NANOMATERIAL BASED DETECTION AND DEGRADATION OF BIOLOGICAL AND CHEMICAL CONTAMINANTS IN A MICROFLUIDIC SYSTEM

by

Harikrishnan Jayamohan

A dissertation submitted to the faculty of
The University of Utah
in partial fulfillment of the requirements for the degree of

Doctor of Philosophy

Department of Mechanical Engineering

The University of Utah

August 2015

Copyright © Harikrishnan Jayamohan 2015

All Rights Reserved

The University of Utah Graduate School

STATEMENT OF DISSERTATION APPROVAL

The dissertation of **Harikrishnan Jayamohan**

has been approved by the following supervisory committee members:

Bruce K. Gale	, Chair	**5/7/2015** Date Approved
Bart Raeymaekers	, Member	**5/4/2015** Date Approved
Manoranjan Misra	, Member	**5/4/2015** Date Approved
Swomitra K. Mohanty	, Member	**5/4/2015** Date Approved
Tim A. Ameel	, Member	**5/6/2015** Date Approved

and by **Tim A. Ameel**, Chair/Dean of

the Department/College/School of **Mechanical Engineering**

and by David B. Kieda, Dean of The Graduate School.

ABSTRACT

Monitoring and remediation of environmental contaminants (biological and chemical) form the crux of global water resource management. There is an extant need to develop point-of-use, low-power, low-cost tools that can address this problem effectively with minimal environmental impact. Nanotechnology and microfluidics have made enormous advances during the past decade in the area of biosensing and environmental remediation. The "marriage" of these two technologies can effectively address some of the above-mentioned needs [1]. In this dissertation, nanomaterials were used in conjunction with microfluidic techniques to detect and degrade biological and chemical pollutants.

In the first project, a point-of-use sensor was developed for detection of trichloroethylene (TCE) from water. A self-organizing nanotubular titanium dioxide (TNA) synthesized by electrochemical anodization and functionalized with photocatalytically deposited platinum (Pt/TNA) was applied to the detection. The morphology and crystallinity of the Pt/TNA sensor was characterized using field emission scanning electron microscope, energy dispersive x-ray spectroscopy, and X-ray diffraction. The sensor could detect TCE in the concentrations ranging from 10 to 1000 ppm. The room-temperature operation capability of the sensor makes it less power intensive and can potentially be incorporated into a field-based sensor. In the second part, TNA synthesized on a foil was incorporated into a flow-based microfluidic format and applied to degradation of a model pollutant, methylene blue. The system was demonstrated to have enhanced photocatalytic performance at higher flow rates (50-200 μL/min) over the same microfluidic format with TiO_2 nanoparticulate (commercial P25) catalyst. The microfluidic format with TNA catalyst was able to achieve 82% fractional conversion of 18 mM methylene blue in comparison to 55% in the case of the TiO_2 nanoparticulate layer at a flow rate of 200 L/min. The microfluidic device was fabricated using non-cleanroom-based methods, making it suitable for economical large-scale manufacture. A computational model of the microfluidic format was developed in COMSOL Multiphysics® finite element software to evaluate the effect of diffusion coefficient and rate constant on the photocatalytic performance. To further enhance the photocatalytic performance of the microfluidic device, TNA synthesized on a mesh was used as the catalyst.

The new system was shown to have enhanced photocatalytic performance in comparison to TNA on a foil. The device was then employed in the inactivation of E. coli O157:H7 at different flow rates and light intensities (100, 50, 20, 10 mW/cm^2).

In the second project, a protocol for ultra-sensitive indirect electrochemical detection of *E. coli* O157:H7 was reported. The protocol uses antibody functionalized primary (magnetic) beads for capture and polyguanine (polyG) oligonucleotide functionalized secondary (polystyrene) beads as an electrochemical tag. The method was able to detect concentrations of *E. coli O157:H7* down to 3 CFU/100 mL (S/N=3). We also demonstrate the use of the protocol for detection of *E. coli* O157:H7 seeded in wastewater effluent samples.

"ekam sad vipra bahudha vadanti" – Truth is one; the wise call it many names

– Rig Veda 1.164.46

CONTENTS

ACKNOWLEDGMENTS

Firstly, I would like to thank my advisor, Dr. Bruce Gale, for his guidance and support and for allowing me the freedom to explore new directions and ideas. Also a great deal of thanks goes to Drs. Mano Mista and Swomitra Mohanty for their guidance and total freedom in use of their laboratory facilities. I also thank their respective lab members for their help and friendship. I would like to thank Dr. Shelley Minteer for all the help with electrochemical methods and for patiently enduring my several queries on the subject.

I would like to acknowledge the institutions that have funded my research endeavors. The Nano Institute of Utah Nanotechnology training program, U.S. Department of Defense SBIR program, Lassonde Entrepreneur Institute scholarship, Utah Technology Commercialization and Innovation Program (TCIP), and the Utah Science and Technology Research Initiative (USTAR) supported much of the work presented here.

I would also like to thank my other committee members, Drs. Bart Raeymaekers and Tim Ameel, for their service and valuable input. I would also like to thank some colleagues and co-authors who have contributed to this work: Dr. York Smith, Metallurgical Engineering; Dr. Himanshu Sant, Jordan Davis, Christopher Lambert, and B.J.Minson, Espira Inc. For this dissertation, I would like to thank my friends, Anshul Joshi, James Skowronek, and Prashant Bagri, for their help with proofreading.

I am thankful to my dear wife for being supportive (emotionally and financially), encouraging, and patient during my endeavor. I am indebted to my parents for their kind words of encouragement during my tough times. I also thank my dear grandparents, sister, in-laws, and friends for their encouragement. Last but not the least, I would like to thank my dear friend, Harish Krishnamurthy, for planting the idea to get a Ph.D. in my mind and being a source of inspiration for me.

CHAPTER 1

INTRODUCTION

This dissertation explores the applicability of nanostructured materials in sensing and purification of biological and chemical environmental pollutants in a microfluidic format. This chapter delves into the problem and the significance of the approach using nanomaterials in a microfluidic format as a solution to the same.

1.1 Motivation and Significance

According to the World Health Organization, 780 million people worldwide do not have access to safe water [2]. More than 2200 children succumb to water-borne diseases every day [3]. In 2011, reports of the presence of *E. coli* superbug (NDM-1) in the public water supply in New Delhi, the capital of India and a city with over 22 million residents, sent public health officials into panic mode [4]. In the same year, a novel strain of *E. coli* O104:H4 affected close to 4000 people in Germany [5]. In the United States, diseases due to waterborne pathogens are estimated to have cost $20 billion in lost productivity annually [6]. Water-based hazards of biological and chemical nature pose a serious challenge to both developing and developed nations.

Biological pollutants include waterborne pathogens like viruses, bacteria, and parasites. Many of these are highly virulent and resistant to standard methods of water treatment [7]. For example, the pathogen *E. coli* O157:H7 is highly virulent with an extremely low infectious dose required to cause disease [8, 9, 10, 11]. Other infectious agents like viruses are resistant to conventional treatment methods like UV and combined chlorine disinfection [12].

The rapid growth of industries, especially in the developing economies, has contributed to the increased repertoire of chemical contaminants in water bodies. These include toxic metal ions, polyaromatic hydrocarbons, haloacetic acids and other disinfectant by-products, pesticides and herbicides, organic peroxides, phenols, chlorinated compounds, and nitrates [13, 14]. Increasing regulatory push is driving the need for effective analytical tools to

identify and quantify these pollutants [13]. Monitoring of these pollutants plays a significant role in the design and implementation of water safety plans, and can be used in surveillance, operational, and investigative means [7].

The challenges related to the measurement of water-borne pollutants are numerous:

1. Current analysis techniques (Gas chromatographymass spectrometry/GC-MS, culturing) are time-consuming and are not always field-based. For instance, conventional methods to detect and identify pathogens require growing a small number of bacteria into colonies of higher numbers. These take 18-24 hours, at a minimum. Methods like GC-MS or cell culture techniques require complex equipment, highly trained technicians, and are not field deployable, nor can they be used in point-of-care (POC) settings [15, 16].

2. The analytes (pathogens and chemical pollutants) of interest are in low concentrations (PPM-PPB).

3. A large number of interferents exist, and hence highly selective and discriminative sensing is required. For example, more recent ultra-sensitive detection methods like PCR suffer from significant loss of sensitivity during detection from samples in complex background [15].

1.2 Water Purification

As mentioned in the previous section, access to clean water is a global necessity that needs to be met. Purification, along with monitoring of polluting agents, are key elements of the solution to this global challenge. Recent advances in water treatment research are expected to mitigate some of the issues involved [12].

Reuse of treated municipal waste water or rural waste water could be an attractive option [17]. Recycling of the waste water is usually associated with the presence of biological contaminants like coliforms and soluble organic compounds that are both tedious and expensive to treat. Conventional water treatment techniques like adsorption and coagulation merely concentrate the pollutants by transferring them to other phases and do not completely eliminate them. Other techniques like sedimentation, filtration, and chemical and membrane technologies involve high operating costs and could potentially leave harmful by-products (disinfection by-products or DBPs). For instance, the use of chlorine, a common disinfectant, results in the generation of DBPs that are mutagenic and carcinogenic [17].

Moreover, chemically intensive technologies are not viable in many regions of the world due to the lack of appropriate infrastructure [12].

However, there is a move toward technologies which reduce the need for chemical treatment, instead relying on more natural systems for water treatment. Some of the recent advances in water purification technologies are described below [12].

1.2.1 Disinfection

Using sunlight to treat drinking water has been around since antiquity, as described in ancient Sanskrit and Greek writings [18]. Irradiation with ultraviolet (UV) light for photochemical inactivation of pathogens has seen a resurgence in the recent years. Treatment with UV light combined with chlorine has been applied in many drinking water utilities. In comparison with standalone free chlorine, UV/chlorine sequential disinfection is very effective in controlling durable waterborne pathogens like *C. parvum* [19, 12]. However, viruses are still resistant to both UV and chlorine disinfection. One solution to viral disinfection is the use of ozone. However, ozone could potentially react with bromide ions in water, forming DBP carcinogen bromate ions. Hence, it is essential to develop alternatives to chlorine and UV-based disinfection for the control of waterborne viruses [12].

1.2.2 Decontamination

The goal of decontamination is to detect and remove toxic substances such as arsenic, heavy metals, halogenated aromatics, nitrosoamines, nitrates, and phosphates from bodies of water in an affordable and robust fashion. There are two key issues involving such agents: the amount of these substances in the water supply is increasing, and these agents are toxic even in trace quantities.

Some of the current methods applied toward the remediation of these agents include chemical precipitation, ion exchange, adsorption, membrane filtration, and electrochemical treatment technologies [20]. Each of these methods has inherent advantages as well as limitations. For instance, chemical precipitation, primarily used for removal of heavy metals from aqueous solutions, is simple and inexpensive. However, it is ineffective when metal ion concentration is low. So it is used primarily for treating wastewater containing high metal ion levels. Also, an unwanted by-product of chemical precipitation is sludge, which is difficult to treat and dispose of properly. For an in-depth analysis of each of these methods mentioned above, the reader can refer to the review by Fenglian Fu et al. [20].

1.3 The Solution: Nanotechnology and Microfluidics

Microfluidics and nanomaterials have both received wide interest as standalone technologies for detection of biological and chemical pollutants as well as their remediation. However, used in tandem, the synergistic effects can be significant [1]. For instance, in coupled systems, the water purification capabilities are enhanced in comparison to stand-alone techniques [21]. The immobilization or growth of photocatalytic nanomaterials as a film, and their use in a microfluidic reactor, can significantly enhance their degradation performance in comparison to macroscale reactors for use in water remediation [22].

Nanomaterials can be used to improve separation in microchip-based capillary electrochromatography or to enhance the sensitivity in microfluidic detection systems [1].

1.4 Microfluidics

Microfluidic systems have been widely applied in sensing of analytes for clinical [23] and environmental applications [24]. The availability of fabrication methods to manufacture small hand-held devices on a large scale is a key enabler in driving down costs of biosensing and diagnostic devices for point-of-use. The capability of microfluidic devices to manipulate small volumes of sample requiring lower amounts of reagents would also help drive down costs. The smaller length-scales associated with microfluidic systems result in faster analysis and higher separation efficiencies, reducing response times. The high-speed analysis also makes microfluidics a suitable candidate for high throughput applications. Highly parallel analyses will allow multiple tests to be run simultaneously, either on the same sample or multiple samples. This is of key benefit when multiple analytes like *E. coli*, Salmonella, etc. are present in the same sample. Still there exist multiple challenges in microfluidic analysis applications due to complexity and diversity of environmental sample matrices and contaminants (biological and chemical) they carry [13]. These would require complex on-chip sample preparation with high throughput capabilities. There are other unique challenges at microfluidic scale such as capillary forces, surface roughness, surface fouling, laminar flow-limiting reagent mixing to diffusion, and finally issues related to interfacing electronics and fluid with the macro-world. In spite of these challenges, there have been increasing numbers of commercial bench-top systems that leverage the unique capabilities of microfluidic technology [25].

Chapter 2 of this dissertation delves in detail into the application of microfluidics in biosensing. Some of the advances in microfluidic biosensing in the last three years is listed in the section below.

1.4.1 Microfluidics in Biosensing: Recent Advances

Araz et al. reported a simple "single inlet, single outlet" microfluidic barcode assay for multiplexed detection of analytes [26]. A streptavidin-functionalized polyacrylamide gel was fabricated in a microchannel, and biotin and biotinylated capture reagents were patterned in discrete regions, resulting in a barcode-like pattern of capture reagents and spacers. They applied the assay to the detection of human antibodies against hepatitis C virus and human immunodeficiency virus antigens [26].

Paper and flexible material-based biosensing platforms are an exciting prospect from the perspective of developing affordable tools for drug development, water and environment quality monitoring, and infectious diseases diagnosis in resource-limited settings [27]. Abbas et al. designed a microfluidic paper-based platform that allowed the separation and pre-concentration of the different components of a complex sample over a small surface area. The platform achieved subattomolar detection limit by applying label-free optical detection (surface-enhanced Raman scattering) [28]. Costa et al. developed a paper-based microfluidic format for colorimetric detection of enzymatic reactions (glucose detection), immunoassays (antibodies anti-*Leishmania* detection), and nucleic acid sequence identification (*Mycobacterium tuberculosis* complex detection) [29]. A microfluidic channel with integrated cellulose paper and flexible polyester films was applied to the selective capture, and the sensitive detection, of multiple biotargets, including viruses (Human Immunodeficieny Virus-1), bacteria (*E. coli* and *Staphylococcus aureus*), and cells ($CD4^+$ T lymphocytes) [27]. Recently, Warren et al. [30] developed a POC platform for the detection of noncommunicable diseases using synthetic biomarkers for enzyme activity and lateral flow assay-based urine analysis with scanner readout[31]. Paper microfluidic devices have also been applied in the detection of pathogens [32] and in the area of electrochemical detection [33]. Paper-based microfluidics is still in its infancy and many interesting developments are expected in the future [34].

For advances in fabrication methods for microfluidics, the reader can refer to the work by Tseng et al. [35].

1.4.1.1 Advances in Pathogen Detection

Study of pathogens is of importance in areas ranging from diagnostics to biological warfare. Conventional techniques of pathogen detection like cell culture are time-consuming (>7 hours), laborious, and require trained personnel [36]. POC pathogen detection requires the method to be inexpensive, portable, and simple to use, without the need for centralized

analysis equipment. The ability to perform multiplexed detection of multiple pathogens is another key requirement.

The detection of pathogenic strains involve two principles: by identifying genetic contents (using nucleic acid-based probes, or by specific epitopes on the pathogen membrane) or by identifying the produced toxins (using antibodies or their alternatives). For a list of different biomarkers used for detection of pathogens, the reader can refer to a review by Foudeh et al. [36].

Antibody-based detection, though labour-intensive, has proven to be a crucial and important factor in the specific and high-affinity detection of pathogens. However, this can be offset by the use of automated microfluidic systems that could help reduce the number of manual steps involved in the detection. Klemm et al. developed a immunological assay using antibody array integrated in a microfluidic chip [37]. The platform was able to detect *Francisella tularensis* and *Yersinia pestis* in about 30 minutes. The automated system (Assay Reader) was used to control the fluidic processes of the chip like actuation of the on-chip turning valves, and time controlled metering and transfer of the reagents. The integrated lab-on-a-chip approach ensured that all waste liquids remain on-chip to avoid any contamination risks. However, antibodies can be expensive and often involve challenges due to cross-reactivity. They can also easily become denatured and lose their ability to bind to pathogens [38]. Aptamers are oligonucleic acids or peptide molecules that bind to a specific target molecule. Unlike antibodies, aptamers are stable. Due to the chemical nature of nucleic acids, aptamers can be easily synthesized and modified [38]. An integrated aptamer-functionalized graphene oxide biosensor in a PDMS/paper/glass hybrid microfluidic chip for detection of pathogens *Lactobacillus acidophilus*, *Staphylococcus aureus*, and *Salmonella enterica* was reported by Zuo et al. [38]. The paper reported the novel use of porous chromatography paper as a simple 3D storage substrate for the aptamer functionalized graphene oxide nano-biosensor in microwells. The device was able to detect pathogens without any cumbersome sample preparation steps, making it suitable for field-based applications [39]. Yoo et al. incorporated antimicrobial peptide labeled microbeads into a weir inside the channel of a microfluidic chip for capture and detection of *E. coli*. Although the device was able to detect down to 10^3 cells per mL, lower limits are necessary since even low levels of *E. coli* (10-100 viable organisms) can cause human infections [40].

The use of immunomagentic beads enable extraction of pathogens from real-world samples that experience interference from background microflora [40]. The incorporation of this

technique in a automated system could significantly reduce the time and effort involved in detection of pathogens. An automated in-situ pathogen detection system was developed for detection and quantification of *E. coli* O157:H7-specific *eaeA* gene [41]. The assay employed the hybridization of target DNA with quantum dot-labeled magnetic beads and probe DNA for quantification of the target bacterial gene. The authors developed the automated version of the assay (earlier reported by Kim et al. [42]), incorporating automated sample and reagent introduction, DNA hybridization, magnetic separation of complexes, and sample collection. However, for the fluorescence detection, a bench-top microplate spectrofluorometer was used. Incorporation of a more portable detection mechanism into the automated system could enable POC use of the platform. A microfluidic nano-biosensor was developed for the rapid detection of *Salmonella* from food samples by Kim et al. [43]. The device used immunomagnetic separation for extraction of *Salmonella* combined with antibody-conjugated quantum dots as fluorescence labels. The fluorescence signal was measured using a custom-built fluorometer, making it suitable for POC use. The device was able to detect levels of *Salmonella* down to 10^3 CFU/mL.

Among various nucleic acid amplification tests, PCR is the most commonly used. PCR amplifies and detects specific nucleic acid sequences from cells and can potentially speed up the detection of infectious pathogens with very high specificity and sensitivity [44]. It can in principle detect a single copy of a target DNA sequence, and hence can be used to detect a single pathogenic organism. It is a promising technology since it detects the organism by amplifying the target rather than the signal. Hence, it is also less prone to false-positives [39]. However, PCR is one of the most sophisticated techniques among the various methods for pathogen detection. Currently available PCR tests rely on complex sample preparation procedures, which prevent their use in a POC setting. Hence, the integration of simple, highly efficient and high throughput sample preparation capability on a microfluidic chip would be a key enabler compared to conventional PCR techniques for POC use. A microfluidic device utilizing dielectrophoresis and multiplex PCR was applied to the detection of pathogens in biological samples like blood [45]. The device was fabricated using SlipChip technologies [46, 47] and integrated four channels processing independent samples. The pathogens were extracted from the blood by dielectrophoresis, retained in an array of grooves, and identified by multiplex array PCR in nanoliter volumes with fluorescence detection. The system was used in the simultaneous identification of *Pseudomonas aeruginosa*, *Staphylococcus aureus*, and *Escherichia coli* O157:H7 within 3 hours. Julich et al. reported an lab-on-a-chip system for the detection of pathogens [48].

The system involved separate modules for on-chip sample preparation and PCR. The sample preparation involved utilizing paramagnetic particles for concentration of bacteria and thermal lysis of the captured bacteria. Stationary and a flow-through PCR technologies were integrated in the on-chip modules for specific detection of six highly pathogenic bacteria. The work did not demonstrate integration of the separate modules.

1.4.2 Microfluidics in Environmental Remediation

Microfluidics has been widely applied to molecular analysis, biodefense, molecular biology, and microelectronics [49]. It has unique properties that can be applied in photocatalysis. Some of these include [21]:

1. **High surface-area-to-volume ratio (SA:V)**: Microfluidic reactors have SA:V at least two orders of magnitude larger than bulk reactors. This is because the volume of fluid flowing through the channel is small in comparison to the surface area of the microfluidic channel. Hence, significant enhancement in the reaction rate can be achieved in a microfluidic reactor in comparison to bulk reactors.

2. **Short diffusion distance**: Due to the relatively small thickness of the microfluidic layer, the pollutants can diffuse faster from the bulk solution to the catalyst surface.

3. **Uniform residence time**: The flow in the microfluidic channel is in the laminar regime. Hence, due to the steady state nature of the flow, the degradation performance is less variable and hence, more predictable.

4. **Higher photon efficiency**: Lesser photons are lost due to scattering in microfluidic reactors due to the thin layer of liquid over the catalyst (unlike in the case of macroscale reactors).

5. **Large mass transfer efficiency**: The mass transfer efficiency determines the ease with which reagents in the liquid are moved to the catalyst surface and the rate at which the reaction products are in turn removed from the catalyst surface. The high SA:V and the short diffusion distance in the case of microfluidic reactors lead to a large mass transfer efficiency.

6. **Self refreshing effect**: The large mass transfer efficiency helps in refreshing the catalyst surface by removing the degradation products away from the surface of the catalyst. This ensures a longer life of the catalyst in a microfluidic system in comparison to bulk reactors.

Microfluidic reactors have been applied to photocatalytic applications like water purification, water splitting [50, 51], photosynthesis, bioparticle deactivation, and heavy metal ion mineralization [52, 53, 54, 55, 56, 57, 58]. Most of the microfluidic reactors for photocatalytic water purification reported in literature are of fairly simple design and can be broadly classified into four configurations, viz. micro-capillary, single-microchannel, multi-microchannel, and planar reactors (Figure 1.1) [21]. Table 1.1 lists the set of published work in the area of microfluidic photocatalytic remediation. It is evident that TiO_2 is the most widely used photocatalytic material in most of the reported microfluidic reactors. Interestingly, the majority of the work pertains to the degradation of methylene blue. Future work will need to focus on applying microfluidic reactors towards the remediation of other agents including biological pathogens.

1.5 Nanotechnology/Nanostructured Materials

1.5.1 Nanotechnology in Biosensing

Nanotechnology is a disruptive technology that holds promise in enabling development of tools that are inexpensive, convenient, and yet accurate in biosensing applications. The inherent size of many of the analytes (pathogens, chemical entities) is in the nanoscale. Hence, nanotechnology provides windows into the environment to look for these biological/chemical agents and quantify them [23]. Nanomaterials have unique optical, magnetic, mechanical, chemical, and physical properties that are absent in the bulk scale, and can been used for sensitive and precise detection [71]. Also, the surface-area-to-volume ratio increases as we go down to the nanoscale, which means nanoparticles will have very high surface area compared to their volume, to attach to and detect entities of interest. Since the last decade, the integration of nanomaterials has had significant impact in the area of biological and chemical sensing [72, 73]. There have been significant advances in terms of new materials and their properties like "highly controllable size, shape, surface charge, and physicochemical characteristics" [72]. The ease of surface functionalization of the nanomaterials with different moieties render them useful in sensing and catalytic applications.

1.5.1.1 Nanomaterial-based Electrochemical Biosensors

Electrochemical sensors offer several advantages. They offer "elegant routes for interfacing, at the molecular level, biological recognition events and electronic signal-transduction processes" [73]. Electrochemical detection has been used to achieve low detection limits (atto- and zeptomole) in immunoassays with little or no sample preparation. Electrochemi-

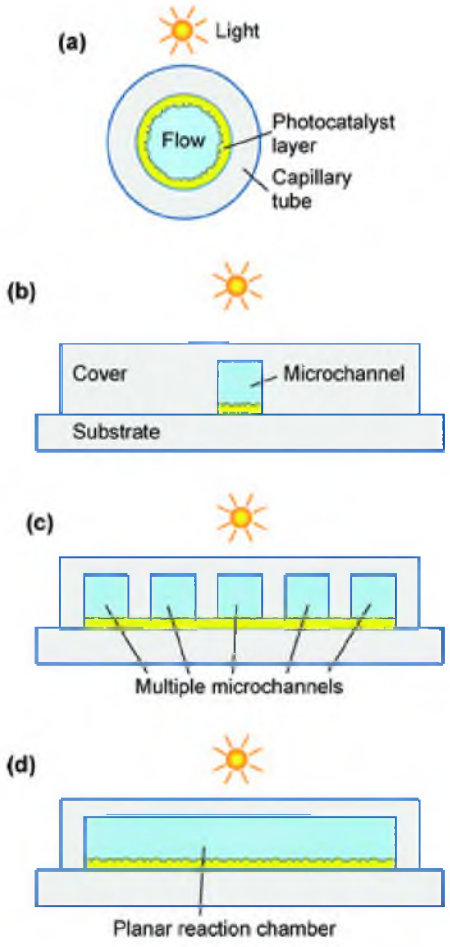

Figure 1.1. Various configurations of microfluidic reactors for photocatalytic water purification. (a) Transverse cross-section of micro-capillary reactor; (b) single-microchannel reactor; (c) multi-microchannel reactor; and (d) planar microreactor. Reproduced with permission from Royal Society of Chemistry [21].

Table 1.1. Summary of reported photocatalytic microfluidic reactor systems.

Photocatalyst	**Light source**	**Chemical degraded**	**Ref.**
TiO_2/SiO_2	UV light	Methylene blue	[59]
P25 TiO_2 coated fiber glass	AM 1.5	Methylene blue	[60]
P25 TiO_2 film	UV light	Methylene blue	[61]
P25 TiO_2 film	AM 1.5	Methylene blue	[22]
Electrospun nanofibrous TiO_2	UV LED	Methylene blue	[62]
TiO_2 nanotube array	AM 1.5	Methylene blue	[22]
TiO_2	UV light	4-Chlorophenol	[63]
TiO_2 microbeads	UV-A LED	4-Chlorophenol	[64]
ZnO nanowires	UV light	Methylene blue	[65]
TiO_2	UV LED	Rhodamine 6G	[66]
TiO_2	UV lamp	Methylene orange	[67]
TiO_2	UV LED	New coccine	[68]
TiO_2	UV Nd-YAG laser	Salicylic acid	[69]
TiO_2	UV LED	Chelate (Cu-EDTA)	[70]

cal detection can be very effective in the case of homogeneous immunoassays with no separation step to isolate the antibody-antigen complex from the unbound assay constituents. This is because electrochemical detection is not affected by sample components like chromophores and fluorophores that could potentially interfere with spectrophotometric detection. Therefore, electrochemical detection can be performed on colored and turbid samples like whole blood containing interferents like red blood cells, hemoglobin, fat globules, and bilirubin [74].

Electrochemical devices are also attractive from the perspective of developing decentralized point-of-use systems, by meeting the requirements of size, cost, low volume, and power. They offer a great promise for a wide range of applications in biomedical and environmental scenarios [73].

Electrochemical sensors rely on conventional electrochemical techniques like differential pulse voltammetry (DPV), electrochemical impedance spectroscopy (EIS), potentiometric stripping analysis (PSA), square wave voltammetry (SWV), cathodic stripping voltammetry (CSV), adsorptive transfer stripping voltammetry (AdSTV), linear voltammetry (LV), and linear square voltammetry (LSV) [75]. Electrochemical sensors rely on a measurable current generated by the reaction being monitored (amperometry), a measurable charge accumulation or potential (potentiometry), or alters the conductive properties of the medium between electrodes (conductometry). EIS-based methods work by monitoring both resistance and reactance in the biosensor [74].

In recent years, the use of nanomaterial-enabled electrochemical DNA sensing strategies have become one of the most exciting forefronts in analytical chemistry. Various nanomaterials like magnetic nanoparticles, nanoparticles labeled with metal tags, nanotubes, and nanowires [75, 72] enable signal amplification and multiplexing capabilities to electrochemical sensing [76, 73].

1.5.1.2 Carbon-based Nanomaterials

Carbon nanomaterials have unique advantages such as a high surface-to-volume ratio, high electrical conductivity, chemical stability, biocompatibility, and robust mechanical strength, which makes them an attractive material for biosensing applications. These materials include carbon nanotubes, fullerenes, and graphene. The readers can refer to the following reviews for advances in the area of carbon nanotube and fullerene-based electrochemical sensing [77, 78, 72].

1.5.1.3 Graphene

Graphene is a two-dimensional material that has attracted much attention owing to its fascinating physical properties like high surface area, excellent conductivity, quantum hall effect, high mechanical strength, and ease of functionalization and mass production [79]. It has shown great promise in many applications, such as energy storage and conversion, electronics, and biosensing [79, 80, 81]. They have extensively been applied in DNA sensing and environmental analysis due to their excellent electron transfer promoting ability [79, 82].

Graphene is used as transducer in bio-field-effect transistors, electrochemical biosensors, impedance biosensors, electrochemiluminescence and fluorescence biosensors, as well as biomolecular labels [81]. For an in-depth discussion on the use of graphene in non-electrochemical biosensors, the reader can refer to [81].

Graphene has been applied to direct electrochemical detection of enzymes. In the case of direct electrochemistry, there is a direct transfer of electrons between the electrode and the active center of the enzyme without the participation of any mediators or other reagents [79]. Such a capability is difficult to achieve in the case of common electrodes since the active centers of most redox enzymes are located deep in a hydrophobic cavity of the molecule. The use of graphene for direct electron transfer-based detection of glucose oxidase enzyme (glucosensing applications) has been widely reported [81]. They have also been applied to electrochemical detection of small biomolecules like hydrogen peroxide, nicotinamide adenine dinucleotide (NADH), and dopamine [79].

Electrochemical detection of DNA using graphene-based sensors has received significant amount of attention recently [83, 82, 84, 85]. They work by direct detection of DNA, by reading the oxidative signals of DNA bases or by using electroactive labels. Although direct detection is advantageous due to it being label free, it offers poorer sensitivity than label-based DNA assays [81].

1.5.1.4 Titania Nanotube Arrays

Titania nanotube arrays (TNA) have received significant interest due to ease of synthesis and tunable size (nanotube diameter and length) over other nanomaterials [22]. TiO_2 can be fabricated into different shapes like nanotubes, nanofibers, nanosheets, and nanoparticles [86]. Of these, TNA have improved properties over other forms especially for applications like photocatalysis, sensing, and photoelectrolysis [87]. They have been applied to applications like energy conversion/storage, electroluminescent hybrid devices [86], drug delivery [88], and chemical and biological sensing [89]. They have been extensively applied in photocatalytic applications due to properties like strong oxidizing ability for organic

decomposition, superhydrophilicity, chemical stability, durability, nontoxicity [90], and low cost of preparation [91].

Titania nanotube arrays have also been applied in chemical/gas sensing applications. They have been used in the detection of hydrogen [92, 93, 94], oxygen [95], and formaldehyde [96]. The large surface area of nanostructured TNA enables higher sensitivity since the interaction of a gas with the sensor is a surface phenomenon. They can also be photocatalytically functionalized with catalysts like platinum for specific gas sensing capabilities [97]. Banerjee et al. applied Zn^{2+} metal ion functionalized TNA for the detection of triacetone triperoxide (TATP), a peroxide-based explosive [98]. The interaction between the functionalized metal and TATP resulted in a change in the electrical resistivity of the sensor platform[99]. Ray et al. used density functional theory to study affinity of different metals to TATP and found Co^{2+} metal ion to have a higher affinity towards TATP [99]. Hence, such an approach to study the affinity of metals to the analyte gas of interest would be effective in enhancing the sensitivity of the platform. TNA have also been used as humidity sensors [100]. Electrodes utilizing TNA have been applied in electrochemical detection of various analytes. The large surface area and high aspect ratio of the nanotubular structure make TNA an attractive material in electrochemical detection applications. Nanocrystalline anatase TNA was applied to the direct electrochemical detection of a single-chain protein, Myoglobin [101]. Guo et al. developed a reagentless hydrogen peroxide biosensor utilizing direct electrochemistry of hemoglobin on carbonized TNA [102]. Direct electrochemical detection of hemeprotein was reported utilizing gold nanoparticle functionalized TNA [103]. Benvenuto et al. reported a glucose biosensor using glucose oxidase immobilized with chitosan onto TNA modified by prussian blue and gold [104]. TNA modified with palladium, platinum, and gold nanoparticles was used for the simultaneous detection of uric acid and ascorbic acid [105].

A variety of methods have been applied to the fabrication of TNA, including deposition into a nanoporous alumina template, solgel transcription using organo-gelators as templates, seeded growth, and hydrothermal processes. Of these methods, anodization of highly ordered TNA via anodization of titanium in fluoride-based solution exhibit remarkable properties, including ability to precisely tune dimensions like pore size, wall thickness, and lengths [22].

1.5.2 Nanotechnology in Environmental Remediation

Nanomaterials been widely applied for environmental remediation of gaseous (SO_x, NO_x, CO, NH_3), chemical (arsenic, heavy metals), organic (volatile organic compounds/VOCs),

and biological pollutants (bacteria, virus) [106, 107]. They are excellent adsorbents and catalysts, and hence exhibit enhanced performance in environmental remediation applications. This is primarily due to their large specific surface area and associated high reactivity. The high surface area-to-mass ratio of nanomaterials can greatly enhance their adsorption capacities. Due to their reduced size and large radii of curvature, nanomaterials have a surface that is particularly reactive (due to the high density of low-coordinated atoms at the surface, edges, and vortices) [107]. These unique properties make them an attractive choice in degradation and scavenging of pollutants in water and air.

1.6 Dissertation Overview

The overarching theme of this dissertation is the application of microfluidic techniques and nanomaterials in detection and degradation of chemical and biological pollutants.

Chapter 3 talks about a platinum functionalized TNA sensor for detection of trichloroethylene in water. This chapter is published in its entirety in the *Proceedings of IEEE Sensors* 2013 [89].

Chapter 4 presents a protocol for ultra-sensitive indirect detection of *E. coli* O157:H7 using immunomagnetic capture, and polyguanine (polyG) oligonucleotide functionalized polystyrene beads as an electrochemical tag. This chapter is published in its entirety in the peer-reviewed journal *Sensors* [40].

Chapter 5 presents a novel microfluidic reactor with TNA as the catalyst, applied to the photocatalytic degradation of an organic dye (methylene blue). This chapter is published in its entirety in the peer-reviewed journal *Applied Catalysis B: Environmental* [22].

Chapter 6 applies TNA grown on a mesh as a catalyst in a microfluidic reactor. The system shows enhanced performance in comparison to TNA on a foil (described in Chapter 5) in a microfluidic reactor during photocatalytic degradation of methylene blue. The device is also applied to the inactivation of *E. coli* O157:H7 at different flow rates and light intensity.

Lastly, Chapter 7 provides a conclusion, highlighting the knowledge gained from above dissertation-projects, scientific and technological contributions, as well as a future work section.

1.7 References

[1] M. Pumera, "Nanomaterials meet microfluidics," *Chemical Communications*, vol. 47, no. 20, pp. 5671–5680, 2011.

[2] World Health Organization. (2012, March) The history of drinking water treatment. [Online]. Available: "http://www.who.int/water_sanitation_health/publications/2012/jmp_report/en"

[3] L. Liu, H. L. Johnson, S. Cousens, J. Perin, S. Scott, J. E. Lawn, I. Rudan, H. Campbell, R. Cibulskis, M. Li *et al.*, "Global, regional, and national causes of child mortality: an updated systematic analysis for 2010 with time trends since 2000," *The Lancet*, vol. 379, no. 9832, pp. 2151–2161, 2012.

[4] T. R. Walsh, J. Weeks, D. M. Livermore, and M. A. Toleman, "Dissemination of ndm-1 positive bacteria in the new delhi environment and its implications for human health: an environmental point prevalence study," *The Lancet infectious diseases*, vol. 11, no. 5, pp. 355–362, 2011.

[5] F. Scheutz, E. M. Nielsen, J. Frimodt-Moller, N. Boisen, S. Morabito, R. Tozzoli, J. Nataro, and A. Caprioli, "Characteristics of the enteroaggregative shiga toxin/verotoxin-producing escherichia coli o104: H4 strain causing the outbreak of haemolytic uraemic syndrome in germany, may to june 2011," *Euro surveill*, vol. 16, no. 24, p. 19889, 2011.

[6] T. M. Straub and D. P. Chandler, "Towards a unified system for detecting waterborne pathogens," *Journal of Microbiological Methods*, vol. 53, no. 2, pp. 185–197, 2003.

[7] H. Bridle, B. Miller, and M. P. Desmulliez, "Application of microfluidics in waterborne pathogen monitoring: A review," *water research*, vol. 55, pp. 256–271, 2014.

[8] O. Tokarskyy and D. L. Marshall, "Immunosensors for rapid detection of escherichia coli O157: H7-perspectives for use in the meat processing industry," *Food microbiology*, vol. 25, no. 1, pp. 1–12, 2008.

[9] L. Yang and R. Bashir, "Electrical/electrochemical impedance for rapid detection of foodborne pathogenic bacteria," *Biotechnology advances*, vol. 26, no. 2, pp. 135–150, 2008.

[10] B. Ge and J. Meng, "Advanced technologies for pathogen and toxin detection in foods: current applications and future directions," *Journal of the Association for Laboratory Automation*, vol. 14, no. 4, pp. 235–241, 2009.

[11] M. Barreiros dos Santos, J. Agusil, B. Prieto-Simon, C. Sporer, V. Teixeira, and J. Samitier, "Highly sensitive detection of pathogenescherichia coli o157: h7 by electrochemical impedance spectroscopy," *Biosensors and Bioelectronics*, vol. 45, pp. 174–180, 2013.

[12] M. A. Shannon, P. W. Bohn, M. Elimelech, J. G. Georgiadis, B. J. Mariñas, and A. M. Mayes, "Science and technology for water purification in the coming decades," *Nature*, vol. 452, no. 7185, pp. 301–310, 2008.

[13] J. C. Jokerst, J. M. Emory, and C. S. Henry, "Advances in microfluidics for environmental analysis," *Analyst*, vol. 137, no. 1, pp. 24–34, 2012.

[14] E. M. E. Zahran, *Nanostructured materials and sensors for environmental applications*, 2011.

[15] H. Sharma and R. Mutharasan, "Review of biosensors for foodborne pathogens and toxins," *Sensors and Actuators B: Chemical*, vol. 183, pp. 535–549, 2013.

[16] H. Jayamohan, H. J. Sant, and B. K. Gale, "Applications of microfluidics for molecular diagnostics," in *Microfluidic Diagnostics*. Springer, 2013, pp. 305–334.

[17] M. N. Chong, B. Jin, C. W. Chow, and C. Saint, "Recent developments in photocatalytic water treatment technology: a review," *Water research*, vol. 44, no. 10, pp. 2997–3027, 2010.

[18] United States Environmental Protection Agency. (2007, February) Progress on drinking water and sanitation: 2012 update. [Online]. Available: "http://www.epa.gov/ogwdw/consumer/pdf/hist.pdf"

[19] W. Hijnen, E. Beerendonk, and G. J. Medema, "Inactivation credit of uv radiation for viruses, bacteria and protozoan (oo) cysts in water: a review," *Water research*, vol. 40, no. 1, pp. 3–22, 2006.

[20] F. Fu and Q. Wang, "Removal of heavy metal ions from wastewaters: a review," *Journal of Environmental Management*, vol. 92, no. 3, pp. 407–418, 2011.

[21] N. Wang, X. Zhang, Y. Wang, W. Yu, and H. L. Chan, "Microfluidic reactors for photocatalytic water purification," *Lab on a Chip*, vol. 14, no. 6, pp. 1074–1082, 2014.

[22] H. Jayamohan, Y. R. Smith, L. C. Hansen, S. K. Mohanty, B. K. Gale, and M. Misra, "Anodized titania nanotube array microfluidic device for photocatalytic application: Experiment and simulation," *Applied Catalysis B: Environmental*, vol. 174, pp. 167–175, 2015.

[23] J. R. Heath and M. E. Davis, "Nanotechnology and cancer," *Annual review of medicine*, vol. 59, p. 251, 2008.

[24] H.-A. Keserue, H. P. Füchslin, and T. Egli, "Rapid detection and enumeration of giardia lamblia cysts in water samples by immunomagnetic separation and flow cytometric analysis," *Applied and environmental microbiology*, vol. 77, no. 15, pp. 5420–5427, 2011.

[25] C. D. Chin, V. Linder, and S. K. Sia, "Commercialization of microfluidic point-of-care diagnostic devices," *Lab on a Chip*, vol. 12, no. 12, pp. 2118–2134, 2012.

[26] M. K. Araz, A. A. Apori, C. M. Salisbury, and A. E. Herr, "Microfluidic barcode assay for antibody-based confirmatory diagnostics," *Lab on a Chip*, vol. 13, no. 19, pp. 3910–3920, 2013.

[27] H. Shafiee, W. Asghar, F. Inci, M. Yuksekkaya, M. Jahangir, M. H. Zhang, N. G. Durmus, U. A. Gurkan, D. R. Kuritzkes, and U. Demirci, "Paper and flexible substrates as materials for biosensing platforms to detect multiple biotargets," *Scientific reports*, vol. 5, 2015.

[28] A. Abbas, A. Brimer, J. M. Slocik, L. Tian, R. R. Naik, and S. Singamaneni, "Multifunctional analytical platform on a paper strip: separation, preconcentration, and subattomolar detection," *Analytical chemistry*, vol. 85, no. 8, pp. 3977–3983, 2013.

[29] M. Costa, B. Veigas, J. Jacob, D. Santos, J. Gomes, P. Baptista, R. Martins, J. Inácio, and E. Fortunato, "A low cost, safe, disposable, rapid and self-sustainable paper-based

platform for diagnostic testing: lab-on-paper," *Nanotechnology*, vol. 25, no. 9, p. 094006, 2014.

[30] A. D. Warren, G. A. Kwong, D. K. Wood, K. Y. Lin, and S. N. Bhatia, "Point-of-care diagnostics for noncommunicable diseases using synthetic urinary biomarkers and paper microfluidics," *Proceedings of the National Academy of Sciences*, vol. 111, no. 10, pp. 3671–3676, 2014.

[31] E. Petryayeva and W. R. Algar, "Toward point-of-care diagnostics with consumer electronic devices: the expanding role of nanoparticles," *RSC Advances*, vol. 5, no. 28, pp. 22 256–22 282, 2015.

[32] T. Park and J. Yoon, "Smartphone detection of escherichia coli from field water samples on paper microfluidics," 2015.

[33] B. Liu, D. Du, X. Hua, X.-Y. Yu, and Y. Lin, "Paper-based electrochemical biosensors: From test strips to paper-based microfluidics," *Electroanalysis*, vol. 26, no. 6, pp. 1214–1223, 2014.

[34] P. Tabeling, "Recent progress in the physics of microfluidics and related biotechnological applications," *Current opinion in biotechnology*, vol. 25, pp. 129–134, 2014.

[35] P. Tseng, C. Murray, D. Kim, and D. Di Carlo, "Research highlights: printing the future of microfabrication," *Lab on a Chip*, vol. 14, no. 9, pp. 1491–1495, 2014.

[36] A. M. Foudeh, T. F. Didar, T. Veres, and M. Tabrizian, "Microfluidic designs and techniques using lab-on-a-chip devices for pathogen detection for point-of-care diagnostics," *Lab on a Chip*, vol. 12, no. 18, pp. 3249–3266, 2012.

[37] R. Klemm, H. Becker, N. Hlawatsch, S. Julich, P. Miethe, C. Moche, S. Schattschneider, H. Tomaso, and C. Gärtner, "A microfluidic platform with integrated arrays for immunologic assays for biological pathogen detection," in *SPIE Defense+ Security*. International Society for Optics and Photonics, 2014, pp. 907 311–907 311.

[38] P. Zuo, X. Li, D. C. Dominguez, and B.-C. Ye, "A pdms/paper/glass hybrid microfluidic biochip integrated with aptamer-functionalized graphene oxide nano-biosensors for one-step multiplexed pathogen detection," *Lab on a Chip*, vol. 13, no. 19, pp. 3921–3928, 2013.

[39] R. Singh, M. D. Mukherjee, G. Sumana, R. K. Gupta, S. Sood, and B. Malhotra, "Biosensors for pathogen detection: A smart approach towards clinical diagnosis," *Sensors and Actuators B: Chemical*, vol. 197, pp. 385–404, 2014.

[40] H. Jayamohan, B. K. Gale, B. Minson, C. J. Lambert, N. Gordon, and H. J. Sant, "Highly sensitive bacteria quantification using immunomagnetic separation and electrochemical detection of guanine-labeled secondary beads," *Sensors*, vol. 15, no. 5, pp. 12 034–12 052, 2015.

[41] K. A. Mitchell, B. Chua, and A. Son, "Development of first generation in-situ pathogen detection system (gen1-ipds) based on nanogene assay for near real time e. coli o157: H7 detection," *Biosensors and Bioelectronics*, vol. 54, pp. 229–236, 2014.

[42] G.-Y. Kim and A. Son, "Development and characterization of a magnetic bead-quantum dot nanoparticles based assay capable of escherichia coli o157: H7 quantification," *Analytica chimica acta*, vol. 677, no. 1, pp. 90–96, 2010.

[43] G. Kim, J.-H. Moon, C.-Y. Moh, and J.-g. Lim, "A microfluidic nano-biosensor for the detection of pathogenic salmonella," *Biosensors and Bioelectronics*, 2014.

[44] J. Casalta, F. Gouriet, V. Roux, F. Thuny, G. Habib, and D. Raoult, "Evaluation of the lightcycler® septifast test in the rapid etiologic diagnostic of infectious endocarditis," *European journal of clinical microbiology & infectious diseases*, vol. 28, no. 6, pp. 569–573, 2009.

[45] D. Cai, M. Xiao, P. Xu, Y.-C. Xu, and W. Du, "An integrated microfluidic device utilizing dielectrophoresis and multiplex array pcr for point-of-care detection of pathogens," *Lab on a Chip*, vol. 14, no. 20, pp. 3917–3924, 2014.

[46] W. Du, L. Li, K. P. Nichols, and R. F. Ismagilov, "Slipchip," *Lab Chip*, vol. 9, no. 16, pp. 2286–2292, 2009.

[47] R. F. Ismagilov, W. Du, L. Li, F. Shen, K. P. F. Nichols, D. Chen, and J. E. Kreutz, "Slip chip device and methods," Mar. 23 2010, uS Patent App. 13/257,811.

[48] S. Julich, R. Kopinč, N. Hlawatsch, C. Moche, A. Lapanje, C. Gärtner, and H. Tomaso, "Lab-on-a-chip modules for detection of highly pathogenic bacteria: from sample preparation to detection," in *SPIE Sensing Technology+ Applications*. International Society for Optics and Photonics, 2014, pp. 91 070R–91 070R.

[49] G. M. Whitesides, "The origins and the future of microfluidics," *Nature*, vol. 442, no. 7101, pp. 368–373, 2006.

[50] Y. Matsushita, H. M. A. Mohamed, and S. Ookawara, "Micro-flow reaction systems for photocatalytic carbon dioxide recycling and hyrdrogen generation," *Proc. MicroTAS 2012 (Okinawa, Japan, 1 November 2012) Micro*, 2012.

[51] X. Zhang, Y. L. Chen, R.-S. Liu, and D. P. Tsai, "Plasmonic photocatalysis," *Reports on Progress in Physics*, vol. 76, no. 4, p. 046401, 2013.

[52] J. R. Adleman, D. A. Boyd, D. G. Goodwin, and D. Psaltis, "Heterogenous catalysis mediated by plasmon heating," *Nano letters*, vol. 9, no. 12, pp. 4417–4423, 2009.

[53] J. H. Kim, M. Lee, J. S. Lee, and C. B. Park, "Self-assembled light-harvesting peptide nanotubes for mimicking natural photosynthesis," *Angewandte Chemie International Edition*, vol. 51, no. 2, pp. 517–520, 2012.

[54] Y. Matsushita, T. Ichimura, N. Ohba, S. Kumada, K. Sakeda, T. Suzuki, H. Tanibata, and T. Murata, "Recent progress on photoreactions in microreactors," *Pure and Applied Chemistry*, vol. 79, no. 11, pp. 1959–1968, 2007.

[55] Y. Matsushita, N. Ohba, S. Kumada, T. Suzuki, and T. Ichimura, "Photocatalytic n-alkylation of benzylamine in microreactors," *Catalysis Communications*, vol. 8, no. 12, pp. 2194–2197, 2007.

[56] Y. Matsushita, N. Ohba, T. Suzuki, and T. Ichimura, "N-alkylation of amines by photocatalytic reaction in a microreaction system," *Catalysis Today*, vol. 132, no. 1, pp. 153–158, 2008.

[57] M. Neumann and K. Zeitler, "Application of microflow conditions to visible light photoredox catalysis," *Organic letters*, vol. 14, no. 11, pp. 2658–2661, 2012.

[58] P. C. Vesborg, S.-i. In, J. L. Olsen, T. R. Henriksen, B. L. Abrams, Y. Hou, A. Kleiman-Shwarsctein, O. Hansen, and I. Chorkendorff, "Quantitative measurements of photocatalytic co-oxidation as a function of light intensity and wavelength over tio2 nanotube thin films in μ-reactors," *The Journal of Physical Chemistry C*, vol. 114, no. 25, pp. 11 162–11 168, 2010.

[59] X. Li, H. Wang, K. Inoue, M. Uehara, H. Nakamura, M. Miyazaki, E. Abe, and H. Maeda, "Modified micro-space using self-organized nanoparticles for reduction of methylene blue," *Chemical Communications*, no. 8, pp. 964–965, 2003.

[60] L. Li, R. Chen, X. Zhu, H. Wang, Y. Wang, Q. Liao, and D. Wang, "Optofluidic microreactors with tio2-coated fiberglass," *ACS applied materials & interfaces*, vol. 5, no. 23, pp. 12 548–12 553, 2013.

[61] L. Lei, N. Wang, X. Zhang, Q. Tai, D. P. Tsai, and H. L. Chan, "Optofluidic planar reactors for photocatalytic water treatment using solar energy," *Biomicrofluidics*, vol. 4, no. 4, p. 043004, 2010.

[62] Z. Meng, X. Zhang, and J. Qin, "A high efficiency microfluidic-based photocatalytic microreactor using electrospun nanofibrous tio2 as a photocatalyst," *Nanoscale*, vol. 5, no. 11, pp. 4687–4690, 2013.

[63] R. Gorges, S. Meyer, and G. Kreisel, "Photocatalysis in microreactors," *Journal of Photochemistry and Photobiology A: Chemistry*, vol. 167, no. 2, pp. 95–99, 2004.

[64] T.-H. Yoon, L.-Y. Hong, and D.-P. Kim, "Photocatalytic reaction using novel inorganic polymer derived packed bed microreactor with modified tio2 microbeads," *Chemical Engineering Journal*, vol. 167, no. 2, pp. 666–670, 2011.

[65] Z. Han, J. Li, W. He, S. Li, Z. Li, J. Chu, and Y. Chen, "A microfluidic device with integrated zno nanowires for photodegradation studies of methylene blue under different conditions," *Microelectronic Engineering*, vol. 111, pp. 199–203, 2013.

[66] K. Oda, Y. Ishizaka, T. Sato, T. Eitoku, and K. Katayama, "Analysis of photocatalytic reactions using a tio2 immobilized microreactor," *Analytical Sciences*, vol. 26, no. 9, pp. 969–972, 2010.

[67] Z. Zhang, H. Wu, Y. Yuan, Y. Fang, and L. Jin, "Development of a novel capillary array photocatalytic reactor and application for degradation of azo dye," *Chemical Engineering Journal*, vol. 184, no. 0, pp. 9 – 15, 2012.

[68] N. Tsuchiya, K. Kuwabara, A. Hidaka, K. Oda, and K. Katayama, "Reaction kinetics of dye decomposition processes monitored inside a photocatalytic microreactor," *Phys. Chem. Chem. Phys.*, vol. 14, no. 14, pp. 4734–4741, 2012.

[69] G. Charles, T. Roques-Carmes, N. Becheikh, L. Falk, J.-M. Commenge, and S. Corbel, "Determination of kinetic constants of a photocatalytic reaction in micro-channel reactors in the presence of mass-transfer limitation and axial dispersion," *Journal of Photochemistry and Photobiology A: Chemistry*, vol. 223, no. 2, pp. 202–211, 2011.

[70] D. Daniel and I. G. Gutz, "Microfluidic cell with a tio 2-modified gold electrode irradiated by an uv-led for in situ photocatalytic decomposition of organic matter and its potentiality for voltammetric analysis of metal ions," *Electrochemistry communications*, vol. 9, no. 3, pp. 522–528, 2007.

[71] Y.-E. Choi, J.-W. Kwak, and J. W. Park, "Nanotechnology for early cancer detection," *Sensors*, vol. 10, no. 1, pp. 428–455, 2010.

[72] A. Chen and S. Chatterjee, "Nanomaterials based electrochemical sensors for biomedical applications," *Chemical Society Reviews*, vol. 42, no. 12, pp. 5425–5438, 2013.

[73] J. Wang, "Nanomaterial-based electrochemical biosensors," *Analyst*, vol. 130, no. 4, pp. 421–426, 2005.

[74] N. J. Ronkainen, H. B. Halsall, and W. R. Heineman, "Electrochemical biosensors," *Chemical Society Reviews*, vol. 39, no. 5, pp. 1747–1763, 2010.

[75] A. Erdem, "Nanomaterial-based electrochemical dna sensing strategies," *Talanta*, vol. 74, no. 3, pp. 318–325, 2007.

[76] J.-M. Nam, S. I. Stoeva, and C. A. Mirkin, "Bio-bar-code-based dna detection with pcr-like sensitivity," *Journal of the American Chemical Society*, vol. 126, no. 19, pp. 5932–5933, 2004.

[77] C. B. Jacobs, M. J. Peairs, and B. J. Venton, "Review: Carbon nanotube based electrochemical sensors for biomolecules," *Analytica Chimica Acta*, vol. 662, no. 2, pp. 105–127, 2010.

[78] S. K. Vashist, D. Zheng, K. Al-Rubeaan, J. H. Luong, and F.-S. Sheu, "Advances in carbon nanotube based electrochemical sensors for bioanalytical applications," *Biotechnology advances*, vol. 29, no. 2, pp. 169–188, 2011.

[79] Y. Shao, J. Wang, H. Wu, J. Liu, I. A. Aksay, and Y. Lin, "Graphene based electrochemical sensors and biosensors: a review," *Electroanalysis*, vol. 22, no. 10, pp. 1027–1036, 2010.

[80] A. Ambrosi, A. Bonanni, Z. Sofer, J. S. Cross, and M. Pumera, "Electrochemistry at chemically modified graphenes," *Chemistry-A European Journal*, vol. 17, no. 38, pp. 10 763–10 770, 2011.

[81] M. Pumera, "Graphene in biosensing," *Materials Today*, vol. 14, no. 7, pp. 308–315, 2011.

[82] A. Bonanni, A. Ambrosi, and M. Pumera, "Nucleic acid functionalized graphene for biosensing," *Chemistry-A European Journal*, vol. 18, no. 6, pp. 1668–1673, 2012.

[83] M. Muti, S. Sharma, A. Erdem, and P. Papakonstantinou, "Electrochemical monitoring of nucleic acid hybridization by single-use graphene oxide-based sensor," *Electroanalysis*, vol. 23, no. 1, pp. 272–279, 2011.

[84] L. Feng, Z. Zhang, J. Ren, and X. Qu, "Graphene platform used for electrochemically discriminating dna triplex," *ACS applied materials & interfaces*, vol. 6, no. 5, pp. 3513–3519, 2014.

[85] Q. Gong, H. Yang, Y. Dong, and W. Zhang, "A sensitive impedimetric dna biosensor for the determination of the hiv gene based on electrochemically reduced graphene oxide," *Analytical Methods*, 2015.

[86] H.-H. Ou and S.-L. Lo, "Review of titania nanotubes synthesized via the hydrothermal treatment: Fabrication, modification, and application," *Separation and Purification Technology*, vol. 58, no. 1, pp. 179–191, 2007.

[87] G. K. Mor, O. K. Varghese, M. Paulose, K. Shankar, and C. A. Grimes, "A review on highly ordered, vertically oriented tio 2 nanotube arrays: fabrication, material properties, and solar energy applications," *Solar Energy Materials and Solar Cells*, vol. 90, no. 14, pp. 2011–2075, 2006.

[88] Y.-Y. Song, F. Schmidt-Stein, S. Bauer, and P. Schmuki, "Amphiphilic tio2 nanotube arrays: an actively controllable drug delivery system," *Journal of the American Chemical Society*, vol. 131, no. 12, pp. 4230–4232, 2009.

[89] H. Jayamohan, Y. R. Smith, B. K. Gale, M. Misra, and S. K. Mohanty, "Platinum functionalized titania nanotube array sensor for detection of trichloroethylene in water," *Proc. Sensors 2013 (Baltimore, MD, 3–6 November 2013) IEEE*, pp. 1–4, 2013.

[90] K. Nakata and A. Fujishima, "Tio 2 photocatalysis: design and applications," *Journal of Photochemistry and Photobiology C: Photochemistry Reviews*, vol. 13, no. 3, pp. 169–189, 2012.

[91] J. M. Macak, M. Zlamal, J. Krysa, and P. Schmuki, "Self-organized tio2 nanotube layers as highly efficient photocatalysts," *Small*, vol. 3, no. 2, pp. 300–304, 2007.

[92] O. K. Varghese, D. Gong, M. Paulose, K. G. Ong, and C. A. Grimes, "Hydrogen sensing using titania nanotubes," *Sensors and Actuators B: Chemical*, vol. 93, no. 1, pp. 338–344, 2003.

[93] M. Paulose, O. K. Varghese, G. K. Mor, C. A. Grimes, and K. G. Ong, "Unprecedented ultra-high hydrogen gas sensitivity in undoped titania nanotubes," *Nanotechnology*, vol. 17, no. 2, p. 398, 2006.

[94] E. Şennik, Z. Colak, N. Kılınç, and Z. Z. Öztürk, "Synthesis of highly-ordered tio 2 nanotubes for a hydrogen sensor," *International Journal of Hydrogen Energy*, vol. 35, no. 9, pp. 4420–4427, 2010.

[95] H. F. Lu, F. Li, G. Liu, Z.-G. Chen, D.-W. Wang, H.-T. Fang, G. Q. Lu, Z. H. Jiang, and H.-M. Cheng, "Amorphous tio2 nanotube arrays for low-temperature oxygen sensors," *Nanotechnology*, vol. 19, no. 40, p. 405504, 2008.

[96] S. Lin, D. Li, J. Wu, X. Li, and S. Akbar, "A selective room temperature formaldehyde gas sensor using tio 2 nanotube arrays," *Sensors and Actuators B: Chemical*, vol. 156, no. 2, pp. 505–509, 2011.

[97] C.-H. Han, D.-W. Hong, I.-J. Kim, J. Gwak, S.-D. Han, and K. C. Singh, "Synthesis of pd or pt/titanate nanotube and its application to catalytic type hydrogen gas sensor," *Sensors and Actuators B: Chemical*, vol. 128, no. 1, pp. 320–325, 2007.

[98] S. Banerjee, S. K. Mohapatra, M. Misra, and I. B. Mishra, "The detection of improvised nonmilitary peroxide based explosives using a titania nanotube array sensor," *Nanotechnology*, vol. 20, no. 7, p. 075502, 2009.

[99] R. S. Ray, B. Sarma, S. Mohanty, and M. Misra, "Theoretical and experimental study of sensing triacetone triperoxide (tatp) explosive through nanostructured tio 2 substrate," *Talanta*, vol. 118, pp. 304–311, 2014.

[100] Q. Wang, Y. Pan, S. Huang, S. Ren, P. Li, and J. Li, "Resistive and capacitive response of nitrogen-doped tio2 nanotubes film humidity sensor," *Nanotechnology*, vol. 22, no. 2, p. 025501, 2011.

[101] A. Liu, M. Wei, I. Honma, and H. Zhou, "Direct electrochemistry of myoglobin in titanate nanotubes film," *Analytical chemistry*, vol. 77, no. 24, pp. 8068–8074, 2005.

[102] C. Guo, F. Hu, C. M. Li, and P. K. Shen, "Direct electrochemistry of hemoglobin on carbonized titania nanotubes and its application in a sensitive reagentless hydrogen peroxide biosensor," *Biosensors and Bioelectronics*, vol. 24, no. 4, pp. 819–824, 2008.

[103] G. Zhao, Y. Lei, Y. Zhang, H. Li, and M. Liu, "Growth and favorable bioelectrocatalysis of multishaped nanocrystal au in vertically aligned tio2 nanotubes for hemoprotein," *The Journal of Physical Chemistry C*, vol. 112, no. 38, pp. 14 786–14 795, 2008.

[104] P. Benvenuto, A. Kafi, and A. Chen, "High performance glucose biosensor based on the immobilization of glucose oxidase onto modified titania nanotube arrays," *Journal of Electroanalytical Chemistry*, vol. 627, no. 1, pp. 76–81, 2009.

[105] S. Mahshid, C. Li, S. S. Mahshid, M. Askari, A. Dolati, L. Yang, S. Luo, and Q. Cai, "Sensitive determination of dopamine in the presence of uric acid and ascorbic acid using tio2 nanotubes modified with pd, pt and au nanoparticles," *Analyst*, vol. 136, no. 11, pp. 2322–2329, 2011.

[106] S. Wang, H. Sun, H.-M. Ang, and M. Tadé, "Adsorptive remediation of environmental pollutants using novel graphene-based nanomaterials," *Chemical Engineering Journal*, vol. 226, pp. 336–347, 2013.

[107] M. M. Khin, A. S. Nair, V. J. Babu, R. Murugan, and S. Ramakrishna, "A review on nanomaterials for environmental remediation," *Energy & Environmental Science*, vol. 5, no. 8, pp. 8075–8109, 2012.

CHAPTER 2

APPLICATIONS OF MICROFLUIDICS FOR MOLECULAR DIAGNOSTICS

©2013 Springer Science+Business Media, LLC. Reprinted, with permission, from Springer. This was published in Microfluidic Diagnostics, Methods in Molecular Biology, Volume 949, 2013, pp 305-334, DOI:10.1007/978-1-62703-134-9_20. Authors are Harikrishnan Jayamohan, Himanshu J. Sant, and Bruce K. Gale.

Chapter 20

Applications of Microfluidics for Molecular Diagnostics

Harikrishnan Jayamohan, Himanshu J. Sant, and Bruce K. Gale

Abstract

Diagnostic assays implemented in microfluidic devices have developed rapidly over the past decade and are expected to become commonplace in the next few years. Hundreds of microfluidics-based approaches towards clinical diagnostics and pathogen detection have been reported with a general theme of rapid and customizable assays that are potentially cost-effective. This chapter reviews microfluidics in molecular diagnostics based on application areas with a concise review of microfluidics in general. Basic principles of microfabrication are briefly reviewed and the transition to polymer fabricated devices is discussed. Most current microfluidic diagnostic devices are designed to target a single disease, such as a given cancer or a variety of pathogens, and there will likely be a large market for these focused devices; however, the future of molecular diagnostics lies in highly multiplexed microfluidic devices that can screen for potentially hundreds of diseases simultaneously.

Key words: Microfluidics, Micro-total-analysis-systems, Lab-on-a-chip, Point-of-care devices, Sample preparation, MEMS, Rapid prototyping, Biomarker detection, Personalized medicine, Global health care

1. Introduction

The role of molecular diagnostics is critical in today's global health care environment. In the developing world, 95% of deaths are due to a lack of proper diagnostics and the associated follow-on treatment of infectious diseases; i.e., acute respiratory infections (ARIs), malaria, HIV, and tuberculosis (TB) (1). Recent pandemics like the 2009 H1N1 Influenza A pandemic, have accentuated the need for tools to effectively detect and control infectious diseases. Factors like "rapid pathogen mutation rates, transformation of nonhuman pathogens into human pathogens, and recombination of nonhuman pathogen with human pathogens" have added to the challenge of managing novel infectious diseases (2). Increased global

Gareth Jenkins and Colin D. Mansfield (eds.), *Microfluidic Diagnostics: Methods and Protocols*, Methods in Molecular Biology, vol. 949, DOI 10.1007/978-1-62703-134-9_20, © Springer Science+Business Media, LLC 2013

mobility has aided the rapid spread of infectious diseases from region of origin to other parts of the world as seen during the 2009 H1N1 pandemic. This mobility has highlighted the need for rapid, portable diagnostic (point-of-care [POC]) devices at ports of entry to prevent global spread of infections. Current laboratory culture methods for pathogens take a day or more to provide results (2). Clearly, methods need to be developed to aid rapid and site-relevant diagnosis of disease.

For certain other types of infections, in both the developed and developing worlds, the diagnostic tests need to be repeated periodically to measure response to therapy and monitor the disease condition. One such case is monitoring the viral load (number of viral particles per milliliter of blood) for infections like HIV (Human immunodeficiency virus) and hepatitis C. Sub-Saharan Africa is a region heavily affected by the AIDS pandemic. The lack of standard laboratory facilities and trained laboratory technicians in these regions is a serious bottleneck (3). Similar problems exist in medically underserved areas of the USA. A simple POC platform could enable increased access to treatment for patients in such low-resource settings.

In the developed world, the strategy to deal with major disease burdens such as cancer is shifting from a therapeutic to diagnostic mode (4), as the cost of treating disease falls dramatically if it is found early. Ischemic heart diseases and cerebrovascular diseases, which are the major causes of mortality in the developed world, can be targeted by effective diagnostics (1). With projected US healthcare costs of $4.4 trillion by 2018, expanding conventional expensive diagnostic solutions is not a viable option (5). Rapid, low-cost diagnostic tools that can be dispersed throughout a community for easy access, possibly even in the home, would provide substantial benefit by allowing more rapid diagnosis and monitoring of disease and infection.

Homeland security is another key sector where portable molecular biology tools are needed to detect a variety of biological agents (6). The US Departments of Health and Human Services (HHS) and Agriculture (USDA) maintains a list of biological agents and toxins defined as select agents "that have the potential to pose a severe threat to public, animal or plant health, or to animal or plant products" (7). Again, there is a need for rapid, inexpensive detection, identification, and quantification of pathogens to help reduce this threat.

Hence, there is an unmet need for simple, low-cost/cost-effective, accurate, portable/point-of-care diagnostic tools for rapid identification of disease markers and pathogens in a variety of settings. The FDA (Food & Drug Administration), definition of a "simple test" provides a benchmark for features for an ideal diagnostic tool (Table 1, (1, 8)).

Table 1
Features of the ideal diagnostic tool based on FDA's definition of a "simple test"

Is a fully automated instrument or a unitized or self-contained test
Uses direct unprocessed specimens, such as capillary blood (fingerstick), venous whole blood, nasal swabs, throat swabs, or urine
Needs no operator intervention during the analysis steps
Needs no electronic or mechanical maintenance beyond simple tasks, e.g., changing a battery or power cord
Produces results that require no operator calibration, interpretation, or calculations
Produces results that are easy to determine, such as "positive" or "negative," a direct readout of numerical values, the clear presence or absence of a line, or obvious color gradations
Has test performance comparable to a traceable reference method, as demonstrated by studies in which intended operators perform the test? (Intended operator refers to a test operator with limited or no training or hands-on experience in conducting laboratory testing)
Contains a quick reference instruction sheet that is written at no higher than a seventh grade reading level

There is consensus that for such an ideal diagnostic tool, microfluidics will certainly be required and will likely make up the critical components of the device (9). Microfluidics can be defined as "science and technology of systems that process or manipulate small (10^{-9} to 10^{-18} liters) amounts of fluids, using channels with dimensions of tens to hundreds of micrometers" (10). Lab-on-a-chip (LOC) refers to the application of microfluidics in chemical, biological analysis and diagnostics. The ultimate objective of LOC devices is to integrate the entire gamut of laboratory capabilities on a microfluidic chip (11–13).

Some of the features of microfluidics that make the technology attractive for lab-on-a-chip point-of-care applications are:

- The availability of fabrication methods to manufacture small hand-held devices on a large scale at a lower cost.
- The ability to manipulate small volumes of sample, requiring lower amounts of reagents.
- The ability to analyze small volumes for applications like single-cell analysis, multiplexed analysis, or forensic trace analysis (14).
- Smaller length scales result in faster analyses and higher separation efficiencies, reducing response times. The high speed analysis also makes microfluidics a suitable candidate for high-throughput applications.

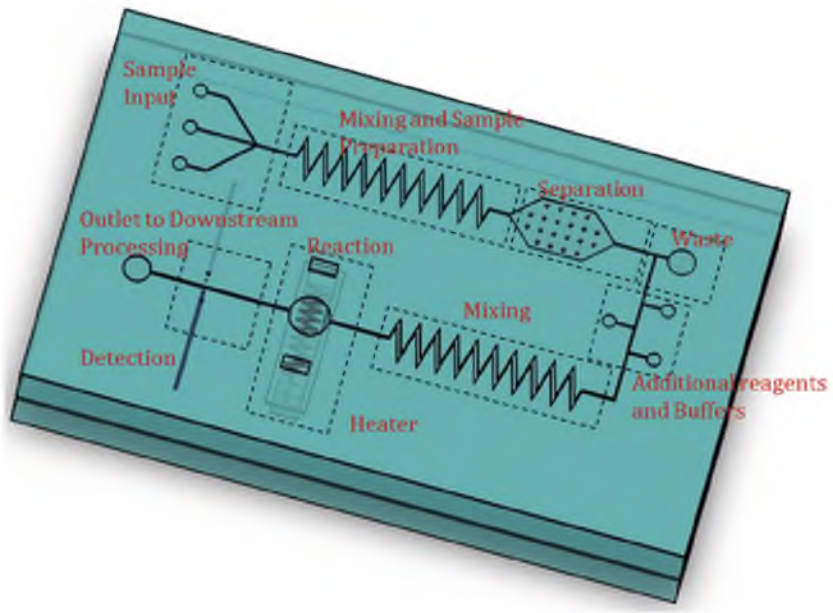

Fig. 1. A schematic diagram of a conceptual lab-on-a-chip device designed to perform a variety of unit operations and unit processing steps including: sample preparation (e.g., fluid handling, , derivatization, lysis of cells, concentration, extraction, and amplification), sample separation (e.g., electrophoresis, liquid chromatography, molecular exclusion, field-flow fractionation), and detection (e.g., fluorescence, UV/Vis absorption, amperometric, conductivity, Raman, electrochemical).

- Straightforward integration of multiple components/functionalities (sample preparation, detection, data processing) on a single device.
- Potentially fully automated and simple to use, enabling use by laypeople.
- Portability and a small footprint should allow field and clinic use, as well as possibly allowing more widespread diagnostics. Pervasive diagnostics should greatly increase the likelihood of personalized medicine having a significant impact on society.
- Highly parallel analyses will allow multiple tests to be run simultaneously, either on the same sample or multiple samples. Microfluidic devices can in principle be used to obtain parameters like proteomic, metabolomic, and genetic data of each individual for personalized care (15).

Figure 1 provides a basic generalized schematic of a microfluidic LOC device with sample-in/readout capabilities. The figure shows some of the various technologies that might be involved in sample preparation, analysis or separation, and detection. Figure 2 is an example of a real nucleotide analysis system developed at the State of Utah Center of Excellence for Biomedical Microfluidics.

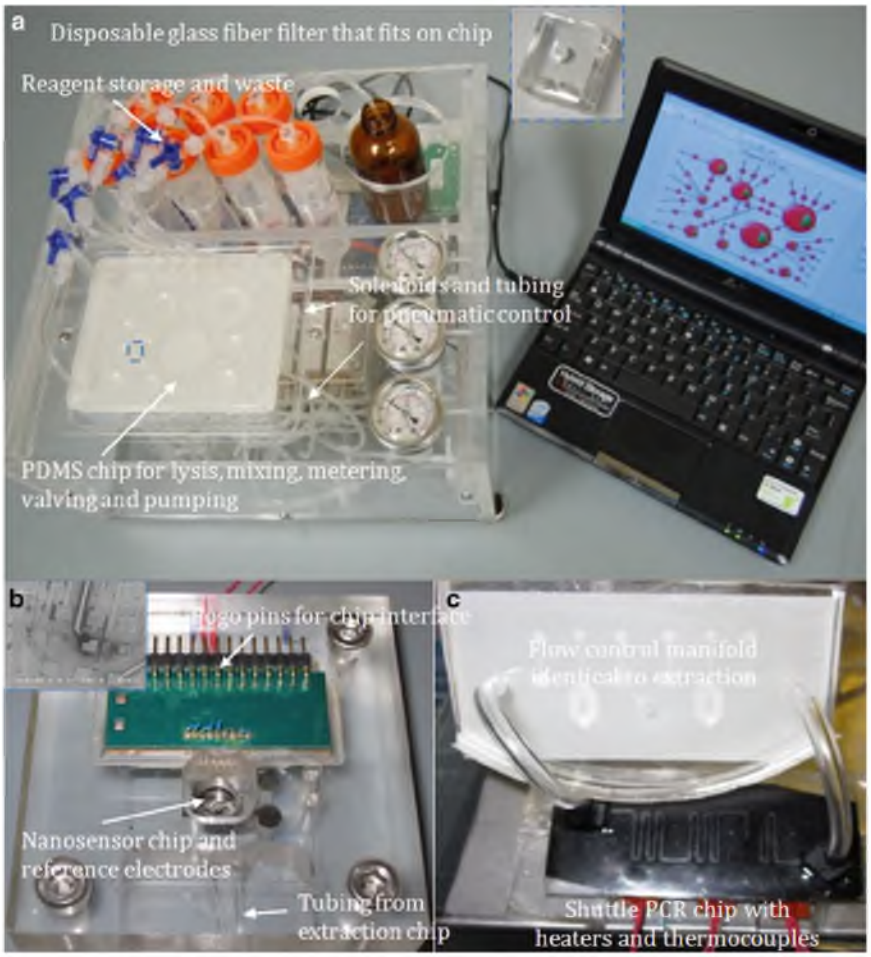

Fig. 2. (**a**) Prototype of an automated nucleotide extraction platform. The microfluidic system consists of five different components: (i) a disposable microfluidic cartridge containing a glass fiber filter (inset figure); (ii) a PDMS-microfluidic chip for flow control; (iii) microfluidic chambers for mixing, metering, pumping, and reactions; (iv) a pneumatic micropump to deliver the eluted sample to downstream assays; and (v) a vacuum pump to control the on-chip valves. The extraction chip also has provision for thermal lysis and reverse transcription (not shown). (**b**) Prototype of a test socket for characterization of a carbon nanotube-based electrochemical nanosensor array. The test socket provides both fluidic and electrical interface to the nanosensor chip (inset figure) that detects nucleotide hybridization. (**c**) Prototype of a shuttle PCR chip with three temperature zones and which is fabricated using polycarbonate lamination. The heaters and thermocouples are shown with a manifold for on-chip fluidic control. The fluidic interface for the extraction system is designed so that it can be readily connected to the downstream assays such as hybridization and PCR.

2. Early Development of Microfluidics

Microfluidic devices have been steadily developing over the past 30 years, but most of the progress related to diagnostic applications has been made in about the past 15 years (10, 16). A major driver for microfluidic development was the focus on genomics and

molecular biology in the 1980s especially on microanalysis techniques like high-throughput DNA sequencing. The initial microfluidic devices were inspired by the microelectronics industry and relied on photolithography and MEMS fabrication techniques. Hence, most of the earliest microfluidic devices were fabricated in silicon and glass.

The origins of microfluidics as used in diagnostic and molecular biology applications can be traced to microanalytical tools like gas-phase chromatography (GPC), high-pressure liquid chromatography (HPLC), and capillary electrophoresis (CE) developed in the mid-1990s (16). Rapid progress was made on these tools at this time and many of the developed concepts are still in use today. A summary of some of the best examples follow: Jacobson et al. reported separation of complexed metal ions in polyacrylamide-modified channels (17) using electrophoresis. Micellar electrokinetic capillary chromatography (MECC) separation of biological samples (18) and neutral dyes (19) were reported. Wooley et al. reported ultra-high-speed DNA sequencing and separation using microfabricated capillary electrophoresis chips (20). Surface passivation of silicon-based PCR chips to obtain amplifications comparable to conventional PCR systems was accomplished (21). Koutny et al. reported a competitive immunoassay for separation and quantification of free and bound labeled antigens by capillary electrophoresis (CE) (22). Hadd et al. presented an automated enzyme assay in which nanoliter volumes of substrate, enzyme, and inhibitor were mixed using electrokinetic flow (23). Microchip-based capillary electrophoresis (CE) for separation and relative quantitation of human serum proteins was achieved (24). Some of the other separation methods like free-flow electrophoresis (FFE) (25), capillary gel electrophoresis (26) and capillary array electrophoresis (CAE) (27) were reported. These devices were primarily fabricated in silicon and glass and lead to the work on related components like micropumps, microvalves and sensors.

There are a few examples of plastic devices before 2000. Delamarche et al. used elastomeric microfluidic networks to pattern immunoglobulin with high resolution on a variety of substrates (gold, glass, polystyrene) (28). Freaney et al. developed a prototype miniaturized chemical analysis system comprising biosensors and a microdialysis interface for on-line monitoring of glucose and lactate in blood (29).

In the 1990s, to counter the threat of biological and chemical weapons, the US Defense Advanced Research Projects Agency (DARPA) supported development of "field-deployable microfluidic" devices and was a driver for academic research in microfluidics (10). The first lab-on-a-chip emerged with the concept of a "miniaturized total analysis system" or μTAS, involving a silicon chip analyzer with sampling, sample pretreatment, separation, and detection functionalities embedded on an integrated system (30).

Electroosmotic pumping was the primary actuation mode used in these early μTAS systems especially since separation was one of the objectives and pumping could be controlled using simple electronics and no moving parts (31). Seiler et al. reported amino-acid separation on chip and their detection using laser-induced fluorescence (32). Other applications involving biomolecules and cells emerged during the period. These include flow cytometry (33), DNA amplification (PCR) (34) and cellular metabolism studies (35) on a microfabricated chip.

A host of innovations in microfluidic devices came forth in the period from 1994 to 1997. These include, "reactor chambers for continuous precolumn and postcolumn labeling reactions" (36, 37), high speed efficient separations (38), on-chip static mixing (39), separation of oligonucleotides (40), DNA (41), and amino acids (42), and cell manipulation by electrical fields (43). There was also work on separation modes like synchronized cyclic capillary electrophoresis (44) and free flow electrophoresis (FFE) (45). Verpoorte et al. devised a 3D microflow manifold system incorporating electrochemical and optical detection systems (46). Seiler et al. studied current and electroosmotic fluid flows in microchannels using Kirchhoff's law (47). Jacobson et al. developed glass microchips with octadecylsilane surface modified channels as a stationary phase for open channel chromatography (48). Feustel et al. came up with a miniaturized mass spectrometer incorporating an integrated plasma chamber for electron generation, an ionization chamber, and an array of electrodes acting as the mass separator (49). All of these systems would find their way into later diagnostic microfluidic devices.

The introduction of polymer-based soft lithography offered a cheaper alternative to silicon and glass in microfluidic device fabrication (50). Most of the exploratory research in microfluidics is currently performed on polymer-based devices primarily made of poly(dimethylsiloxane) (PDMS), a soft elastomer (10). Soft lithography techniques for microfluidic devices have been reviewed multiple times along with many of the structures and devices than can be produced (51, 52). Related polymer-based methods like microcontact printing and microtransfer molding enabled rapid fabrication of micrometer scale structures (53). Three dimensional structures were reported using a layer-by-layer structuring using microtransfer molding (54).

Other plastics, hybrid materials, and packaging techniques were soon developed, including a variety of low cost plastic prototyping and manufacturing methods for microfluidics (55, 56). Martynova et al. reported microfluidic devices fabricated in Poly-(methyl methacrylate) (PMMA) by imprinting them with an inverse three-dimensional image of the device micromachined on silicon (57). Wang et al. developed a low temperature bonding process using a sodium silicate layer as an adhesive for glass

microfluidic devices. Microfluidic interconnects for connecting vertically stacked micromachined channels and to external tubing on the same plane was demonstrated by Gonzalez and co-workers (58).

Additional landmark work included Johnson et al. fabricating nanometer wide channels on silicon, SiO_2, and gold substrates by exposing them to a metastable argon atom beam in the presence of dilute vapors of trimethylpentaphenyltrisiloxane (59). Lorenz et al. reported the characterization of SU-8 negative photoresist for the fabrication of high aspect-ratio structures (60). Larsson et al. fabricated 3D microstructures by conventional CD-injection molding against a silicon master produced by wet and deep reactive ion etching (DRIE) (61). Silicon micromachining methods based on DRIE, silicon fusion bonding (SFB) (62), and electron cyclotron resonance (ECR) source were reported (63). Dozens of other techniques have also been reported, but cannot all be reviewed here.

3. Modern Microfluidics Fabrication

Microfluidics was inspired by the microelectronics industry and hence most of the initial devices were fabricated in silicon using photolithography and related technologies. The success of the microelectronics and MEMS industries in manufacturing thousands of miniaturized components in parallel at very low costs was thought to be applicable to microfluidics. While this may eventually prove to be true, low cost microfluidic devices made using photolithographic techniques have proven to be the exception rather than the rule, since the numbers of identical microfluidic chips manufactured for current and foreseeable markets tend to be more in the 10,000 s –100,000 s, where batch processing does not provide sufficient cost savings. Packaging and other post processing steps like reagent introduction have also proven challenging and expensive, and consequently other manufacturing methods currently appear to be more in favor. Thus, while most of the earliest work in microfluidics was in silicon, the majority of current devices are now made in glass or a variety of plastics. Nonetheless, silicon and glass manufacturing technique are important in microfluidics, because molds for rapid and inexpensive manufacturing of plastic devices are still often made of silicon or glass.

Standard silicon and glass manufacturing techniques are based on microlithography, subtractive techniques (etching), and additive techniques (64). Microlithography involves the use of an energy beam to transfer a geometric pattern to a substrate. Depending on the type of energy beam used, these can be divided into: photolithography, electron beam lithography, X-ray lithography, and ion lithography. Photolithography involves using light to transfer a geometric pattern from a photo mask to a light sensitive chemical

called photoresist. This is followed by a development process using a developer solution to create a positive or negative image of pattern onto the photoresist. Other techniques like X-ray lithography, extreme ultraviolet (UV) lithography, ion particle lithography, scanning probe lithography, and nanoimprint lithography are being increasingly used due to their capability in producing sub-100 nm structures. Of these, nanoimprint lithography, a type of embossing, is a low cost, high throughput and high resolution method that has the potential to be used for low-cost mass manufacture of micro and nanofluidic devices in a variety of materials, but especially for direct embossing of plastics (65).

Subtractive techniques involve dry and wet etching, which are primarily used with glass and silicon devices. Wet etching involves chemical removal of layers from a material and is typically used to etch silicon, silicon dioxide, silicon nitride, metals, and glass. Dry etching refers to the removal of material by bombarding it with ions. Sputtering, ion beam milling and plasma etching (reactive ion etching and deep reactive ion etching) are some of other methods used in silicon etching.

Additive technologies involve techniques to deposit films. Methods to deposit thin films include: thermal oxidation of silicon, chemical vapor deposition (CVD), and physical vapor deposition (PVD). Methods to deposit thick films usually involve a spinning or electroplating technique. These thick films are often patterned using photolithography and then used as molds for microfluidic devices. The reader can refer to the text by Madou (64) for an in-depth description of the techniques described above, as well as a description of other micromanufacturing techniques.

In the past decade, silicon and glass have been largely displaced by plastics as the ideal substrate for microfluidic devices (10). Six primary considerations have been behind this transition. First, silicon is relatively expensive compared to plastics because microfluidics tends to take up larger areas than microelectronic chips (and silicon costs are measured by area). Second, the electronic advantages of silicon are not typically required in microfluidic devices. Third, silicon is not transparent, so troubleshooting microfluidic devices during development can be difficult and optical detection techniques cannot be employed. Fourth, silicon processing typically requires processes found in expensive cleanrooms that are also relatively slow. The development of rapid and inexpensive polymer processing methods has proven compelling. Fifth, silicon is relatively brittle and is not ideal for devices that experience significant "handling." Sixth, silicon is incompatible with the strong potentials used in electrokinetic pumping and capillary electrophoresis (CE). Silicon does have some advantages, such as well controlled surface properties, but these have not proven sufficient to drive microfluidic development.

Polymers, due to their lower cost, ease of fabrication and physical properties, are now the primary materials used in microfluidic research. Many microfluidic components, such as pumps and valves, work better when fabricated in the less rigid polymer medium as compared with silicon. The permeability of polymer to gases make it suitable for work with living mammalian cells. PDMS, an optically transparent, soft elastomer has been used for various microfluidic devices since its introduction (10). Most polymer devices are made using a molding, embossing, or casting techniques, although direct processing means, such as laser-based or knife-based manufacturing is increasing (56). Soft lithography is the technique of replicating structures from a master mold or stamp onto an elastomeric (PDMS) substrate. Fabrication using PDMS is simple and does not require expensive facilities, and prototyping can often be done in less than a day. The reader can refer to in-depth reviews of soft lithography for detailed insight into the method (51, 52). Interestingly, not many commercial products use devices fabricated in PDMS due to a gap between academic and industrial practices, although this is starting to change (66). In addition, PDMS has limited application due to its hydrophobic surface and tendency to swell in organic solvents (67). Although polymers are the preferred material for most microfluidic applications today, silicon and glass are still relied upon for building specialized devices that need chemical and thermal stability (68). In the nascent field of nanofluidics, silicon and glass are used due to their mechanical stability (10). Some of other methods that are used in microfluidic fabrication are xerography (69), laser micromachining (70) and polymer stereolithography (71).

An innovative method for creating low cost disposable microfluidic diagnostic devices (paper-based analytical devices [μPADs]) was introduced by Martinez et al. (72, 73). The fluid movement is controlled primarily by evaporation and capillary forces. Although the technology is very promising, more work needs to be done to bring forth real world μPAD applications. Recently, microfluidic devices fabricated on engineered plastics, such as cyclo-olefin copolymers (COC) (74), and photocurable perfluoropolyether (PFPE) (65) have been reported.

4. Microfluidic Diagnostics in the Past Decade

A major boom in microfluidics research has occurred in the last 10–12 years as is reflected by the number of published journal papers using the term: 26 papers were published before 1990, 341 in the 1990s, 15773 in the 2000s and 3,322 in the first 2 years of this decade. While the number of papers each year appears to be leveling off, the impact of microfluidics is likely to continue to

grow. Another consequence of this large body of literature is that it becomes infeasible to cover all the important papers and developments in a chapter such as this. As most reviews on microfluidics for diagnostic applications have focused on the physical methods behind the device operation and not as much on the applications, this work will focus on some specific diagnostic developments and application areas. We examine the microfluidic applications in diagnostics for diabetes, cardiac related conditions, and infections related to bacteria, virus, and HIV. We also review the applications in pharmacogenomics and devices for low resource settings. We discuss some of the methods used in fabricating these microfluidic devices and the challenges in mass production. Included is a section on some of the commercial diagnostic products using microfluidic technology. The reader may refer to supplemental reviews for the theory behind microfluidics (10, 75–78) and methods used in microfluidic LOC detection (14, 67, 79).

5. A Global Health Perspective

There is an increasing need in the developing and developed world for new cost-effective diagnostic technologies, albeit for different reasons. In developed countries, health care costs are rising rapidly, and containment is an issue. In developing countries, delivery of medical services to remote and resource poor areas is difficult and the needs are enormous, as infectious disease is a critical barrier to economic and social development. Interestingly, the two problems tend to converge towards one solution: microfluidic diagnostic devices. The Grand Challenges in Global Health (GCGH) initiative, a major effort to achieve scientific breakthroughs against infectious diseases that cause significant problems in the developing world, has identified seven long-term goals in global health (80), most of which revolve around eliminating infectious disease.

Infectious diseases constitute a huge burden in developing countries (32.1%) using disability-adjusted life year (DALY) metrics compared to developed countries (3.7%) and account for 50% of infant deaths (1, 81). The major concerns in terms of DALY are infections due to viruses (HIV/AIDS, measles, hepatitis B, hepatitis C, and viral gastroenteritis [rotavirus]); bacteria (cholera, tuberculosis, pertussis, tetanus, and meningitis); and parasites (malaria, Lymphatic filariasis, leishmaniasis, and trypanosomiasis). The three most devastating diseases are malaria, tuberculosis, and HIV. In 2009, there was an estimated 169–294 million cases of malaria worldwide, resulting in about 781,000 deaths. Of these 85% of deaths were in children under 5 years of age [82]. There was an estimated 14 million people infected with TB and about 1.7 million related deaths in 2009. TB is a major cause of deaths in

HIV infected patients with about 380,000 of the 1.7 million deaths being reported in people with HIV (83). An estimated 33.3 million people are living with HIV worldwide of which about 67.5% live in sub-Saharan Africa (84). There has been an estimated 1.8 million AIDS related deaths, 73% of those being in sub-Saharan Africa. Thus, early infectious disease detection and management is a high priority in low-resource settings and a major driver of microfluidic diagnostic devices. Infectious diseases are not limited to developing countries. Recent outbreaks like H1N1 influenza A demonstrate the rapid spread of infectious diseases from a country of origin to the rest of the world. In April 2009, USA and Mexico reported 38 cases of H1N1 influenza. By June 2009 when World Health Organization declared a pandemic, there were a reported 28,774 cases and 144 deaths in 74 countries. The H1N1 influenza pandemic had a total of 43,677 reported cases in the USA as of July 2010 (85). Estimates of unreported cases are a much higher figure at 1.8–5.7 million cases (86).

In contrast, chronic diseases that require consistent monitoring are the major disease burden for high-income countries. These diseases include: ischemic heart disease, cerebrovascular disease, cancers, and diabetes mellitus. Global mortality and disease burden projections suggest that these chronic conditions common to high-income countries will also become a priority for low-income countries by the year 2030 (1). Thus, the driver for microfluidic diagnostics in developed countries is the need for consistent, accurate, and affordable diagnostics for chronic disease.

6. Microfluidics in Diagnostics

6.1. Bacterial Detection

Bacterial detection is a key need in areas including: clinical diagnostics, monitoring of food-borne pathogens, and detection of biological threat agents. Harmful bacteria are the source of diseases like gastroenteritis and cholera. From a bioterrorism perspective, pathogenic bacteria pose serious risk. Under favorable temperature and in the presence of moisture and nutrition, bacteria spread rapidly. For a list of bacterial diseases and corresponding causative agents the reader can refer to a review by Ivnitski et al. (87).

Conventional methods to detect and identify bacteria require growing a small number of bacteria into colonies of higher numbers. Hence conventional methods take 18–24 h at a minimum (87). Also, conventional methods require complex equipment, highly trained technicians, and cannot be field deployable or used in point-of-care settings.

There are primarily two modes of pathogen detection: immunosensing and nucleic acid-based detection. In immunosensing, a binding interaction between probing antibodies and antigens of

target cells (analyte) is detected. A variety of mechanisms can be used to detect this interaction, such as: optical, electrical or electrochemical impedance, cantilever, quartz crystalline microbalance, surface plasmon resonance (SPR), and magnetoresistivity. Nucleic acid-based sensors detect DNA or RNA targets from the analyte organisms (88, 89). The polymerase chain reaction (PCR) or reverse transcription PCR (RT-PCR) is used to amplify the nucleic acids to enhance the detection signal (90).

Optical detection methods are often preferred due to their high selectivity and sensitivity (91, 92). A variety of microfluidic devices have been developed for bacteria using optical means. A microfluidic system for detection of Escherichia coli using laser-optical fiber fluorescence detection was reported by Xiang et al. They reported detection limits an order of magnitude higher than that achieved for conventional fluorescence microscope (93). Gao et al. developed a multiplexed microfluidic device for the fluorescence detection of bacterial antibodies in human serum. TRITC-labeled detection antibodies were captured by antigens pre-patterned on the microchannels (94). An integrated microfluidic platform for fluorescence-based detection of Shiga toxin I (*Shigella dysenteriae*) and Staphylococcal enterotoxin B (*Staphylococcus aureus*) was developed by Meagher et al. (95).

Electrical and electrochemical modes of bacterial detection have also been widely reported. The primary advantage of the method is the ease of fabricating microelectrodes in the microchannel by lithography and the absence of labeling steps (96). A microfluidic sensor based on impedance measurement of *E. coli* was constructed by Boehm et al. (97). The selectivity of the sensor to different bacterial strains was demonstrated by positive identification of E. coli in a suspension of E. *coli* and M. *catarrhalis*. A microfabricated electrochemical sensor array for detection of bacterial pathogens in human clinical fluid samples was demonstrated. The device consisting of a set of 16 sensors was able to detect relevant bacterial urinary pathogens (*E. coli*, *Proteus mirabilis, Pseudomonas aeruginosa, Enterococcus spp.,* and Klebsiella–Enterobacter group) and could in principle be used as a point-of-care device for rapid diagnosis of urinary tract infections (98). Table 2 lists a number of detection methods for bacterial diagnostics and, for a comprehensive list of electrical and electrochemical bacterial detection, the reader can refer to a review by Jinseok et al. (96).

Microfluidic devices have also been applied to the detection of parasites. A "microfluidic flow-through membrane immunoassay with on-card dry reagent storage" was developed by Stevens et al. for the detection of *Plasmodium falciparum* (99).

6.2. Viral Detection and Disease Management

As noted earlier in this chapter, effective virus detection and disease management is critical in public health, the biotechnology industry, and biodefense. Some of the most deadly historical epidemics

Table 2
Detection methods of POC devices for bacterial diagnostics

Analyte	Detection method	Material	Limit of detection	Reference
Escherichia coli O157:H7	Fluorescence	PDMS	0.3 ng/μL	(76)
Escherichia coli O157:H7	Fluorescence	PDMS	0.02 μg/mL	(77)
Helicobacter pylori	Fluorescence	PDMS	0.1 μg/mL	(77)
Shiga toxin I	Fluorescence	Glass	500 pM	(78)
Staphylococcal enterotoxin B	Fluorescence	Glass	300 pM	(78)
Escherichia coli	Electrical (impedance)	Silicon	10^4 CFU/mL	(80)
Escherichia coli, *Proteus mirabilis*, *Pseudomonas aeruginosa*, Enterococcoccus spp., and the Klebsiella–Enterobacter group	Electrochemical (amperometric)	Au on plastic	Not specified	(81)
Plasmodium falciparum	Optical	Mylar/PMMA	10 ng/mL	(98)

like smallpox, yellow fever, and Spanish flu were due to viral agents. In the twenty-first century, HIV, rotavirus, and measles are found to be among the leading contributors to global disease burden (100). Many deadly viruses such as Variola virus (small pox), Rift Valley fever virus, and Venezuelan Equine Encephalomyelitis virus have been known to be developed as potential biological agents (101). POC devices to detect these bio-agents are extremely critical for global biosecurity. The small size, simple biology, and lack of reproductive ability outside the host cell add to the complexity in detecting viruses.

The primary methods for virus detection are serology, viral antigen detection, and nucleic acid detection. Serologic tests detect the presence of antibodies that the immune system produces in response to viral infection. Viral antigen detection typically relies on immunoassays as described previously. Nucleic acid detection involves amplification of the viral genome using PCR and the subsequent detection of the amplified genome.

6.3. HIV Detection and Monitoring

HIV is one of the primary targets of microfluidic diagnostic research efforts. Conventional HIV diagnostic assays are based on an enzyme assay (EIA/ELISA) followed by western blot and requires trained laboratory personnel. Universal access to HIV diagnostics is stymied by the lack of trained technicians, patient motivation, and laboratory access especially in rural areas and the developing world. For instance, about 83% of HIV patients remain undiagnosed in Kenya (102). Thus, a simple, inexpensive diagnostic tool for HIV would be readily welcomed.

The number of $CD4^+$ T-lymphocytes per microliter of HIV-infected blood is a critical monitor of disease state and this measurement is needed to make informed antiretroviral therapy (ART) treatment decisions. Therefore, the primary mechanisms for HIV detection in POC microfluidic devices are enumeration of $CD4^+$ T-lymphocytes and HIV viral load quantification. To be successful, the POC device needs to detect around 200 $CD4^+$ cells/μL and 400 copies/mL of HIV from whole blood (103). Towards this goal, Sia et al. reported a microfluidic immunoassay, "POCKET (portable and cost-effective)" for quantifying anti-HIV-1 antibodies in the sera of HIV-1 infected patients. The device consisted of a PDMS slab with microchannels placed orthogonally to a polystyrene stripe patterned with HIV-enveloped antigen. The HIV-1 infected patient serum sample is flowed through the microchannels to quantify anti-HIV-1 antibodies. Although the device was able to identify the sera of HIV-1-infected patients from those of non-infected patients, it could not make a correlation of the output data with HIV disease states (103). Lee et al. developed a RT-PCR-based POC diagnostic chip for HIV. The chip relies on HIV markers p24 (a major core protein encoded by the HIV gag gene) and gp120 (an external envelope protein encoded by envelope gene) for diagnostic purposes (104). Cheng et al. reported a POC microfluidic $CD4^+$ T-cell counting device. The device works in two stages, initial depletion of monocytes from whole blood and subsequent $CD4^+$ T cell capture. The strategy of contaminant (monocytes) depletion prior to $CD4^+$ T cell isolation enhances the performance in low CD4 count (200 cells/μL) scenarios (105). Other label-free $CD4^+$ T-lymphocyte capture techniques have been reported. Although the microfluidic devices themselves are disposable and usually cheap, they still require expensive optical microscopes to count the captured $CD4^+$ T-cells (106, 107). A lensless portable CCD-based microfluidic platform developed by Demirci et al. overcomes this limitation. The captured label-free $CD4^+$ T-lymphocytes are detected by a charge coupled device (CCD) sensor using lensless shadow imaging techniques and counted using automatic cell counting software in a few seconds (108). Cheng et al. developed a non-optical method of counting CD^+ T-cells. The cell count is enumerated by measuring the changes in conductivity of the surrounding medium due to ions released from the surface-immobilized cells within a microfluidic channel (109). Gohring et al. demonstrated the detection of $CD4^+$ and $CD8^+$ T-Lymphocyte whole cells and $CD4^+$ T-Lymphocyte cell lysis using an optofluidic ring resonator (OFRR) sensor. This sensor measures the presence of T cells based on a change in refractive index in the microfluidic channel due to the presence of immobilized T cells (110). Wang et al. reported a microfluidic chip with an integrated micromixer for fluorescent labeling of $CD4^+/CD8^+$ T-cells and their subsequent counting using a microflow cytometer (111).

6.4. Diagnostics for Other Viral Agents

Microfluidic diagnostics have been designed for other viral agent infections like influenza, severe acute respiratory syndrome (SARS) and dengue fever. These diseases have been of serious concern to global public health organizations especially in the last few years.

The influenza virus causes respiratory tract infection and is found to be severely morbid in children and the elderly (112). The challenge with diseases like influenza is that there is a large variety of the viruses and they are constantly changing. For example, the influenza A virus can subdivided into H1N1 and H1N3 based on the glycoproteins (hemagglutinin and neuraminidase) present in the viral envelope. The 2009 influenza pandemic was caused by a novel H1N1 strain with genes from five different flu viruses (113). Thus, the diagnosis of influenza alone is not sufficient; discovery of the type of influenza is also critical.

Some of the conventional diagnostic methods for influenza virus are enzyme-linked immunosorbent assays (ELISA), immunofluorescence assays, serological hemagglutination inhibition assays, real-time polymerase chain reaction (PCR) assays, and complement fixation tests. Most of these methods are complicated, relatively costly and require a lengthy process and expensive apparatus (114).

Several microfluidic systems have been shown for influenza detection. An immunomagnetic bead-based microfluidic system for detection of influenza A virus has been demonstrated recently. Influenza A viral particles are initially bound to monoclonal antibody (mAb)-conjugated immunomagnetic beads using a suction type micro-mixer. Subsequently the virus-bound magnetic complexes are fluorescently labeled by developing mAb with R-phycoerythrin. An external optical detection module is used to analyze the optical intensity of the magnetic complex. The system displayed better performance than conventional flow cytometry systems in terms of limit of detection (114). However, the expensive external optical detection module could restrict its use in POC low-resource settings. Yamanaka et al. reported a microfluidic RT-PCR chip for rapid detection of influenza (AH1pdm) virus of swine-origin. A disposable electrical printed chip was used for electrochemical detection of the PCR amplicon (112). The electrochemical method is better for use in low-resource settings compared to the optical methods reported above due to the absence of expensive external detection units. A Magnetic Integrated Microfluidic Electrochemical Detector (MIMED) for detection of H1N1 influenza virus from throat swab samples has recently been developed (115).

Microfluidics detection methods for other types of viral agents have been reported. Weiss et al. reported a microfluidic chip-based electrophoretic analysis and laser-induced fluorescence detection of human rhinovirus serotype 2 (116). Zhu et al. developed an optofluidic micro-ring resonator-based system for detection of bacteriophage M13 (117). They reported a detection limit

of 2.3×10^3 PFU/mL. An on-chip surface enhanced Raman spectroscopy (SERS)-based biomolecular device for detection of Dengue virus sequences was developed by Huh et al. (118). The fluid is actuated using electrokinetic methods and the limit of detection was reported to be 30 pM. Weng et al. developed a suction-type, pneumatically driven microfluidic device for the detection of dengue infection (119). A detection limit of 10 PFU/ml was reported for the device. A "lab-on-a-disc" centrifugal microfluidics-based portable ELISA system was developed for detection of the antigen and the antibody of Hepatitis B virus (120). The limit of detection of antigen and antibody were reported as 0.51 ng/mL and 8.6 mIU/mL, respectively. Heinze et al. developed a microfluidic immunosensor for detection of bovine viral diarrhea virus (121). An integrated microfluidic assay for targeted ribonucleic acid (RNA) extraction and a one-step reverse transcription loop-mediated-isothermal-amplification (RT-LAMP) process for the detection of nervous necrosis viruses was reported by Wang et al. (122).

6.5. Cancer Biomarker Detection

In 2010, there were an estimated 1,500 cancer related deaths per day in the USA and about 1.4 million new cases of cancer were reported. By 2020, cancer related deaths are estimated to be 10.3 million globally. The cancer mortality rate per 100,000 Americans has dropped from 194 to 190 since 1950, an insignificant drop compared to drop in mortality rates for other diseases. Most of the improvements in cancer survival rates are due to improvements in early diagnosis rather than treatment. For instance, for cancers of the breast, colon, rectum, and cervix, early detection has proved to reduce mortality significantly. Hence, the National Cancer Institute has emphasized a shift from therapeutic to preventive mode in its 2010 vision document.

Existing methods of cancer diagnostics rely on invasive techniques like taking a biopsy and then examining the cell morphology. Further, conventional methods could be inconclusive in disease detection in its early stages (123). Other techniques like immunoassays (ELISA) have been used to detect cancer biomarkers. Although ELISAs are very sensitive, they can be time consuming, expensive and are mostly carried out in a laboratory requiring skilled personnel. In most cases, immunoassays look for only one biomarker and are not sensitive enough to detect very low biomarker levels especially at early stages of the disease. POC devices which are accurate, fast and economic are needed. This would enable improved diagnosis, monitoring of the progress of the disease, and response to therapy.

Advances in oncology have led to identification of biomarkers associated with different kinds of cancers. For a comprehensive list of cancer biomarkers, the reader can refer to reviews in literature (124–129). There are multiple factors responsible for carcinogenesis.

This along with the "heterogeneity in oncogenic pathways" makes it imperative that a range of biomarkers need to be analyzed for cancer diagnostics (123, 130). Hence POC devices with multiplexed capability to detect multiple biomarkers are needed. Although research into cancer diagnostic devices is moving forward, commercialization of the technology still remains a challenge (123).

Here, we review some of the recent research in microfluidics POC devices for cancer diagnostics. Legendre et al. reported work into the design and development of a microfluidic device for diagnosis of T-cell lymphoma. The system accepts a whole blood sample as the input, extracts the DNA, amplifies target sequences of the T-cell receptor-gene, and eletrophoretically resolves the products for detection of a signature consistent with monoclonality (131). Diercks et al. demonstrated a microfluidic device that measured multiple proteins (tumor necrosis factor, CXC chemokine ligand 2, interleukin 6 and interleukin 1b) at pg/mL concentrations in nanoliter volumes. Antibody-coupled polystyrene microspheres labeled with embedded fluorophores were used to detect the analyte (proteins). Optical detection of captured analyte was performed off-chip using a confocal microscope, which proved to be a disadvantage in terms of lack of device portability (132). A similar fluorescence approach has been used to detect vascular endothelial growth factors in human plasma (133). An on-chip nuclear magnetic resonance (NMR)-based biosensor was developed for the multiplexed identification of cancer markers (epidermal growth factor receptors EGFR and Her2/neu). The design consists of a microcoil array for NMR measurements, microfluidic channels for sample handling and a permanent magnet to generate a polarizing magnetic field, all integrated into a handheld device (134). Mass spectroscopy-based microfluidic detection of cancer-specific biomarkers (proliferating cell nuclear antigen, cathepsin D, and keratins K8, K18, and K19) was demonstrated by Lazar (135).

Other mass-based methods like quartz crystal microbalance (QCM) have been used in cancer biomarker detection. For instance, Zhang et al. demonstrated detection of human lung carcinoma cells using a microfluidic surface modified piezoelectric sensor (136). Recently, Von Muhlen et al. have reported a microcantilever-based "suspended microchannel resonator" sensing device for detection of activated leukocyte cell adhesion molecules (137). Zani et al. demonstrated an electrochemical method for detection of prostate specific antigen (PSA) cancer markers. The method works based on the differential pulse voltammetry-based electrochemical detection of protein coated paramagnetic microparticles that selectively capture the analyte (PSA) (138). Similar electrochemical detection methods for breast cancer markers have been reported (139). A microfluidic-based amperometric electrochemical detection system for carcinoembryonic antigen (CEA) and cancer antigen 15–3 (CA15-3) was developed by Kellner et al.

The on-chip fluid function is handled by computer controlled syringe pumps and reports enhanced performance due to fully automated fluidic operations (140). But the external computer control system and syringe pumps prove to be a bottleneck in their use for POC applications. Hence miniaturization and integration of the fluid handling functions within the microfluidic chip is necessary for POC use.

6.6. Cardiac Biomarker Detection

Cardiovascular diseases (CVD) are responsible for nearly half of the deaths in the western world. Studies suggest the acute and long term financial burden of cardiac disease to be substantial (141). It is reported that 5% of myocardial infarction (MI) patients are incorrectly discharged from emergency departments (ED). Hence for timely and effective intervention against cardiovascular diseases, there is a need for rapid and accurate diagnostic tools (142).

For the accurate "diagnosis, prognosis, monitoring and risk stratification of patients with acute coronary syndromes" (ACS), biochemical markers play a fundamental role (142). In clinical settings, in 50–70% of patients with ACS related cases, ECGs give ambiguous results. In such cases, cardiac marker levels could provide critical information for informed decision on the suitable treatment. As a definite indicator of disease condition a combination of cardiac markers need to be explored (143). For a review of cardiac biomarkers, the reader can refer to McDonnell et al. (142).

There is a difference of opinion with regard to the use of POC technologies for cardiac biomarker diagnostic, with some suggesting it to be an alternative to conventional lab analyzers (144, 145) and others questioning the accuracy of the technologies (146, 147). The following section provides a review of microfluidic devices used in cardiac biomarker detection.

Most of the diagnostic mechanisms for biomarkers involve two steps, an initial immunoassay to capture the analyte (biomarker) and subsequent detection of the captured analyte. Using optical methods, Jönsson et al. demonstrated a lateral flow polymer chip for detection of C Reactive Protein (CRP) (148). Gervais et al. demonstrated a microfluidic device for one step detection of CRP in serum. The device works based on capillary action for fluid actuation and does not need any external power requirements (149), which makes it extremely useful in a POC, low-cost setting. A multiplexed cardiac biomarker detection prototype device was developed by Hong et al. The MEMS-based device detected four different cardiac markers viz. myoglobin, CRP, cTnI and BNP using Au nanoparticle-based fluorescence detection (150). Bhattacharyya & Klapperich developed a disposable microfluidic chip for detection of CRP including an on-board detection module (151). A microfluidic chemiluminescence-based immunoassay system for detection of cardiac troponin I (cTnI) was reported by Cho et al. (152). Huang et al. demonstrated a microfluidic

chemiluminescence-based detection sensor for alpha-fetoprotein (AFP). Super-paramagnetic microbeads were used to capture the biomarker (153). Use of magnetic microbeads results in higher surface to volume ratio for efficient analyte capture and enables on-chip actuation using an integrated electromagnet. A digital microfluidic platform detection device for cTnI was developed by Sista et al. (154). The fluidic actuation is performed by electrowetting, obviating the need for any off-chip fluid handling apparatus. SPR-based microfluidic detection of cardiac marker B-type natriuretic peptide (BNP) was reported by Kurita et al. (155).

Electrochemical methods have been applied to detection of cardiac markers. Unlike optical methods, these do not need an often expensive, off-chip optical detection device and could be suitable for POC applications. Tweedie et al. presented a microfluidic-based impedimetric sensing device for cardiac enzymes (156). The i-STAT system (Abbott Point of Care Inc., USA) is a commercial test cartridge for electrochemical detection of cTnI (157). The device can detect cTnI in the range of 0–50 ng/ml and has gained good acceptance as a diagnostic tool for MI (143). Other electrochemical-based detection methods for detection of myoglobin (158), cTnI (159) and CRP (160) have been reported. Recently, Mitsakakis and Gizeli have developed an integrated microfluidic surface acoustic wave (SAW) platform for detection of cardiac markers creatine kinase MB (CK-MB), CRP, and D-dimer (161).

Many commercial systems for cardiac marker detection are currently available, which could possibly limit the impact of microfluidic devices in this area. These include Triage® [Biosite Diagnostics Inc., USA] (myoglobin, CK-MB, and cTnI), Stratus® CS STAT fluorometric analyzer [Siemens Medical Diagnostics, USA] (myoglobin, CK-MB, and cTnI), Roche cardiac reader [Roche Diagnostics, USA] (cTnT, myoglobin), RAMP™ cardiac marker testing [Response Biomedical Inc., Canada] (cTnI, CK-MM), and Cardiac STATus™ device [Nanogen Inc., USA] (myoglobin, CK-MB mass, and cTnI) (157). Table 3 lists the set of published work and commercial devices for microfluidic cardiac marker detection.

6.7. High Throughput and Multiplexed Diagnostic Screening

Microfluidic-based technology is ideal for developing highly parallel diagnostic assays that would allow high-throughput screening, but there has been limited success in this area. The lack of success is not due to problems with microfluidic devices; for example, drug screening requires high-throughput methods to find and test different drug candidates. Microfluidic high-throughput screening (HTS) techniques have been applied to drug discovery to perform thousands of tests in parallel with some success (162–164). As of now these methods haven't been applied in microfluidic diagnostics for several reasons. Current diagnostics are typically performed in large hospitals or reference labs. In these labs, most tests are

Table 3
Performance and detection methods of POC devices for cardiac marker diagnostics

Biomarkers	Detection method	Material/Device	Detection Limit	Reference
Published work				
CRP	Fluorescence	Thermoplastic (Zeonor™)	2.6 ng/ml	(147)
CRP	Fluorescence	PDMS	1 ng/ml	(148)
Myoglobin, BNPCRP cTnI	Fluorescence	Cyclic Olefin Copolymer (COC)	70 ng/ml 0.1 ng/ml700 ng/ ml0.7 ng/ml	(149)
CRP	Chemiluminescence	Thermoplastic (Zeonex™)	100 ng/ml	(150)
cTnI	Chemiluminescence	Polycarbonate	0.027 ng/ml	(151)
AFP	Chemiluminescence	PMMA	0.23 ng/ml	(152)
cTnI	Chemiluminescence	Glass/Polymer	Not reported	(153)
BNP	SPR	PDMS & Glass	5 pg/ml	(154)
Cardiac enzyme (myoglobin)	Electrochemical (impedimetric)	Pressure sensitive adhesive & PMMA	100 ng/ml	(155)
cTnICRP	Electrochemical (anodic stripping voltammetry)	PDMS	0.01–50 μg/l 0.5–200 μg/l	(158)
CK-MB CRPD-dimer	SAW	PDMS & PMMA	0.25 μg/ml 1 μg/ml5 μg/ml	(160)
Commercial devices				
Troponin ICK-MBBNP	Electrochemical	i-STAT®	0–50 ng/ml Not reportedNot reported	(142)
Troponin IMyoglobin CK-MB	Fluorescence	Triage®	Not reported	(142)
Troponin T Myoglobin NT-proBNP D-dimer CK-MB	Fluorescence	Roche cardiac reader	0.1–2.0 ng/ml 30–700 ng/ml 60–3,000 pg/ml 0.1–4.0 μg/ml 1.0–25 ng/ml	(142)
Troponin ICK-MB Myoglobin NT-proBNP	Fluorescence	RAMP™ 3.2	0.2 ng/ml 7.2 ng/ml 100.0 ng/ml Not reported	(142)
Troponin IMyoglobin CK-MB	Chemiluminescence	Cardiac STATus™	Not reported	(142)

batched and performed using robots in a highly parallel, high throughput approach. Replacing these robots by using microfluidics is unlikely in the short term due to the large infrastructure already developed. Essentially, a solution to this problem already exists, so adoption of microfluidics for these assays will only occur if there are compelling assay improvements. In addition, if an assay can be performed in a batch mode using microfluidics, it is likely to be able to be performed in the clinic or POC setting, and for nearly the same price. Thus, microfluidics is likely to be driven to the POC rather than to large reference laboratories.

The reverse of high-throughput screening (multiple samples with one target) is multiplexed screening, where one sample is tested for multiple agents or biomarkers. A few examples of multiplexed screening have already been provided, especially for cardiac biomarkers, but highly multiplexed diagnostics are still being developed. Multiplexed screening is likely to have a more significant impact on diagnostics than high throughput screening, especially with the move towards personalized medicine. Microfluidics has been combined with microarray technology, which is used regularly in genomics and proteomics, and which will likely have diagnostic applications in the future; however, this is beyond the scope of the chapter. More relevant are microfluidic devices that can diagnose multiple diseases simultaneously. A recently released product that uses "mesoscale" fluidics can simultaneously diagnose 15 respiratory diseases associated with viruses (165). A challenge with getting the device to commercialization is that regulatory agencies such as the FDA require individual validation of each assay, meaning that multiplexing must clear very challenging regulatory requirements, which will likely limit substantial multiplexing in the near future. Nevertheless, microfluidics will probably lead to highly multiplexed assays that can perform 100s or 1,000s of diagnostic assays on one sample.

7. Microfluidic Commercialization

About 1,200 patents related to microfluidics have been issued in the USA through 2010. In spite of immense academic interest in microfluidics and significant research investment directed towards both academic and industrial organizations, relatively few commercial products based on microfluidics have been introduced into the market (166, 167); however, the rate of introduction is increasing and many barriers are coming down. One of the reasons cited for lack of commercial success is the lack of a potential "blockbuster" end-user product that could generate billions of dollars in revenue. Until the industry can find a product with high volume demand, the fabrication costs due to lack of "economies of scale" are going to remain high. Existing materials like PDMS, which are hugely popular

Table 4
Leading POC diagnostic companies and products (168)

Company	Product	Application
Abbott Point of Care	i-STAT®	POC blood analyzer
Agilent	Agilent 2100 Bioanalyzer	Microfluidics-based platform for sizing, quantification and quality control of DNA, RNA, proteins and cells on a single platform, PCR/QPCR products
Beckman Coulter	AmpliSpeed	Thermal cycler, single-cell analysis platforms
Biosite	Triage® Cardiac Panel	POC diagnosis of acute myocardial infarction
Caliper Life Sciences	LabChip GX	Nucleic acid and protein separations system
Cepheid	GeneXpert	Integrated real-time PCR system
Cynvenio Biosystems	Under development	Integrated System for molecular analysis of circulating tumor cells
Daktari Diagnostics	Under development	POC CD4 cell counting system
Eksigent	NanoLC	Microfluidic flow control based nanospray mass spectrometry system
Fluidgm	BioMark™ HDFluidigm EP1	Microfluidic devices for molecular diagnostics and personalized medicine
LeukoDx	Under development	POC flow cytometry device
Microfluidic Systems		Microfluidic systems for detection, processing of biological samples and biodefense
Micronics	PanNAT™	Multiplexed nucleic acid amplification device
RainDance Technologies	RDT 1000	Microdroplet-based solutions for human health and disease research
Rheonix	CARD®	Disposable microfluidic chip technology for multiplexed endpoint analysis for diagnostic applications
Shimadzu Biotech	PPSQ-31A/33A	Technologies to aid the protein research work flow and drug discovery
Siloam Biosciences	Optimiser™	Diagnostic systems using microfluidic and microsensor technology
Veridex	CellSearch®	Commercializing microfluidic circulating tumor cell diagnostics

in research, have not succeeded in the industry due to issues with manufacturability and scaling (168). Most of the LOC products are still focused on the business-to-business segment and not the business-to-consumer (167). There needs to be more focused research on microfluidic product development including issues like manufacturability and cost dynamics and a simultaneous search for new application areas where microfluidics could be applied. Table 4 provides a sample of microfluidic companies and products in the market. More comprehensive lists are available (169).

8. Summary and Future Outlook

Microfluidic diagnostic devices have been developing at a rapid rate over the past few years. While the potential for these devices was first recognized more than 20 years ago, the realization of that potential has been slow, even though thousands of devices and methods have been published. The continuing development of applications and microfluidic manufacturing methods, including platform technologies that can be customized easily for each diagnostic test, will be the drivers of success. Very recent progress and an emphasis on global health has helped move the field towards POC devices that will likely become ubiquitous in the years ahead. While most microfluidic devices have one diagnostic target, devices capable of diagnosing 100s or 1,000s of diseases will likely be developed and commercialized in the next decade, making microfluidics a major driver of disease diagnostics.

Acknowledgments

The authors thank Keng-Min Lin for the schematic diagram in Fig. 1. The authors would like to thank the Nano Institute of Utah for funding this work through a nanotechnology training fellowship.

References

1. Yager P, Domingo GJ, Gerdes J (2008) Point-of-care diagnostics for global health. Annu Rev Biomed Eng 10:107–144
2. Kiechle FL, Holland CA (2009) Point- of-Care Testing and Molecular Diagnostics: Miniaturization Required. Clin Lab Med 29(3):555–560
3. UNAIDS (2010) UNAIDS Report on the global AIDS epidemic, UNAIDS.
4. Steven J, Zullo SS, Patrick Looney J, Barker PE (2010) Nanotechnology: Emerging Developments and Early Detection of Cancer, A Two-Day Workshop sponsored by the National Cancer Institute and the National Institute of Standards and Technology, National Cancer Institute, Gaithersburg.
5. Foster RS, Heffler SK (2009) Updated and Extended National Health Expenditure Projections, 2010–2019, Office of the Actuary. Centers for Medicare & Medicaid Services, Maryland
6. Cirino NM, Musser KA, Egan C (2004) Multiplex diagnostic platforms for detection of biothreat agents. Expert Rev Mol Diagn 4:841–857
7. (USDA) U S D o HHS H a A (ed) (2011) National select agent registry: overview. Department of Health & Human Service, Washington DC
8. Food and Drug Administration (2008) Recommendations: Clinical Laboratory Improvement Amendments of 1988 (CLIA Waiver Applications for Manufacturers of In Vitro Diagnostic Devices.
9. Sia SK, Kricka LJ (2008) Microfluidics and point-of-care testing. Lab Chip 8:1982–1983
10. Whitesides GM (2006) The origins and the future of microfluidics. Nature 442:368–373
11. Arora A et al (2010) Latest developments in micro total analysis systems. Anal Chem 82:4830–4847
12. Salieb-Beugelaar GB et al (2010) Latest developments in microfluidic cell biology and analysis systems. Anal Chem 82:4848–4864
13. West J et al (2008) Micro total analysis systems: latest achievements. Anal Chem 80:4403–4419

14. Trietsch SJ et al (2011) Lab-on-a-chip technologies for massive parallel data generation in the life sciences: A review Chemometr Intell Lab 108:64–75.
15. Weston AD, Hood L (2004) Systems biology, proteomics, and the future of health care: toward predictive, preventative, and personalized medicine. J Proteome Res 3:179–196
16. Reyes DR (2002) Micro Total Analysis Systems. 1. Introduction. Theory, and Technology 74(12):2623–2636
17. Jacobson SC, Moore AW, Ramsey JM (1995) Fused quartz substrates for microchip electrophoresis. Anal Chem 67:2059–2063
18. von Heeren F et al (1996) Micellar electrokinetic chromatography separations and analyses of biological samples on a cyclic planar microstructure. Anal Chem 68:2044–2053
19. Moore AW Jr, Jacobson SC, Ramsey JM (1995) Microchip separations of neutral species via micellar electrokinetic capillary chromatography. Anal Chem 67:4184–4189
20. Woolley AT, Mathies RA (1995) Ultra-high-speed DNA sequencing using capillary electrophoresis chips. Anal Chem 67:3676–3680
21. Shoffner MA et al (1996) Chip PCR. I. Surface passivation of microfabricated silicon-glass chips for PCR. Nucleic Acids Res 24:375–379
22. Koutny LB et al (1996) Microchip electrophoretic immunoassay for serum cortisol. Anal Chem 68:18–22
23. Hadd AG et al (1997) Microchip device for performing enzyme assays. Anal Chem 69:3407–3412
24. Colyer CL, Mangru SD, Harrison DJ (1997) Microchip-based capillary electrophoresis of human serum proteins. J Chromatogr A 781:271–276
25. Raymond DE, Manz A, Widmer HM (1996) Continuous separation of high molecular weight compounds using a microliter volume free-flow electrophoresis microstructure. Anal Chem 68:2515–2522
26. von Heeren F et al (1996) Characterization of electrophoretic sample injection and separation in a gel filled cyclic planar microstructure. J Microcolumn Separations 8:373–381
27. Woolley AT, Sensabaugh GF, Mathies RA (1997) High-speed DNA genotyping using microfabricated capillary array electrophoresis chips. Anal Chem 69:2181–2186
28. Delamarche E et al (1997) Patterned delivery of immunoglobulins to surfaces using microfluidic networks. Science 276:779
29. Freaney R et al (1997) Novel instrumentation for real-time monitoring using miniaturized flow systems with integrated biosensors. Ann Clin Biochem 34:291–302
30. Manz A, Graber N, Widmer HM (1990) Miniaturized total chemical analysis systems: a novel concept for chemical sensing. Sensors Actuators B: Chemical 1:244–248
31. Harrison DJ, Manz A, Glavina PG (1991) Electroosmotic pumping within a chemical sensor system integrated on silicon. In: Proc. IEEE Int. Conf. Solid-State Sensors and Actuators (Transducers '91), San Francisco, USA, pp 792–795
32. Seiler K, Harrison DJ, Manz A (1993) Planar glass chips for capillary electrophoresis: repetitive sample injection, quantitation, and separation efficiency. Anal Chem 65: 1481–1488
33. Sobek D et al. (1993) A microfabricated flow chamber for optical measurements in fluids. In: Proc. 6th IEEE MEMS, Fort Lauderdale, USA, pp 219–224
34. Northrup MA et al. (1993) DNA amplification with a microfabricated reaction chamber. In: Proc. of The 7th Int. Conf. on Solid-State Sensors and Actuators (Transducers '93), Yokohama, Japan, pp 924–926
35. Bousse L et al (1994) Micromachined multichannel systems for the measurement of cellular metabolism. Sensors Actuators B: Chemical 20:145–150
36. Jacobson SC et al (1994) Precolumn reactions with electrophoretic analysis integrated on a microchip. Anal Chem 66:4127–4132
37. Jacobson SC et al (1994) Microchip capillary electrophoresis with an integrated postcolumn reactor. Anal Chem 66:3472–3476
38. Jacobson SC et al (1994) High-speed separations on a microchip. Anal Chem 66: 1114–1118
39. Mensinger H et al (1995) Microreactor with integrated static mixer and analysis system. Kluwer Academic Publishers, The Netherlands, p 237
40. Effenhauser CS et al (1994) High-speed separation of antisense oligonucleotides on a micromachined capillary electrophoresis device. Anal Chem 66:2949–2953
41. Woolley AT, Mathies RA (1994) Ultra-high-speed DNA fragment separations using microfabricated capillary array electrophoresis chips. Proc Natl Acad Sci 91:11348
42. Fan ZH, Harrison DJ (1994) Micromachining of capillary electrophoresis injectors and separators on glass chips and evaluation of flow at capillary intersections. Anal Chem 66:177–184
43. Fuhr G, and Wagner B. (1994) Electric field mediated cell manipulation, characterisation

and cultivation in highly conductive media. Paper presented at the MicroTAS, University of Twente, Netherlands, 21–22 Nov 1994
44. Manz A et al (1994) Electroosmotic pumping and electrophoretic separations for miniaturized chemical analysis systems. J Micromech Microeng 4:257
45. Raymond DE, Manz A, Widmer HM (1994) Continuous sample pretreatment using a free-flow electrophoresis device integrated onto a silicon chip. Anal Chem 66:2858–2865
46. Verpoorte EMJ et al (1994) Three-dimensional micro flow manifolds for miniaturized chemical analysis systems. J Micromech Microeng 4:246
47. Seiler K et al (1994) Electroosmotic pumping and valveless control of fluid flow within a manifold of capillaries on a glass chip. Anal Chem 66:3485–3491
48. Jacobson SC et al (1994) Open channel electrochromatography on a microchip. Anal Chem 66:2369–2373
49. Feustel A, Muller J, Relling V (1995) A microsystem mass spectrometer. Springer, Berlin, p 299
50. Kim E, Xia Y, Whitesides GM (1995) Polymer microstructures formed by moulding in capillaries. Nature 376:581–584
51. Xia Y, Whitesides GM (1998) Soft lithography. Ann Rev Mat Sci 28:153–184
52. Whitesides GM et al (2001) Soft lithography in biology and biochemistry. Annu Rev Biomed Eng 3:335–373
53. Mrksich M, Whitesides GM (1995) Patterning self-assembled monolayers using microcontact printing: a new technology for biosensors? Trends Biotechnol 13:228–235
54. Zhao XM, Xia Y, Whitesides GM (1996) Fabrication of three dimensional micro structures: Microtransfer molding. Adv Mater 8:837–840
55. Bartholomeusz DA, Boutté RW, Gale BK (2009) Xurography: Microfluidic Prototyping with a Cutting Plotter. In: Herold K, Rasooly A (eds) Lab on a Chip Technology: Fabrication and Microfluidics. Caister Academic Press, United Kingdom, pp 65–82
56. Gale BK et al (2008) Fabrication and packaging: Low-cost MEMS technologies. In: Gianchandani YB, Tabata O, Zappe HP (eds) Comprehensive microsystems. Elsevier, Amsterdam, pp 341–378
57. Martynova L et al (1997) Fabrication of plastic microfluid channels by imprinting methods. Anal Chem 69:4783–4789
58. Gonzalez C, Collins SD, Smith RL (1998) Fluidic interconnects for modular assembly of chemical microsystems. Sens. Actuators B: Chemical 49:40–45
59. Johnson KS et al (1996) Using neutral metastable argon atoms and contamination lithography to form nanostructures in silicon, silicon dioxide, and gold. Appl Phys Lett 69: 2773–2775
60. Lorenz H et al (1997) SU-8: a low-cost negative resist for MEMS. J Micromech Microeng 7:121
61. Larsson O et al (1997) Silicon based replication technology of 3D-microstructures by conventional CD-injection molding techniques. IEEE 1412:1415–1418
62. Klaassen EH et al. (1996) Silicon fusion bonding and deep reactive ion etching; a new technology for microstructures. Sens. Actuators A: Physical 52:132–139
63. Juan WH, Pang SW (1995) A novel etch-diffusion process for fabricating high aspect ratio Si microstructures. In: Proc. 8th Int. Conf. Solid-State Sensors and Actuators (Transducers '95), Stockholm, Sweden, pp 560–563
64. Madou MJ (2002) Fundamentals of microfabrication: the science of miniaturization. CRC, Boca Raton, FL
65. Rolland JP et al (2004) High Resolution Soft Lithography: Enabling Materials for Nanotechnologies. Angewandte Chemie 116:5920–5923
66. Wasatch Microfluidics, LLC, www.microfl.com. 12 Nov 2012
67. Rivet C et al (2010) Microfluidics for medical diagnostics and biosensors. Chem Engine Sci 66:1490–1507
68. Crews N, Wittwer C, Gale B (2008) Continuous-flow thermal gradient PCR. Biomed Microdevices 10:187–195
69. Bartholomeusz DA, Boutté RW, Andrade JD (2005) Xurography: rapid prototyping of microstructures using a cutting plotter. Microelectromechanical Syst J 14: 1364–1374
70. Klank H, Kutter JP, Geschke O (2002) CO2-laser micromachining and back-end processing for rapid production of PMMA-based microfluidic systems. Lab Chip 2:242–246
71. Becker H, Gärtner C (2008) Polymer microfabrication technologies for microfluidic systems. Anal Bioanal Chem 390:89–111
72. Martinez AW, Phillips ST, Whitesides GM (2008) Three-dimensional microfluidic

devices fabricated in layered paper and tape. Proc Natl Acad Sci 105:19606–19611
73. Martinez AW et al (2009) Diagnostics for the developing world: microfluidic paper-based analytical devices. Anal Chem 82:3–10
74. Bhattacharyya A, Klapperich CM (2006) Thermoplastic microfluidic device for on-chip purification of nucleic acids for disposable diagnostics. Anal Chem 78:788–792
75. Yager P et al (2006) Microfluidic diagnostic technologies for global public health. Nature 442:412–418
76. Squires TM, Quake SR (2005) Microfluidics: Fluid physics at the nanoliter scale. Rev Mod Phys 77:977
77. Psaltis D, Quake SR, Yang C (2006) Developing optofluidic technology through the fusion of microfluidics and optics. Nature 442:381–386
78. Demello AJ (2006) Control and detection of chemical reactions in microfluidic systems. Nature 442:394–402
79. Myers FB, Lee LP (2008) Innovations in optical microfluidic technologies for point-of-care diagnostics. Lab Chip 8:2015–2031
80. Singer PA et al (2007) Grand challenges in global health: the ethical, social and cultural program. PLoS Med 4:e265
81. Chin CD, Linder V, Sia SK (2007) Lab-on-a-chip devices for global health: past studies and future opportunities. Lab Chip 7:41–57
82. World Health Organization (2010) World malaria report: 2010. World Health Organization, Geneva
83. World Health Organization (2010) 2010/2011 Tuberculosis Global Facts, Geneva.
84. United Nations (2000) *United Nations Millennium Declaration.*
85. World Health Organization. (2009–2010) Situation updates - Pandemic (H1N1) 2009, World Health Organization, Geneva.
86. Reed C et al (2009) Estimates of the prevalence of pandemic (H1N1) 2009, United States, April-July 2009. Emerg Infect Dis 15: 2004–2007
87. Ivnitski D et al (1999) Biosensors for detection of pathogenic bacteria. Biosens Bioelectron 14:599–624
88. Kim J et al. (2010) Sample to answer: a fully integrated nucleic acid identification system for bacteria monitoring. In: Becker H, Wang W (eds) Proc. SPIE, vol 7593, pp 75930S
89. Kim J et al (2009) Microfluidic sample preparation: cell lysis and nucleic acidpurification. Integr Biol 1:574–586
90. Sant HJ et al (2010) Integrated Microfluidics for Serotype Identification of Foot and Mouth Disease Virus, in Proceedings of The 14th International Conference on Miniaturized Systems for Chemistry and Life Sciences. Groningen, The Netherlands
91. Velusamy V et al (2010) An overview of foodborne pathogen detection: In the perspective of biosensors. Biotechnol Adv 28:232–254
92. Lazcka O, Campo F, Munoz FX (2007) Pathogen detection: A perspective of traditional methods and biosensors. Biosens Bioelectron 22:1205–1217
93. Xiang Q et al (2006) Miniaturized immunoassay microfluidic system with electrokinetic control. Biosens Bioelectron 21(10): 2006–2009
94. Gao Y et al (2008) Multiplexed high-throughput electrokinetically-controlled immunoassay for the detection of specific bacterial antibodies in human serum. Anal Chim Acta 606:98–107
95. Meagher RJ et al (2008) An integrated microfluidic platform for sensitive and rapid detection of biological toxins. Lab Chip 8:2046–2053
96. JinSeok H, Hua SZ (2009) An overview of recent strategies in pathogen sensing. Sensors 9:4483–4502
97. Boehm DA, Gottlieb PA, Hua SZ (2007) On-chip microfluidic biosensor for bacterial detection and identification. Sensors Actuators B: Chemical 126:508–514
98. Liao JC et al (2006) Use of electrochemical DNA biosensors for rapid molecular identification of uropathogens in clinical urine specimens. J Clin Microbiol 44:561–570
99. Stevens DY et al (2008) Enabling a microfluidic immunoassay for the developing world by integration of on-card dry reagent storage. Lab Chip 8:2038–2045
100. Cheng X, Chen G, Rodriguez WR (2009) Micro-and nanotechnology for viral detection. Anal Bioanal Chem 393:487–501
101. Kortepeter MG, Parker GW (1999) Potential biological weapons threats. Emerg Infect Dis 5:523–527
102. Desai D, Wu G, Zaman MH (2010) Tackling HIV through robust diagnostics in the developing world: current status and future opportunities. Lab Chip 11(2):194–211
103. Lee WG et al (2010) Nano/Microfluidics for diagnosis of infectious diseases in developing countries. Adv Drug Deliv Rev 62:449–457
104. Lee SH et al (2008) A polymer lab-on-a-chip for reverse transcription (RT)-PCR based

point-of-care clinical diagnostics. Lab Chip 8:2121–2127

105. Cheng X et al (2009) Enhancing the performance of a point-of-care CD4+ T-cell counting microchip through monocyte depletion for HIV/AIDS diagnostics. Lab Chip 9:1357–1364
106. Cheng X et al (2007) A microfluidic device for practical label-free CD4+ T cell counting of HIV-infected subjects. Lab Chip 7:170–178
107. Cheng X et al (2007) A microchip approach for practical label-free CD4+ T-cell counting of HIV-infected subjects in resource-poor settings. JAIDS J Acquired Immune Deficiency Syndrom 45:257–261
108. Moon SJ et al (2009) Integrating microfluidics and lensless imaging for point-of-care testing. Biosens Bioelectron 24:3208–3214
109. Cheng X et al (2007) Cell detection and counting through cell lysate impedance spectroscopy in microfluidic devices. Lab Chip 7:746–755
110. Gohring JT, Fan X (2010) Label Free Detection of CD4+ and CD8+ T Cells Using the Optofluidic Ring Resonator. Sensors 10:5798–5808
111. Wang JH et al (2011) An integrated microfluidic system for counting of CD4+/CD8+ T lymphocytes. Microfluid Nanofluid 10:531–541
112. Yamanaka K et al (2011) Rapid detection for primary screening of influenza A virus: microfluidic RT-PCR chip and electrochemical DNA sensor. Analyst 136(10):2064–2068
113. Neumann G, Noda T, Kawaoka Y (2009) Emergence and pandemic potential of swine-origin H1N1 influenza virus. Nature 459:931–939
114. Lien KY et al (2011) Rapid detection of influenza A virus infection utilizing an immunomagnetic bead-based microfluidic system. Biosens Bioelectron 26:3900–3907
115. Ferguson BS et al (2011) Genetic Analysis of H1N1 Influenza Virus from Throat Swab Samples in a Microfluidic System for Point-of-Care Diagnostics. J Am Chem Soc 133(23):9129–9135
116. Weiss VU et al (2007) Virus analysis by electrophoresis on a microfluidic chip. J Chromatogr B 860:173–179
117. Zhu H et al (2008) Opto-fluidic micro-ring resonator for sensitive label-free viral detection. Analyst 133:356–360
118. Huh YS et al (2008) Enhanced on-chip SERS based biomolecular detection using electrokinetically active microwells. Lab Chip 9:433–439
119. Weng CH et al (2011) A suction-type microfluidic immunosensing chip for rapid detection of the dengue virus. Biomed Microdevices 13(3):585–595
120. Lee BS et al (2009) A fully automated immunoassay from whole blood on a disc. Lab Chip 9:1548–1555
121. Heinze BC et al (2009) Microfluidic immunosensor for rapid and sensitive detection of bovine viral diarrhea virus. Sensors and Actuators B: Chemical 138:491–496
122. Wang C et al (2011) An integrated microfluidic loop-mediated-isothermal-amplification system for rapid sample pre-treatment and detection of viruses. Biosens Bioelectron 26(5):2045–2052
123. Tothill IE (2009) Biosensors for cancer markers diagnosis. Elsevier, Amsterdam, pp 55–62
124. Choi YE, Kwak JW, Park JW (2010) Nanotechnology for early cancer detection. Sensors 10:428–455
125. Kumar S, Mohan A, Guleria R (2006) Biomarkers in cancer screening, research and detection: present and future: a review. Biomarkers 11:385–405
126. Hanash SM, Pitteri SJ, Faca VM (2008) Mining the plasma proteome for cancer biomarkers. Nature 452:571–579
127. Saerens D et al (2008) Antibody fragments as probe in biosensor development. Sensors 8:4669–4686
128. D'Haeseleer P (2006) How does DNA sequence motif discovery work? Nat Biotechnol 24:959–961
129. Makarov DV et al (2009) Biomarkers for prostate cancer. Annu Rev Med 60:139–151
130. Wang J (2006) Electrochemical biosensors: towards point-of-care cancer diagnostics. Biosens Bioelectron 21:1887–1892
131. Legendre LA et al (2008) Toward a Simplified Microfluidic Device for Ultra-fast Genetic Analysis with Sample-In/Answer-Out Capability: Application to T-Cell Lymphoma Diagnosis. J Assoc Laboratory Automation 13:351–360
132. Diercks AH et al (2009) A microfluidic device for multiplexed protein detection in nano-liter volumes. Anal Biochem 386:30–35
133. Lin DH et al (2010) Internally calibrated quantification of VEGF in human plasma by fluorescence immunoassays in disposable elastomeric microfluidic devices. J Chromatogr B 878:258–263

134. Lee H et al (2008) Chip–NMR biosensor for detection and molecular analysis of cells. Nat Med 14:869–874
135. Lazar IM (2008) Microfluidic bioanalytical platforms with mass spectrometry detection for biomarker discovery and screening In: Severine le Gac, Albert van den Berg (eds) Miniaturization and Mass Spectrometry, Royal Society of Chemistry, 1st ed., pp 151–172
136. Zhang K et al (2010) A microfluidic system with surface modified piezoelectric sensor for trapping and detection of cancer cells. Biosens Bioelectron 26(2):935–939
137. von Muhlen MG et al (2010) Label-free biomarker sensing in undiluted serum with suspended microchannel resonators. Anal Chem 82:1905–1910
138. Zani A et al (2011) A New Electrochemical Multiplexed Assay for PSA Cancer Marker Detection. Electroanalysis 23:91–99
139. Fragoso A et al (2010) Integrated microfluidic platform for the electrochemical detection of breast cancer markers in patient serum samples. Lab Chip 11(4):625–631
140. Kellner C et al (2011) Automated microsystem for electrochemical detection of cancer markers. Electrophoresis 32:926–930
141. O'Sullivan A et al (2011) Cost Estimation of Cardiovascular Disease Events in the US. Pharmacoeconomics 29(8):693–704
142. McDonnell B et al (2009) Cardiac biomarkers and the case for point-of-care testing. Clin Biochem 42:549–561
143. Mohammed MI, Desmulliez MPY (2010) Lab-on-a-chip based immunosensor principles and technologies for the detection of cardiac biomarkers: a review. Lab Chip 11(4):569–595
144. Wu AHB et al (2004) Evaluation of a point-of-care assay for cardiac markers for patients suspected of acute myocardial infarction. Clin Chim Acta 346:211–219
145. Ordonez-Llanos J et al (2006) Risk stratification of chest pain patients by point-of-care cardiac troponin T and myoglobin measured in the emergency department. Clin Chim Acta 365:93–97
146. James SK et al (2004) A rapid troponin I assay is not optimal for determination of troponin status and prediction of subsequent cardiac events at suspicion of unstable coronary syndromes. Int J Cardiol 93:113–120
147. Cramer GE et al (2007) Lack of concordance between a rapid bedside and conventional laboratory method of cardiac troponin testing: impact on risk stratification of patients suspected of acute coronary syndrome. Clin Chim Acta 381:164–166
148. Jönsson C et al (2008) Silane–dextran chemistry on lateral flow polymer chips for immunoassays. Lab Chip 8:1191–1197
149. Gervais L, Delamarche E (2009) Toward one-step point-of-care immunodiagnostics using capillary-driven microfluidics and PDMS substrates. Lab Chip 9:3330–3337
150. Hong B et al (2008) Highly sensitive rapid, reliable, and automatic cardiovascular disease diagnosis with nanoparticle fluorescence enhancer and MEMS. Adv Exp Med Biol 614:265–273
151. Bhattacharyya A, Klapperich CM (2007) Design and testing of a disposable microfluidic chemiluminescent immunoassay for disease biomarkers in human serum samples. Biomed Microdevices 9:245–251
152. Cho IH et al (2009) Chemiluminometric enzyme-linked immunosorbent assays (ELISA)-on-a-chip biosensor based on cross-flow chromatography. Anal Chim Acta 632:247–255
153. Huang H et al (2009) Rapid analysis of alpha-fetoprotein by chemiluminescence microfluidic immunoassay system based on super-paramagnetic microbeads. Biomed Microdevices 11:213–216
154. Sista R et al (2008) Development of a digital microfluidic platform for point of care testing. Lab Chip 8:2091–2104
155. Kurita R et al (2006) On-chip enzyme immunoassay of a cardiac marker using a microfluidic device combined with a portable surface plasmon resonance system. Anal Chem 78:5525–5531
156. Tweedie M et al (2006) Fabrication of impedimetric sensors for label-free Point-of-Care immunoassay cardiac marker systems, with passive microfluidic delivery. IEEE 1: 4610–4614
157. Christenson RH, Azzazy HME (2009) Cardiac point of care testing: a focused review of current National Academy of Clinical Biochemistry guidelines and measurement platforms. Clin Biochem 42:150–157
158. Billah M, Hays HCW, Millner PA (2008) Development of a myoglobin impedimetric immunosensor based on mixed self-assembled monolayer onto gold. Microchimica Acta 160:447–454
159. Zhou F et al (2010) Electrochemical Immunosensor for Simultaneous Detection of Dual Cardiac Markers Based on a Poly (Dimethylsiloxane)-Gold Nanoparticles

Composite Microfluidic Chip: A Proof of Principle. Clin Chem 56:1701–1707

160. Chen X et al (2008) Electrochemical impedance immunosensor based on three-dimensionally ordered macroporous gold film. Anal Chem 80:2133–2140
161. Mitsakakis K, Gizeli E (2011) Detection of multiple cardiac markers with an integrated acoustic platform for cardiovascular risk assessment. Anal Chim Acta 699(1):1–5
162. Hong J, Edel JB, deMello AJ (2009) Micro- and nanofluidic systems for high-throughput biological screening. Drug Discov Today 14:134–146
163. Liu J et al (2009) In Situ Microarray Fabrication and Analysis Using a Microfluidic Flow Cell Array Integrated with Surface Plasmon Resonance Microscopy. Anal Chem 81:4296–4301
164. Caliper LifeSciences-Target ID/Validation Applications. http://www.perkinelmer.com/industries/lifesciencesresearch/default.xhtml. Accessed 26 May 2011
165. The FilmArray Respiratory Panel. http://www.biofiredx.com/FilmArray/RespiratoryTest.html. Accessed 12 Nov 2012
166. (2011) search issued patents for "microfluidic" in title or abstract, United States Patent and Trademark office.
167. Mark D et al (2010) Microfluidic lab-on-a-chip platforms: requirements, characteristics and applications. Chem Soc Rev 39:1153–1182
168. Becker H (2009) It's the economy. Lab Chip 9:2759–2762
169. Kim L (2011) FluidicMEMS.com's list of microfluidics/lab-on-a-chip companies. http://fluidicmems.com/list-of-microfluidics-lab-on-a-chip-and-biomems-companies. Accessed 12 Nov 2012

CHAPTER 3

PLATINUM FUNCTIONALIZED TITANIA NANOTUBE ARRAY SENSOR FOR DETECTION OF TRICHLOROETHYLENE IN WATER

©2013 IEEE. Reprinted, with permission, from Harikrishnan Jayamohan, York R. Smith, Bruce K. Gale, Manoranjan Misra, and Swomitra K. Mohanty, Platinum functionalized titania nanotube array sensor for detection of Trichloroethylene in water, Proceedings of IEEE SENSORS 2013, November 2013, DOI:10.1109/ICSENS.2013.6688608.

Platinum functionalized Titania Nanotube Array Sensor for Detection of Trichloroethylene in Water

Harikrishnan Jayamohan*, York R. Smith†, Bruce K. Gale*, Manoranjan Misra† and Swomitra K. Mohanty‡
*Department of Mechanical Engineering
University of Utah, Salt Lake City, UT 84112
†Metallurgical Engineering Department, University of Utah, UT 84112, USA
‡Chemical Engineering Department, University of Utah, UT 84112, USA
Email: swomitra@chemeng.utah.edu

***Abstract*— A sensor using platinum functionalized titania nanotubes for the detection of Trichloroethylene (TCE) in water samples has been developed. The titania nanotubes were synthesized using an electrochemical anodization technique and platinum was photocatalytically deposited on the nanotubes. The sensor exhibits a good response to TCE concentrations in the range of 10 to 1000 ppm.**

I. Introduction

Chlorinated solvents are a type of chemical that is used in industrial processes (i.e. Aerospace and Electronics Industry, Dry Cleaning) and common household consumer products. They are found in products such as shoe polish, degreasers, waxes, pesticides, drain cleaners and oven cleaners. Unfortunately these chemicals have found their way into groundwater contaminating water sources around the United States and around the world [1]. This is a problem due to the associated toxic and carcinogenic effects these compounds have on the general population [2]. The Environmental Protection Agency (EPA) has estimated that volatile organic compounds (VOCs) are found in an estimated one-fifth of United States water supplies [3]. According to the US Geological Survey estimates, VOC levels were found to be in excess of federal drinking water criteria in about 6 percent of urban wells and 1.5 percent of rural wells. Among VOCs, Trichloroethylene (TCE) is a major ground-water pollutant and found to be present in about 1400 military properties around the US [4]. The actual amount of human exposure to the VOCs like TCE remains uncertain, pointing to a need for point-of-use TCE sensor [5].

The detection of TCE-gas (air, nitrogen, oxygen, argon) mixtures has been widely reported with detection limits in range of pph (parts-per-hundred) [5], down to 1 ppm (parts-per-million) [6]. However, the operating temperatures of these sensors are in the range of 100-400 °C [7], making it power intensive and less amenable for field-based sensing. None of the above sensors have been used to detect TCE levels in water based samples.

Conventional methods for detection of VOCs from water are traditionally performed in central laboratories using sophisticated lab equipment such as gas chromatography (GC) and mass spectroscopy (MS). While these methods are highly sensitive and quantitative, they are not appropriate for field use due to the complexity of the instrument and cost. It is not possible to detect TCE in water using electrochemical methods with a conventional precious metal working electrode, since the reduction potential of TCE is much higher than water. TCE sensors using immobilized microbial membrane have been widely reported and have excellent sensitivity [8], [9]. But these sensors suffer from issues such as complicated preparation process, a long response time and a short shelf-life time [10]. Chen et al. reported a lead modified Platinum-Titanium thin film with detection limit of 100 ppm for TCE in water [11].

Oxide semiconductor nanomaterials have been shown to be effective in detecting VOCs due to their high specific surface area and good selectivity [12]. Titania nanotube array (TNA) have received significant interest due to ease of synthesis and tunable size (nanotube diameter and length) over other methods [13]. Sensors based on TNA have been demonstrated in the detection of gases such as hydrogen, oxygen and organic vapors like toluene, ethanol and formaldehyde [14]–[17]. In this work, detection of TCE in water using Platinum (Pt) functionalized TNA (Pt/TNA) (Figure 2) has been discussed. The TCE is purged from the water using a carrier gas (air) and carried over to the Pt/TNA sensor. When the TCE in carrier air reacts with the Pt functionalized nanotubes, an order of magnitude change in current is measured using a simple potentiostat. This change in current is correlated to the level of TCE present in solution. The sensitivity (S) of the Pt/TNA sensor is calculated as the ratio of change in current ($I_{TCE\,in\,water}$) when the TCE-water vapor mix is introduced to the baseline current in air (I_{Air}):

$$S = \frac{I_{\text{TCE in water}}}{I_{\text{Air}}} \tag{1}$$

II. Materials and Methods

A. Fabrication of TNA

TNA were synthesized by electrochemical anodization similar to previously reported protocols [18]. In summary, Ti foils (0.1 mm thick) were anodized under magnetic stiring in an electrolytic solution consisting of ethylene glycol (Fisher Scientific, Waltham, MA), deionized (DI) water (3 wt. %) and ammonium fluoride (0.5 wt.%, Fischer Scientific). A two-electrode configuration with platinum (Pt) foil as the cathode

was used for anodization. The anodization was carried out at an applied potential of 45 V(D.C.) (Agilent, E3647A) for 60 minutes and subsequently annealed in oxygen (O_2) at 500°C (ramp up at a rate of 1.6 C/min from 25°C) for 2 hours.

B. Pt functionalization of TNA

The annealed TNA were functionalized with metallic Pt nanoparticles via photocatalytic reduction of chloroplatinic acid [19]. Annealed TNA were immersed in a 2mM solution of chloroplatinic acid ($H_2PtCl_6 \cdot 6H_2O$) (Aldrich), in a 50/50 mixture of methanol and water, then subject to UV irradiation (365 nm, 100-W UV lamp) for one hour [20]. The Pt ions in solution are reduced at the TNA surface to form metallic platinum deposits (5-10 nm) as seen in Figure 2. The methanol in solution serves as a scavenger of photo-induced holes. Functionalization of the sensor using nanosized Pt catalyst has shown to improve the response of semiconductor sensors during detection of VOCs [6]. Subsequent to the deposition, one side of the Pt/TNA strip was polished manually with sand-paper and washed in DI water to remove the Pt-Nanotubes and to expose the underlying bare Titanium (Ti) metal (in effect forming a Pt on nanotubes on Ti structure). The morphology of TNAs after functionalization with Pt was analyzed using a field emission scanning electron microscope (FESEM) (Hitachi, S-4800). Energy dispersive x-ray spectroscopy (EDX) analysis of a 25 by 20 μm area of the sample was obtained using an Oxford detector. X-ray diffraction (Rigaku MiniFlex 600) was used to confirm the crystalline phases of the annealed Pt/TNA.

C. Amperometric detection of TCE

The experimental setup for detection of TCE in water is shown in Figure 1. It comprised of an inlet air, a mass flow controller (MFC), potentiostat and detection chamber. The sensor, a 50 mm^2 Pt/TNA strip connected via alligator clips to the external potentiostat (Gamry Reference 600) is placed inside the detection chamber. A low bias voltage of -1 V (two electrode system) is applied using the potentiostat and the current response is measured. Different concentrations of TCE in DI water were prepared in a Büchner flask (250 ml). Air (at 120 Standard Cubic Centimeters per Minute/SCCM controlled using MFC) was bubbled through the respective TCE-DI water solution for 15 seconds and delivered to the sensor through a brass nozzle. This is similar to the protocol used for purging VOCs from water based samples for detection in a Purge and Trap GC/MS system. The TCE-DI water solution was heated to 50°C to enhance TCE transport from the solution to air. After the 15 second detection interval, TCE-DI water vapor flow is cut and air is introduced over the sensor. Experiments were also run with air bubbled through DI water as a negative control (0 ppm TCE). All experiments were conducted at room temperature.

III. Results

The FESEM images of TNA functionalized with Pt and annealed in O_2 are shown in Figure 2. The nanotubes are approximately 1-1.4 μm in length, with a pore diameter of

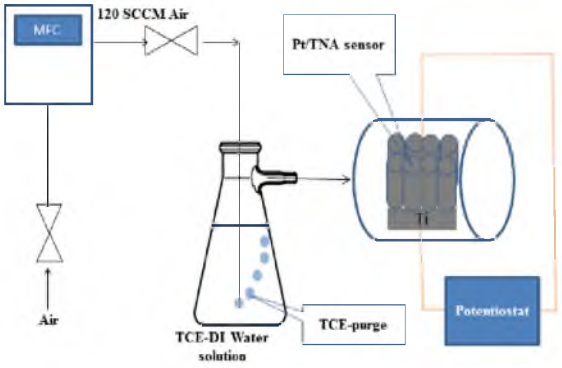

Fig. 1. Experimental set-up for TCE detection. TCE-DI water mixture is placed in a Büchner flask. Air at 120 SCCM is bubbled through the solution and delivered to the Pt/TNA sensor

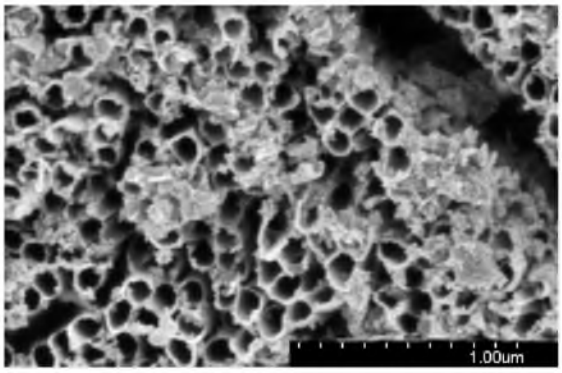

Fig. 2. TNA functionalized with Pt. The deposited Pt particles as well as agglomerates are seen on the walls of TNA

90-100 nm and tube wall thickness of 10-20 nm. From the images, the photocatalytically deposited Pt particles as well as agglomerates can be seen on the walls of TNA. EDX analysis (Figure 3) shows the percentage of Pt to be about 0.3 % wt. in addition to presence of titanium, oxygen and carbon. The presence of carbon is due to anodization in ethylene glycol solution [18].

X-ray diffraction patterns of O_2 annealed TNA samples (not shown) confirmed the predominantly anatase phase TiO_2. TNA samples annealed at 400-500°C in (O_2) have shown to exhibit higher sensitivity of gases like formaldehyde compared to as-prepared (amorphous) TNA samples [17].

Figure 4 shows the current response of the Pt/TNA sensor, when air is bubbled through 10 ppm TCE solution to the sensor. During the Stage I, air (120 SCCM) is introduced over the sensor and the current response represents the baseline (I_{Air}). During the Stage II, air bubbled (at 120 SCCM) through 10 ppm TCE-DI water solution is introduced over the sensor for 15 seconds. An instantaneous (<10 seconds) increase in current response is seen and reaches a maximum value

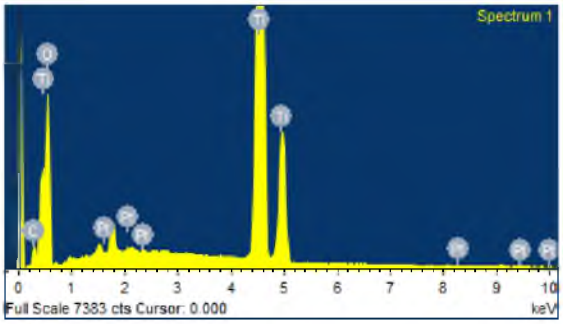

Fig. 3. EDX analysis of the sample showing presence of Pt

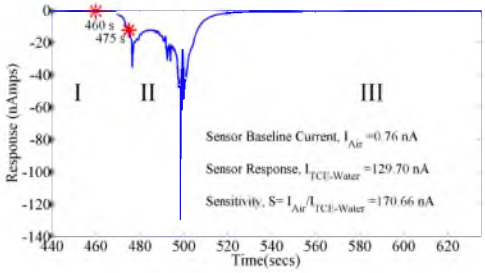

Fig. 4. Potentiostatic (I vs. t) response of Pt/TNA sensor to 10 ppm TCE in water. A representative cycle of 120 s is shown in the figure. The cycle is divided into three stages. Stage I shows the baseline current when air is introduced over the sensor. The current increases (Stage II) when TCE-water vapor is introduced over the sensor for 15 seconds (t=460 to 475 seconds). An instantaneous increase in current response in noticed. The current starts to drop after 40 seconds (t=500 seconds) and drops to 10% of original value after 170 seconds (t=633 seconds) (Stage III)

($I_{TCE\,in\,water}$). Subsequently, the current starts to decrease and goes back to the baseline current after 170 seconds. Figure 5 shows the sensitivity (equation (1)) of the Pt/TNA sensor to different concentrations of TCE in water, ranging from 0 ppm to 1000 ppm. The response time (time taken for the sensor to reach maximum current from the time of injection of air through solution) is around 38 seconds. The non-zero value of response at 0 ppm TCE is likely due to the presence of dissolved gases in adsorbed water molecules on the sensor surface, which are known to change the conductivity of metal oxide sensors [17].

The sensing mechanism of Pt/TNA is based on the reaction of TCE with the chemisorbed reactive oxygen species (primarily O^-) on the surface of the sensor [7], [21]. This reaction leads to a pooling of electrons and causes a change in conductance through the sensor which leads to a change in current. The reaction of TCE with adsorbed O^-, for example, is expressed as:

$$C_2HCl_3 + O^- \longrightarrow C_2HOCl_3(g) + e^- \qquad (2)$$

The higher specific surface area of TNA helps increase the

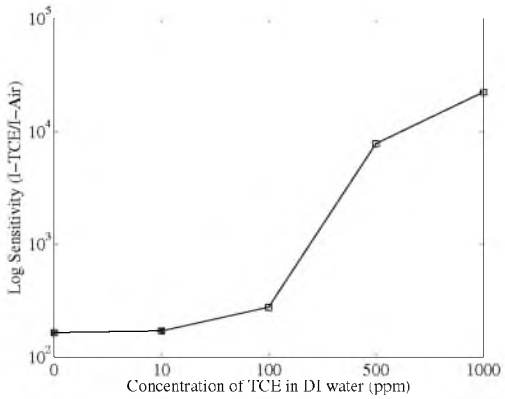

Fig. 5. Log plot of Pt/TNA sensor sensitivity to TCE concentrations (0-1000 ppm in water)

sensitivity to TCE due to increased amount of chemisorbed O_2 via enhanced diffusion.

The Pt deposited on TNA (semiconductor oxide) forms a Schottky contact [22], [23]. This results in an alignment of the Fermi-surface of TiO_2 and Pt, inducing band-bending, leading to a reduction of Schottky-barrier height [22]. This decrease in barrier height could be the reason for good response of the Pt/TNT sensor to TCE at room temperature operation.

IV. Conclusion

In summary, a Pt functionalized TNA sensor for detection of TCE in water sample is reported. The sensor operating at room temperature shows response to TCE in water at concentrations ranging from 10 ppm to 1000 ppm. This is in the concentration range of TCE contamination in sites around the United States [24], [25] and hence can be easily incorporated into a field-based sensor.

References

[1] A. for toxic substances and disease registry, "Publich Health Assessment for Hidden Lane Landfill, Sterling, Loudoun County, Virginia," 2009.

[2] J. Fagliano, M. Berry, F. Bove, and T.Burke, "Drinking water contamination and the incidence of leukemia: an ecologic study," *Am. J. Public Health*, vol. 80, no. 10, pp. 1209–1212, 1990.

[3] B. Himes, "Community meeting to discuss next steps - River Valley ground water contamination site, North Platte, Nebraska," 2006.

[4] L. Siegel, "When is enough, enough? Community perspectives on groundwater treatment at Department of Defense facilities," 2008.

[5] L. Yadava, R. Verma, and R. Singh, "Detection and sensing mechanism of acetone with modeling using Pd/TiO2/Si structure," *Thin Solid Films*, vol. 520, no. 7, pp. 3039–3042, 2012.

[6] M. Kadosaki, Y. Saka, I. Takamura, I. Matsubara, and T. Itoh, "Development of an oxide semiconductor thick film gas sensor for the detection of total volatile organic compounds," *Electronics and Communications in Japan*, vol. 93, no. 10, pp. 125–130, 2010.

[7] S. Ahmadnia-Feyzabad, A. Khodadadi, M. Vesali-Naseh, and Y. Mortazavi, "Highly sensitive and selective sensors to volatile organic compounds using MWCNTs/SnO_2," *Sens. Actuators B"*, vol. 166, pp. 150–155, 2012.

[8] M. Hnaien, F. Lagarde, J. Bausells, and A. E. N. Jaffrezic-Renault, "Impedimetric microbial biosensor based on single wall carbon nanotube modified microelectrodes for trichloroethylene detection," *Electrochim. Acta.*, vol. 56, no. 28, p. 1035310358, 2011.

[9] M. Hnaiena, S. Bourigua, F. Bessueille, J. Bausells, A. Errachid, F. Lagarde, and N. Jaffrezic-Renault, "A new bacterial biosensor for trichloroethylene detection based on a three-dimensional carbon nanotubes bioarchitecture," *Anal. Bioanal. Chem.*, vol. 400, no. 4, p. 10831092, 2011.

[10] M. Chen, C. Liu, and T. Chou, "Thin film trichloroethylene electrochemical sensor," *Biosens. Bioelectron.*, vol. 20, no. 1, pp. 25–32, 2004.

[11] M. Chen, T. Lin, and T. Chou, "Trichloroethylene sensor by using electrodeposited Pb-modified graphite strip electrode," *J. Electrochem. Soc.*, vol. 149, no. 3, pp. H87–H92, 2002.

[12] J. Zheng, Z. Xue, S. Li, S. Li, and Z. Rao, "Development of trichloroethylene gaseous sensor utilizing ZnO-Y_2O_3 as nanocatalyst based on thermal desorption/cataluminescence," *Anal. Methods*, vol. 4, pp. 2791–2796, 2012. [Online]. Available: http://dx.doi.org/10.1039/C2AY25351H

[13] S. Banerjee, S. Mohapatra, M. Misra, and I. Mishra, "The detection of improvised nonmilitary peroxide based explosives using a titania nanotube array sensor," *Nanotechnology*, vol. 20, no. 7, p. 075502, 2009.

[14] M. Seo, M. Yuasa, T. Kida, J. Huh, N. Yamazoe, and K. Shimanoe, "Microstructure control of TiO_2 nanotubular films for improved VOC sensing," *Sens. Actuators B*, vol. 154, no. 2, pp. 251–256, 2011.

[15] O. Varghese, D. Gong, M. Paulose, K. Ong, and C. Grimes, "Hydrogen sensing using titania nanotubes," *Sens. Actuators B*, vol. 93, no. 1, pp. 338–344, 2003.

[16] H. F. Lu, F. Li, G. Liu, Z. Chen, D. Wang, H. Fang, G. Lu, Z. Jiang, and H.M.Cheng, "Amorphous TiO_2 nanotube arrays for low-temperature oxygen sensors," *Nanotechnology*, vol. 19, no. 40, p. 405504, 2008.

[17] S. Lin, D. Li, J. Wu, and S. Akbar, "A selective room temperature formaldehyde gas sensor using TiO_2 nanotube arrays," *Sens. Actuator B*, vol. 156, no. 2, pp. 505–509, 2011.

[18] S. Mohapatra, M. Misra, V. Mahajan, and K. Raja, "Design of a highly efficient photoelectrolytic cell for hydrogen generation by water splitting: Application of $TiO_{2-x}C_x$ nanotubes as a photoanode and Pt/TiO_2 nanotubes as a cathode," *The Journal of Physical Chemistry C*, vol. 111, no. 24, pp. 8677–8685, 2007. [Online]. Available: http://pubs.acs.org/doi/abs/10.1021/jp071906v

[19] E. Bae and W. Choi, "Highly enhanced photoreductive degradation of perchlorinated compounds on dye-sensitized metal/TiO_2 under visible light," *Environ. Sci. Technol.*, vol. 37, no. 1, pp. 147–152, 2003. [Online]. Available: http://pubs.acs.org/doi/abs/10.1021/es025617q

[20] F. Zhang, J. Chen, X. Zhang, W. Gao, R. Jin, N. Guan, and Y. Li, "Synthesis of titania-supported platinum catalyst: The effect of pH on morphology control and valence state during photodeposition," *Langmuir*, vol. 20, no. 21, pp. 9329–9334, 2004. [Online]. Available: http://pubs.acs.org/doi/abs/10.1021/la049394o

[21] B. Zhu, C. Xie, W. Wang, K. Huang, and J. Hu, "Improvement in gas sensitivity of ZnO thick film to volatile organic compounds (VOCs) by adding TiO_2," *Materials Letters*, vol. 58, no. 5, pp. 624–629, 2004.

[22] S. Kandasamy, A. Trinchi, W. Wlodarski, E. Comini, and G. Sberveglier, "Study of Pt/TiO2/SiC schottky diode based gas sensor," in *Proc. IEEE (Sensors '04)*, Oct. 2004, pp. 738–741.

[23] H. Chen, S. Chen, X. Quan, H. Yu, H. Zhaon, and Y. Zhang, "Fabrication of TiO_2Pt coaxial nanotube array schottky structures for enhanced photocatalytic degradation of phenol in aqueous solution," *J Phys. Chem. C*, vol. 112, no. 25, pp. 9285–9290, 2008. [Online]. Available: http://pubs.acs.org/doi/abs/10.1021/jp8011393

[24] Oregon Department of Environmental Quality, "Site summary report - details for site ID 2424, Wirfs property," 2006.

[25] J. Deuren, T. Lloyd, S. Chhetry, and J. P. R. Liou, "Remediation technologies screening matrix and reference guide, 4^{th} edition," 2002.

CHAPTER 4

HIGHLY SENSITIVE BACTERIA QUANTIFICATION USING IMMUNOMAGNETIC SEPARATION AND ELECTROCHEMICAL DETECTION OF GUANINE-LABELED SECONDARY BEADS

This paper was published in the peer-reviewed open access journal Sensors, 2015, 15(5), 12034-12052, DOI:10.3390/s150512034. Authors are Harikrishnan Jayamohan, Bruce K. Gale, B.J. Minson, Christopher J. Lambert, and Himanshu J. Sant.

Sensors **2015**, *15*, 12034-12052; doi:10.3390/s150512034

OPEN ACCESS
sensors
ISSN 1424-8220
www.mdpi.com/journal/sensors

Article

Highly Sensitive Bacteria Quantification Using Immunomagnetic Separation and Electrochemical Detection of Guanine-Labeled Secondary Beads

Harikrishnan Jayamohan [1,*], Bruce K. Gale [1,2], Bj Minson [2], Christopher J. Lambert [3], Neil Gordon [4] and Himanshu J. Sant [1,2,*]

[1] Department of Mechanical Engineering, University of Utah, Salt Lake City, UT 84112, USA; E-Mail: bruce.gale@utah.edu
[2] Espira Inc., 825 N 300 W Suite N-223, Salt Lake City, UT 84103, USA; E-Mail: bjminson@gmail.com
[3] Department of Bioengineering, University of Utah, Salt Lake City, UT 84112, USA; E-Mail: chris.lambert@utah.edu
[4] Guanine Inc., Salt Lake City, UT 84103, USA; E-Mail: neil.gordon@guanineinc.com

* Authors to whom correspondence should be addressed; E-Mails: hari.jayamohan@utah.edu (H.J.); himanshu.sant@utah.edu (H.J.S.); Tel.: +1-801-585-5944 (H.J.S.); Fax: +1-801-585-9826 (H.J.S.).

Academic Editor: Stephane Evoy

Received: 23 March 2015 / Accepted: 7 May 2015 / Published: 22 May 2015

Abstract: In this paper, we report the ultra-sensitive indirect electrochemical detection of *E. coli* O157:H7 using antibody functionalized primary (magnetic) beads for capture and polyguanine (polyG) oligonucleotide functionalized secondary (polystyrene) beads as an electrochemical tag. Vacuum filtration in combination with *E. coli* O157:H7 specific antibody modified magnetic beads were used for extraction of *E. coli* O157:H7 from 100 mL samples. The magnetic bead conjugated *E. coli* O157:H7 cells were then attached to polyG functionalized secondary beads to form a sandwich complex (magnetic bead/*E. coli*/ secondary bead). While the use of magnetic beads for immuno-based capture is well characterized, the use of oligonucleotide functionalized secondary beads helps combine amplification and potential multiplexing into the system. The antibody functionalized secondary beads can be easily modified with a different antibody to detect other pathogens from the same sample and enable potential multiplexing. The polyGs on the secondary beads enable signal amplification up to 10^8 guanine tags per secondary bead (7.5×10^6 biotin-FITC per secondary bead, 20 guanines per oligonucleotide) bound to the target (*E. coli*). A

single-stranded DNA probe functionalized reduced graphene oxide modified glassy carbon electrode was used to bind the polyGs on the secondary beads. Fluorescent imaging was performed to confirm the hybridization of the complex to the electrode surface. Differential pulse voltammetry (DPV) was used to quantify the amount of polyG involved in the hybridization event with tris(2,2'-bipyridine)ruthenium(II) ($Ru(bpy)_3^{2+}$) as the mediator. The amount of polyG signal can be correlated to the amount of *E. coli* O157:H7 in the sample. The method was able to detect concentrations of *E. coli* O157:H7 down to 3 CFU/100 mL, which is 67 times lower than the most sensitive technique reported in literature. The signal to noise ratio for this work was 3. We also demonstrate the use of the protocol for detection of *E. coli* O157:H7 seeded in waste water effluent samples.

Keywords: *Escherichia coli* O157:H7 detection; biosensors; pathogen detection; electrochemical detection; differential pulse voltammetry; immunomagnetic separation

1. Introduction

Food and water-borne diseases are a major source of concern worldwide. According to the World Health Organization, gastrointestinal infections kill around 2.2 million people globally each year [1]. The pathogenic strains of *E. coli* such as O157:H7 are a major source of food and water-borne disease outbreaks around the world [2]. As Escherichia coli (*E. coli*) is a bacterium found in the lower intestine of warm-blooded organisms, it is considered an indicator organism to test environmental samples for fecal contamination [3]. Even low levels of *E. coli* O157:H7 (10–100 viable organisms) can cause human infections [2,4].

Current methods of *E. coli* detection involve conventional techniques like membrane filtration, plate counting [5], turbidimetry and multiple-tube fermentation. These techniques though reliable, are time consuming (24–48 h), complex and require trained personnel [6]. Additionally, none of these techniques are suitable for point-of-use, which is essential in monitoring pathogenic bacteria in geographically remote locations. Recently, biosensing methods including electronic [7], mass-based [8], optical [9,10] and electrochemical (EC) techniques [11–13] have been applied for detecting pathogenic bacteria [4,14]. Among these, EC methods are increasingly relied upon due to advantages like simplicity, accuracy, fast response, low cost, and portability [4,6]. EC sensors can also be integrated on a chip and can be multiplexed for detecting multiple pathogens and strains [15].

EC detection has been shown to be very sensitive in the detection of *E. coli*. Han *et al.* reported an EC immunosensor for *E. coli* using graphene oxide-Ag nanoparticle composite labels with limits of detection down to 10 colony-forming units (CFU) per mL [6]. dos Santos recently reported a limit of detection of 2 CFU/mL using an electrochemical impedance spectroscopy based immunosensor [4]. Note, though that, environmental standards for *E. coli* in water are mostly defined for 100 mL samples. For instance, the U.S Environmental Protection Agency defines protocols for testing *E. coli* limits in the Clean Water Act for 100 mL sampling volumes [16–18], most likely because 1 mL would not be statistically representative of the volumes involved. In addition, real world samples experience interference from

the sample matrix and background microflora, making isolation and detection of bacterial pathogens more challenging [19]. We have coupled immunomagnetic capture and EC detection to enable sensitive detection of *E. coli* from waste water effluent (Figure 1).

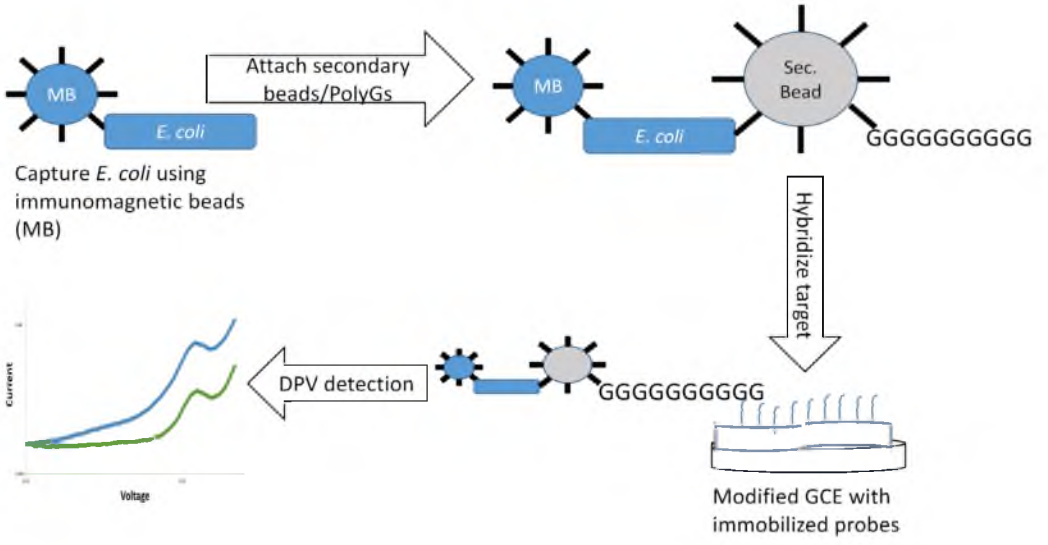

Figure 1. Working principle of the *E. coli* detection mechanism.

Immunoaffinity capture techniques, like immunomagnetic separations (IMS), have been applied to isolate and concentrate *E. coli* from water samples [20]. These techniques purify *E. coli* and remove contaminants that might interfere with *E. coli* detection signals during subsequent detection assays [19]. Sample purification also reduces the incidence of false positive and false negative test results by removing virtually all inhibiting materials that could be incorrectly detected. IMS has also been incorporated into microfluidic point-of-use systems and the process can be automated [21,22]. Zhu *et al.* applied IMS coupled with fluorescent detection (using a spectrofluorometer) of *E. coli* O157:H7 and obtained a limit of detection of 10 CFU/mL [19]. However fluorescent detection requires related optical detection equipment, which is often not miniaturized making the approach less amenable for point-of-use [23–25]. Immunomagnetic beads have been used to capture *E. coli* and subsequently detect the bacteria using electrochemical methods without secondary bead based amplification [26]. To achieve ultra-sensitive detection of pathogens, a signal amplification step was incorporated to the IMS. Nam *et al.* reported the use of immunomagnetic capture combined with secondary beads (bio-barcodes) for signal amplification in the detection of DNA and proteins [27,28]. The work relied on optical methods for detection of the bio-barcodes.

The use of electrochemical methods using bio-barcodes has been reported for the detection of proteins and DNA, including DNA from pathogens (Figure 2) [29–34]. Some of these methods have relied on non-oligonucleotide based electrochemical labels for detection. For instance, Ding *et al.* reported the use of cadmium sulfide nanoparticles as electrochemical labels for the detection of human α-fetoprotein [32]. Zhang *et al.* applied lead sulfide and cadmium sulfide as electrochemical labels for the detection of *Bacillus anthracis* and *Salmonella enteritidis* [33]. The use of metal nanoparticles as electrochemical

labels has disadvantages vis-a-vis oligonucleotides with regard to multiplexing capabilities. The number of entities that can be simultaneously detected is restricted by the number of metals that have a peak potential (ΔE_p) within a given electrochemical range. For instance, the use of Pb^{2+} (anodic oxidation $\Delta E_p = -0.61$ V) and Cd^{2+} (anodic oxidation $\Delta E_p = -0.87$ V) as electrochemical labels restricts the use of any other label with peak potential in between these due to issues with peak separation. In contrast, using oligonucleotide electrochemical labels provides multiplexing possibilities limited only by the number of electrodes with complimentary probes on them. The use of metal nanoparticles also involves an additional step of dissolution of the EC marker from the beads onto the electrodes for detection. Wang *et al.* reported the use of guanine tagged polymeric beads for the detection of proteins [30]. However the guanine tags had to be released from the beads for detection using potentiometric stripping. By releasing the guanine, there was no possibility of distinguishing the tags from different analytes for potential multiplexing. This method, although it enables amplification of the detection signal, does not enable multiplexing. In contrast, keeping oligonucleotide EC labels intact provides multiplexing possibilities with complementary probes on individual working electrodes assigned to specific analytes.

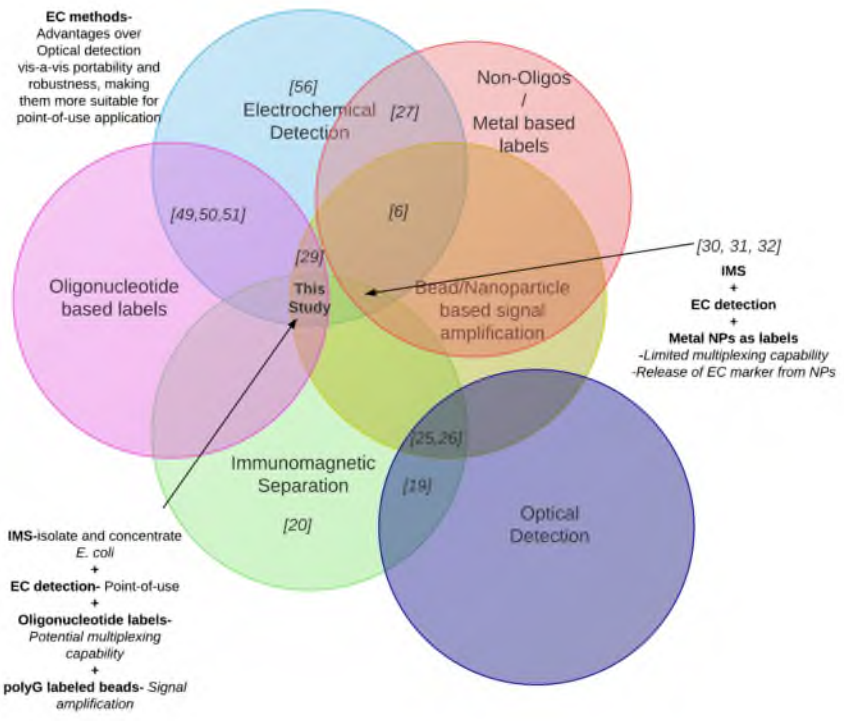

Figure 2. Review of recent point-of-use methods used for detection of proteins and DNA sequences.

In this paper, we report the use of immunomagnetic capture coupled with amplification and indirect EC detection of *E. coli* O157:H7 on an electrochemically reduced graphene oxide glassy carbon

electrode (RGO-GCE). *E. coli* O157:H7 specific antibodies coated magnetic beads were used to capture *E. coli* O157:H7 strains from water samples. The use of polyG functionalized secondary beads in addition to the magnetic beads incorporates signal amplification and potential multiplexing capability. To enable multiplexing and amplification we use synthetic polyguanine oligonucleotides (polyG) as an EC tag and amplification system. The use of biobarcode based signal amplification enables higher sensitivity due to the large number of DNA strands in each single molecular binding event [27,28,35,36]. The bacteria collected using magnetic beads is attached to another set of *E. coli* O157:H7 antibody functionalized nonmagnetic polystyrene (secondary) beads. These secondary beads have an EC tag (polyGs) that can be correlated to the *E. coli* O157:H7 concentration in the sample. The nonmagnetic secondary beads can be easily modified with a different antibody to capture a different pathogen. By using a different polyG sequence on the secondary beads (and using corresponding complementary probe sequence on the RGO-GCE electrode), the system can be modified to detect multiple pathogens. After washing steps, we transfer this complex (magnetic beads, bacteria, and nonmagnetic beads) to the RGO-GCE electrode. These polyGs are hybridized with complementary probes on the electrode surface and upon an EC scan generate a guanine oxidation signal that is correlated to *E. coli* O157:H7 concentration in the sample. Using the protocol we demonstrate detection of *E. coli* O157:H7 in phosphate buffered solution (PBS) and waste water samples. To the best of our knowledge, this is the first instance of combining IMS with oligonucleotide functionalized secondary bead based amplification for electrochemical detection of pathogens. The reported protocol is highly sensitive and selective, and can be potentially multiplexed for detecting multiple pathogens. The protocol has also been applied in the detection of *E. coli* O157:H7 in waste water samples.

2. Experimental Section

2.1. Working Principle of the E. coli O157:H7 Sensor

The mechanism of indirect sensing of *E. coli* O157:H7 is illustrated in Figure 3 [37]. The mechanism consists of four steps which are:

(I) Vacuum filtration to pre-concentrate the *E. coli* O157:H7 in 100 mL samples into a 1 mL sample volume
(II) IMS to selectively capture *E. coli* O157:H7
(III) Analyte amplification consisting of an EC polyG tag attached to secondary beads
(IV) EC detection of the polyG tags

In the IMS step, the bacteria sample is concentrated from water sample (PBS or waste water) by filtration and isolated using *E. coli* O157:H7 specific antibody coated magnetic beads. To enable amplification synthetic polyG oligos are used as an EC tag and amplification system. The bacteria collected using magnetic beads is attached to another set of secondary beads containing EC tag (polyG oligos) and can be correlated to the *E. coli* O157:H7 concentration in the sample. The sample is then washed to remove any unbound secondary beads. The magnetic bead/*E. coli*/secondary bead complexes are transferred to the EC detector and the polyGs on the secondary beads are hybridized with complementary probes on the electrode surface. A DPV scan generates a signal corresponding to

the polyGs on the secondary beads that is indirectly correlated to *E. coli* O157:H7 concentration in the sample. The probes on the electrode surface are specific to the polyGs on the secondary beads to ensure selectivity.

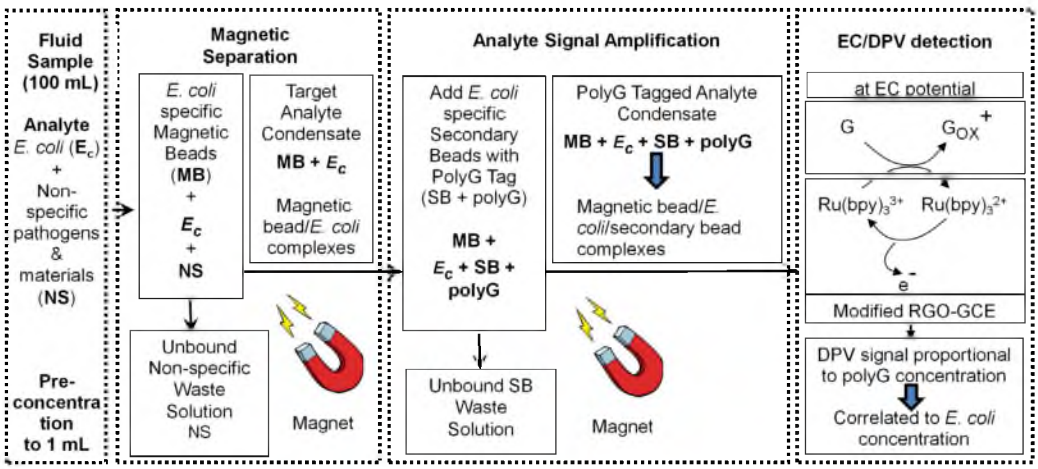

Figure 3. Mechanism of indirect sensing of *E. coli* O157:H7 using IMS and subsequent signal amplification using polyG functionalized secondary beads.

2.2. Apparatus and Reagents

EC deposition and differential pulse voltammetry (DPV) were carried out using a Gamry Reference 600 potentiostat (Gamry Instruments, Warminster, PA, USA). A conventional three-electrode system, which consisted of a modified glassy carbon electrode (GCE-3.0 mm diameter, Catalog no. MF-2012, BASi, West Lafayette, IN, USA) as a working electrode, an Ag/AgCl electrode as a reference electrode and a platinum mesh as an counter electrode, was employed for the DPV and EC deposition.

Graphene oxide for EC deposition was purchased from Graphene Supermarket (Calverton, NY, USA). *E. coli* O157:H7 nonpathogenic strain (Catalog no. 700728) was obtained from ATCC (Manassas, VA, USA). The *E. coli* O157:H7 antibody coated magnetic beads for pathogen extraction were obtained from Invitrogen (Dynabeads MAX *E. coli* O157 kit, Invitrogen, Carlsbad, CA, USA). The streptavidin coated polystyrene (secondary) beads were purchased from Bangs Laboratories (9.78 μm mean diameter, Catalog no. CP01N-11339, Bangs Laboratories Inc., Fishers, IN, USA). Biotin-labeled BacTrace anti-*E. coli* O157:H7 antibody was purchased from Kirkegaard and Perry Laboratories (Catalog no. 16-95-90, KPL Inc., Gaithersburg, MD, USA). Sulfo-NHS (N-hydroxysulfo-succinimide) and EDC (1-ethyl-3(3-dimethly aminopropyl) carbodiimide hydrochloride) were obtained from Pierce/Thermo Fisher Scientific (Rockford, IL, USA). Sodium hydroxide was ordered from Macron Fine Chemicals (Center Valley, PA, USA). Tris(2,2'-bipyridyl)ruthenium(II) chloride hexahydrate ($Ru(bpy)_3Cl_2$) was purchased from Sigma-Aldrich (Catalog no. 224758-1G, St. Louis, MO, USA). The oligonucleotides were obtained from DNA/Peptide synthesis core facility, University of Utah (Salt Lake City, UT, USA).

All reagents were of analytical grade and were used as received without further purification. Ultra-pure deionized (DI) water prepared by Purelab System (ELGA Purelab, UK) was used throughout the experiment.

2.3. Culturing of E. coli O157:H7

E. coli O157:H7 nonpathogenic strain (Catalog no. 700728) was obtained from ATCC. Using manufacturer-supplied protocols [38], the freeze dried pellet was reconstituted using Difco Nutrient Broth (Catalog no. 234000, Becton Dickinson, Sparks, MD, USA). The pellet was hydrated using 1 mL of the Difco Broth and then placed in 5 mL of additional broth. Then 200 µL was taken from the broth and placed on an agar plate prepared using Difco Nutrient Agar (Catalog no. 213000, Becton Dickinson, Sparks, MD, USA). The broth and agar plate were incubated at 37 °C for 36 h. After the incubation period the broth culture was preserved using a protocol supplied by ATCC. The culture broth was centrifuged at 1000 g for 10 min in order to compact the bacteria into a pellet. The broth supernatant was poured off and 3 mL of broth was added to the pellet. Then, 3 mL of sterilized 20% glycerol (vol/vol) was added to the culture. The culture was then placed in Nalgene Cryogenic vials (Thermo Scientific) and placed at −135 °C for storage. To prepare the samples, the stored *E. coli* O157:H7 was initially plated on agar plates for 16 h and subsequently collected using a sterile pipette tip. The *E. coli* O157:H7 was then vortexed with 10 mL of 1× PBS solution. About 2 mL of this solution was tested using a spectrophotometer (Biochrom WPA Biowave DNA spectrophotometer) and diluted as necessary to achieve an OD_{600} of 0.1 (corresponding to a concentration of approximately 50 million *E. coli* O157:H7 per mL). The spectrophotometer was calibrated for *E. coli* O157:H7 using a manual cytometer for bacterial counts before use. Then 100 µL of this solution was serially diluted in 1× PBS buffer to achieve different concentrations of 100 mL samples. The final concentration of *E. coli* O157:H7 was confirmed using plate counting.

2.4. Pre-Concentration of E. coli O157:H7 from Seeded PBS Buffer Sample

Vacuum filtration was employed to pre-concentrate the *E. coli* O157:H7 in 100 mL PBS samples into a 1 mL sample volume. A 0.1 µm Durapore membrane filter (Catalog no. VVLP04700, Millipore, Billerica, MA, USA) was securely held in a custom filtration device and attached to a 2000 mL filtering flask (Catalog no. 5340, Pyrex, Corning Inc., Corning, NY, USA). The flask was vacuum pressurized to −55 kPa and the 100 mL of the *E. coli* O157:H7 sample was loaded into a reservoir above the filtration device. The liquid sample was pulled through the filter trapping bacteria and solids larger than 0.1 µm. The filter was then removed from the device, inserted into a 1.5 mL Eppendorf tube containing 1 mL of 1× PBS and vortexed for a minute to free the bound bacteria. The filter was subsequently removed from the tube and IMS was followed on the 1 mL *E. coli*-PBS buffer sample. The initial and post-filtration *E. coli* O157:H7 samples were plated, incubated at 37 °C for 12 h, and subsequently counted to determine the efficiency of *E. coli* O157:H7 capture during the process.

2.5. Immunomagnetic Separation of E. coli O157:H7

E. coli O157:H7 specific antibody coated magnetic beads (Dynabeads) were used to extract the *E. coli* O157:H7 from the 1 mL samples [39]. Twenty µL of magnetic beads (Dynabeads) was added to the tubes containing 1 mL *E. coli* O157:H7 sample, placed on a Mini-Lab Roller (Labnet International Inc., Edison, NJ, USA) rotating mixer, and rotated at 24 rpm for 10 min. The tubes were inserted into a custom built magnetic capture unit for 3 min with occasional inversion to concentrate the beads into a pellet. Hundred µL of the supernatant solution was pipetted onto another agar plate to test for any *E. coli* O157:H7 not captured by the beads. The remainder of the supernatant was carefully pipetted out so as to not disturb the magnetic pellet. The tube was removed from the magnetic capture unit and 1 mL of 1× Dynabeads wash buffer was added to the tube and returned to the rotating mixer for 3 min. This process of mixing, plating 100 µL, removing supernatant, and washing with 1 mL of 1× buffer was repeated two more times for a total of 3 wash cycles. After the final wash was removed, 100 µL of 1× Dynabeads wash buffer was added to the magnetic beads, resuspended and plated on a final agar plate. The plates were incubated at 37 °C for 12 h before being counted to test the efficiency of magnetic bead extraction process.

While calibration of the spectrophotometer with the *E. coli* O157:H7 allowed for relatively accurate predictions of bacteria concentrations in the dilution series, bacteria samples from the dilution series were also plated in order to obtain the most accurate prediction of the original bacteria concentration of the tested sample.

2.6. Specificity of Immunomagnetic Separation

Three runs of immunomagnetic separation using *E. coli* O157:H7 specific antibody coated magnetic beads (Dynabeads) were performed on samples of 3000 CFUs of *Salmonella* in 1 mL of 1× PBS, similar to the protocol mentioned above. The magnetic beads were resuspended and plated on agar plates to determine the amount of *Salmonella* non-specifically bound to the *E. coli* O157:H7 specific antibody coated magnetic beads.

2.7. Secondary Beads Functionalization Chemistry

2.5 µL of 50 µM 20 m biotinylated polyG (GGGGGGGGGGGGGGGGGGGG/3′-Biotin) was added to 20 µL of streptavidin coated polystyrene (secondary) beads. Subsequently, 12.5 µL of 1 mg/mL anti-*E. coli* O157:H7 antibodies was added to the 20 µL of the polyG functionalized secondary beads [40].

2.8. Attachment of Secondary Beads to Magnetic Bead-E. coli O157:H7 Complexes

The magnetic bead and bacteria complex was bound to the *E. coli* O157:H7 antibody functionalized secondary nonmagnetic polystyrene bead. Magnetic bead/*E. coli* O157:H7 complex was resuspended in 20 µL of 1× PBS and then added to a 20 µL solution of resuspended secondary bead/polyG/antibody complex. The solution was pipet mixed every 5 to 7 min over a 20 min period.

2.9. Preparation of the Electrode-Electrodeposition of Graphene Oxide

We have applied electrodeposition to deposit graphene oxide on the bare GCE (Figure 4). Twenty five mg of graphene oxide was added to 50 mL of 0.1 M PBS. The graphene oxide (GO) in solution was exfoliated by ultra-sonication for 30 min to form a homogeneous brown colloidal dispersion with a concentration of 0.5 mg/mL. The GO in solution was electrodeposited on the GCE using a procedure similar to a previously reported protocol [41]. The GCEs were polished with 0.05 μm alumina slurry and sonicated in anhydrous ethanol and DI water prior to electrodeposition. The cyclic voltammetric (CV) reduction was performed in the GO solution under magnetic stirring, using a three-electrode system. The CV was run from a potential of 1 to −1.5 V at a scan rate of 50 mV/s for 18 cycles. Post-deposition, the reduced graphene oxide-GCE electrode (RGO-GCE) was washed with DI water and dried in nitrogen stream.

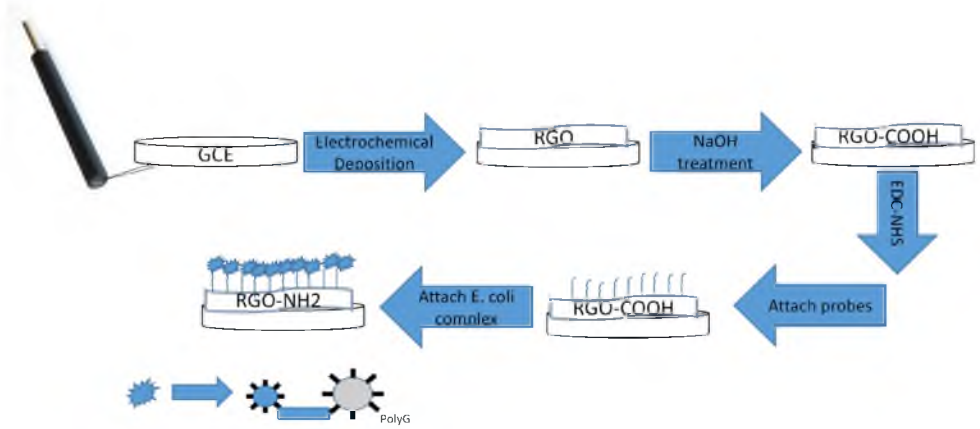

Figure 4. Schematic of GCE preparation for capture of the magnetic bead/*E. coli*/secondary bead complexes.

2.10. Attachment Chemistry for Cytosine Probes on the Electrode and Target Hybridization

The RGO-GCE was functionalized with amine terminated cytosine probes (CCCCCCCCCCCCCCC CCCCC/3′-NH_2). The RGO-GCE was etched in 1 M NaOH at 1.5 V to activate the electrode surface and to create carboxylic acid functional groups on the electrodeposited graphene oxide (Figure 4) [42]. To convert the carboxyl groups on RGO-GCE to amine-reactive NHS esters for attachment to amine terminated probes [43], 10 μL of freshly prepared 100 mM Sulfo-NHS and 400 mM EDC in 0.1 M of MES buffer (pH = 5.9) was pipetted on the RGO-GCE electrode surface for 1 h and then washed with MES buffer [35,44]. Subsequently, 10 μL of 25 μM cytosine probes in 1× PBS was pipetted on the activated RGO-GCE electrode surface for 1 h, followed by washing with 1× PBS to wash off the excess unattached cytosine probes [35]. Finally, the hybridization reactions were performed by incubating the target (magnetic bead/*E. coli*/secondary bead complexes) solution on the probe-RGO-GCE electrode for 1 h. The electrode surface was subsequently washed with 1× PBS before EC detection.

2.11. Fluorescent Microscopy Characterization of Probe-Target Hybridization

The magnetic bead/*E. coli*/secondary bead complexes hybridized on the RGO-GCE electrode was examined under a fluorescent microscope (4×, 500 ms exposure, Olympus IX81 inverted microscope, Olympus DP71 12-bit CCD color camera, FITC filter) using LCGreen (2 μL) intercalating dye (Idaho Technology Inc.). The extraction was also done from DI water with no *E. coli* O157:H7 as the starting sample and was used as the negative control. Another control involved fluorescent imaging of the electrode surface with magnetic bead/*E. coli*/secondary bead complexes without polyGs added to it (no target). Since polyGs specifically bind to the cytosine probes on the electrode surface, the absence of polyGs in the magnetic bead/*E. coli*/secondary bead complexes would enable evaluating any non-specific binding to the electrode surface. The images were analyzed using Olympus DP Controller imaging software (Melville, NY, USA).

2.12. EC Measurements

Initially, DPV measurements were run on the RGO-GCE electrodes with only cytosine probes attached, to record the baseline. Subsequently, the DPV detection was used to detect the target (magnetic bead/*E. coli*/secondary bead complexes) containing different concentrations of captured *E. coli* O157:H7 (0, 3, 20, 200, 300 CFUs) hybridized to the cytosine probes. Five consecutive DPV scans were performed to determine the guanine oxidation peak corresponding to each of the hybridized target. The differential value (S1–S5) was plotted for each target concentration (S1: first scan; S5: fifth scan). The DPV measurements (pulse size: 20 mV and scan rate: 5 mV/s) were conducted from 0.5 to 1.2 V (*vs.* Ag/AgCl) in 0.2 M acetate buffer solution (pH 5) containing 5 μM $Ru(bpy)_3^{2+}$ as the supporting electrolyte. During DPV, the effect of the charging current is minimized and hence enhanced signal-to-noise ratio can be achieved [45].

2.13. Pre-Concentration, IMS and EC Testing of E. coli O157:H7 in Waste Water Sample

To test the effectiveness of the *E. coli* O157:H7 detection process in simulated waste water, filtration, IMS and EC detection assay was run on waste water plant effluent (100 mL sample volume) from the local waste water treatment facility. Initially, vacuum filtration using a 30 μm nylon net filter (NY3004700, Millipore, Billerica, MA, USA) was employed to remove any solids >30 μm. Subsequently, the waste water was concentrated into 1 mL using vacuum filtration similar to the protocol for *E. coli* O157:H7 in PBS buffer samples. Next, IMS was performed to extract the *E. coli* O157:H7 from the 1 mL samples. Filtration, IMS extraction, and EC detection was performed to determine the amount of background *E. coli* O157:H7 in the waste water effluent samples. The waste water effluent was then seeded with 300 CFU *E. coli* O157:H7 and tested. Subsequently, 100 mL of the seeded waste water sample was autoclaved and the process was repeated to determine the signal generated by dead bacteria.

3. Results and Discussion

3.1. E. coli O157:H7 Extraction Efficiency Using Filtration and IMS

Three runs of *E. coli* O157:H7 extraction from 100 mL samples using vacuum filtration yielded an average percentage recovery of 47%. The filtration was employed before IMS to concentrate the *E. coli* O157:H7 from 100 mL samples into a 1 mL sample, because IMS on 100 mL samples directly resulted in only a 22% extraction efficiency. The low extraction percentage is likely due to the relatively low concentration of magnetic beads in the 100 mL sample volume. Increasing the number of beads to bring the concentration up to recommended levels would be cost prohibitive for the 100 mL samples. Pre-concentration using vacuum filtration is a cost-effective alternative for sample enrichment, which can also be incorporated into point-of-use systems [46]. The efficiency of capture of *E. coli* O157:H7 using IMS after vacuum filtration from different concentrations (500, 50, and 5 bacteria/mL in 1 mL 1× PBS sample volume) of *E. coli* O157:H7 was 95%, yielding an overall bacteria extraction efficiency of 46%.

3.2. Specificity of the E. coli O157:H7 IMS Process

Three runs of IMS using *E. coli* O157:H7 specific magnetic beads in non-specific pathogen samples (3000 CFUs *Salmonella*) yielded an average 0.4% extraction efficiency in comparison to the 95% for *E. coli* O157:H7 signifying that the IMS is highly specific to *E. coli* O157:H7.

3.3. Electrodeposition of Graphene Oxide on GCE

Graphene oxide was deposited on the GCE electrodes in preparation for bacteria detection. Electrode modification by deposition of graphene oxide has been applied to a large number of EC biosensing applications [47–50]. The modification of the GCE by graphene oxide enhances the surface area, electron transfer kinetics, and enables attachment of probes by further surface modification of the graphene oxide layers [41,51]. Figure 5 shows the cyclic voltammetry of graphene oxide electrodeposition on a GCE, showing one anodic peak (I) and two cathodic peaks (II and III). The cathodic peak III is attributed to the electrochemical reduction of GO, and the anodic peak I and cathodic peak II are ascribed to the redox pair of some electrochemically active oxygen-containing groups on the graphene plane that are too stable to be reduced by the CV [41,52]. The increase in the peak currents with successive potential scans from cycle 1 to 18 is confirmation of the deposition of reduced graphene oxide on the bare GCE. The graphene electrodeposition happens on conducting surfaces only, and the resultant graphene coating is very stable due to its poor insolubility in common solvents [41].

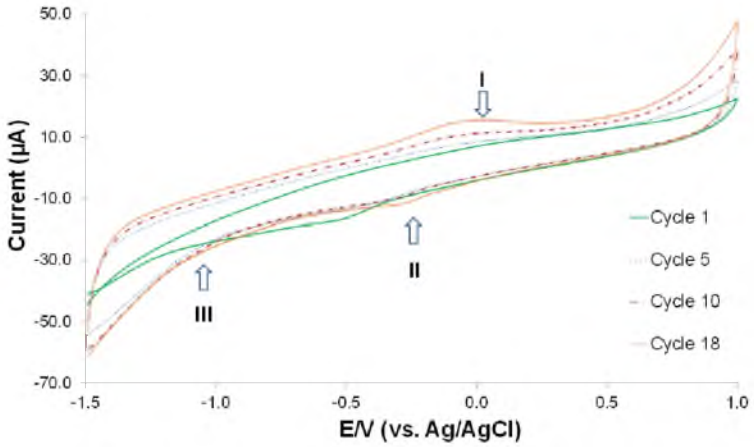

Figure 5. CV curve of graphene oxide electrodeposition on a GCE showing one anodic peak -I and two cathodic peaks -II and III.

3.4. Fluorescent Microscopy Confirmation of Probe-Target Hybridization

Cytosine probe attachment on the RGO-GCE was carried out followed by hybridization of the target magnetic bead/*E. coli*/secondary bead complexes. Fluorescence imaging was done to confirm the capture of magnetic bead/*E. coli*/secondary bead complexes on the cytosine probe functionalized RGO-GCE surface. The fluorescence images shown in Figure 6 generated using an LCGreen intercalating dye clearly show that the appropriate hybridization between the probe DNA and target polyG on the secondary beads has occurred. The number of bound beads was significantly higher than those for the negative control (essentially DI water with no *E. coli* O157:H7 as the starting sample) or the no target (polyGs absent on the magnetic bead/*E. coli*/secondary bead complexes) test. The results suggest that the general process is working and that the secondary beads bind as appropriate to the functionalized RGO-GCE surface and that minimal non-specific binding occurs.

(a) (b) (c)

Figure 6. Fluorescent microscopy images of (**a**) Bound magnetic bead/*E. coli*/secondary bead complexes on RGO-GCE; (**b**) negative control 1 (DI water as starting sample- no *E. coli* present); and (**c**) negative control 2 (polyGs absent on the magnetic bead/*E. coli*/secondary bead complexes).

3.5. In-Direct Electrochemical Detection of E. coli O157:H7

Electrochemical DPV was used to quantitatively measure the amount of hybridized polyG tags on the electrodes and hence indirectly measure the amount of captured *E. coli* O157:H7. The use of $Ru(bpy)_3^{2+}$/$Ru(bpy)_3^{3+}$ as an electron mediator during the oxidation of guanine (polyG) is well documented [53–57]. In the absence of any polyG, the background current/peak signal is due to the oxidation of $Ru(bpy)_3^{2+}$ at the electrode (RGO-GCE) surface. In the presence of polyG, the amplified peak signal during the first scan (S1) is due to the irreversible oxidation of guanine bases [55]. Hence the relative oxidation signals (S1-S5) increases as the concentration of polyG increases. Figure 7 shows the change in absolute DPV signals (S1) with an order of magnitude change in CFUs from 3 to 300 CFUs. These peak signals are observed between 1.06–1.07 V. In addition, a relatively smaller peak is seen at 0.7 V which is possibly due to some contaminants in the tested samples. Figure 8 shows the relative DPV signals (S1–S5) corresponding to varying concentrations of *E. coli* O157:H7 (0 to 300 CFUs enumerated by plate counting) in the initial seeded 100 mL PBS buffer samples.

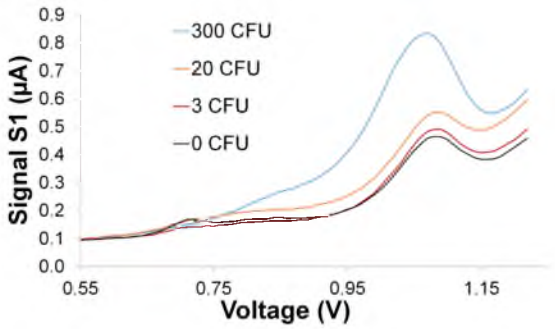

Figure 7. Absolute DPV signals (S1) corresponding to an order of magnitude change in concentration of *E.coli* O157:H7 from 3 to 300 CFUs. EC measurement condition: pulse size: 20 mV, scan rate: 5 mV/s, scan range 0.5 V to 1.2 V (*vs.* Ag/AgCl reference electrode). Supporting electrolyte: 0.2 M acetate buffer solution (pH 5) containing 5 µM $Ru(bpy)_3^{2+}$.

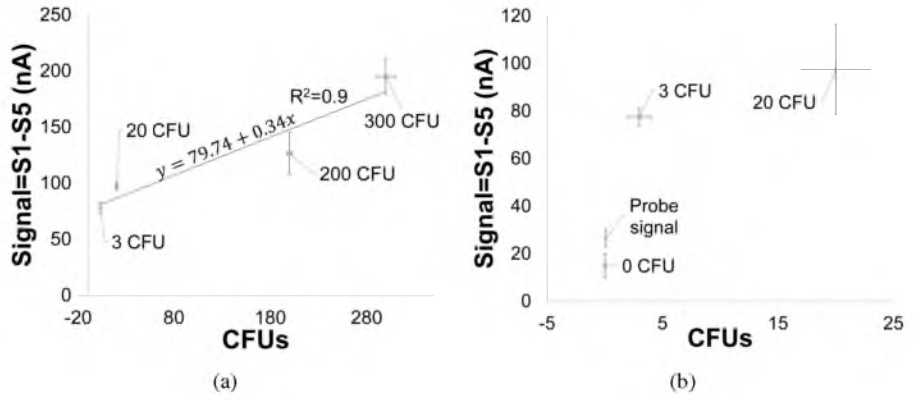

Figure 8. Relative DPV signals (S1-S5) corresponding to varying concentrations of *E. coli* O157:H7 in seeded 100 mL PBS buffer samples.

The relative oxidation signal due to guanine increased from 0 to 300 CFUs. The standard deviation was found to be 56.5% for three successive 300 CFU measurements. From the Figure 8a, the calibration curve is linear in the range from 3–300 CFUs, with regression equation of y = 79.74 + 0.34x with R^2 = 0.9. The detection limit was 3 CFU/100 mL with a signal-to-noise ratio of 3 (the noise being the probe only signal). The 0 CFU does give a signal of 15 nA which corresponds to the base signal due to $Ru(bpy)_3^{2+}$ in the electrolyte (Figure 8b). The average probe only signal (RGO-GCE with functionalized probes) was higher than the signal corresponding to 0 CFU (Figure 8b). This is because there is a drop in signal during DPV cycles due to passivation by acetate buffer in the electrolyte. This was confirmed by a drop in peak signals between first and second scans, seen during DPV performed with RGO-GCE electrodes in acetate buffer solution (not shown). Since the probe scans were initially run for all the electrodes before hybridized target scans was performed, there is a drop in signal for 0 CFU compared to probe only signal (Figure 8b).

3.6. Detection of E. coli O157:H7 in Simulated Waste Water

Our assay was able to detect *E. coli* O157:H7 in waste water plant effluent (Figure 9). The amount of native *E. coli* O157:H7 in waste water effluent samples was unknown. The initial test yielded a 65 nA signal. The waste water effluent was then seeded with 300 CFU *E. coli* O157:H7 and tested. The results in Figure 8, show the electrochemical signal at 225 nA post-seeding with 300 CFU *E. coli* O157:H7. The difference in signal corresponds to 225 − 65 = 180 nA which is 95% of signal corresponding to 300 CFUs tested in PBS buffer solution (Figure 8a). The negative control (DI water) gave a signal of 20 nA which corresponds to signal range for 0 CFUs in buffer. Post autoclaving the waste water sample gave a detection signal, indicating that dead bacteria were also detected. One possible solution to fix this would be to run an additional scan after a prescribed time (about 1 h) to gauge the amount of live bacteria.

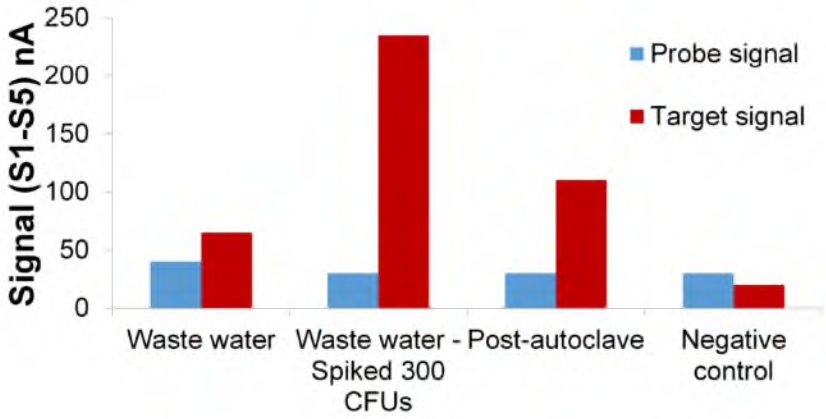

Figure 9. Electrochemical signal corresponding to *E. coli* O157:H7 in waste water effluent samples. Negative control is in the form of DI water without any *E. coli* O157:H7 in it. EC measurement condition: pulse size: 20 mV, scan rate: 5 mV/s, scan range 0.5 V to 1.2 V (*vs.* Ag/AgCl reference electrode). Supporting electrolyte: 0.2 M acetate buffer solution (pH 5) containing 5 μM $Ru(bpy)_3^{2+}$.

4. Conclusions

The protocol utilizing the IMS of *E. coli* O157:H7 and subsequent electrochemical detection of polyG functionalized secondary beads was able to detect 3 CFU *E. coli* O157:H7 in 100 mL samples with a signal-to-noise ratio of 3. The detection time was approximately 2 h. A linear relationship was found between the *E. coli* O157:H7 concentration and the relative electrochemical signal in the 3–300 CFU range with R^2 = 0.9. The IMS indicated a 95% extraction efficiency for *E. coli* O157:H7 with only a 0.4% non-specific capture. The overall extraction efficiency of *E. coli* O157:H7 from 100 mL samples was 46%. Detection of CFU levels below 3 CFU runs into statistical and repeatability issues especially in 100 mL samples. The detection limits of *E. coli* are two orders of magnitude better than what is reported in literature [4], when measured and demonstrated limits of detection are compared directly. The protocol was also able to detect *E. coli* O157:H7 in waste water samples. While not demonstrated in this work, the protocol can be easily modified for detecting multiple pathogens simultaneously by incorporating different oligonucleotide targets on the secondary beads and multiple electrodes (*i.e.*, microarray) with corresponding complementary probes.

Acknowledgments

The authors would like to thank Manoranjan Misra and Swomitra Mohanty at the University of Utah Nanomaterials Characterization Core Facility for the use of their facilities. We would like to thank Shelley Minteer (Department of Chemistry, University of Utah) for her guidance on electrochemical methods. This work was partially supported by a SBIR grant N00024-13-P-4543 from the U.S. Department of Defense.

Author Contributions

H.J., B.K.G., C.J.L., N.G., and H.J.S. conceived and designed the experiments; H.J., B.M. and C.J.L. performed the experiments; H.J., B.K.G., C.J.L., and H.J.S. analyzed the data; H.J., B.K.G. and H.J.S. wrote the paper.

Conflicts of Interest

Bruce K. Gale and Himanshu J. Sant have financial interest in Espira Inc., which has a license to the patent associated with this technology.

References

1. World Health Organization. *Water-Related Diseases*; WHO: Geneva, Switzerland, 2014.
2. Yang, L.; Li, Y. Simultaneous detection of Escherichia coli O157:H7 and Salmonella Typhimurium using quantum dots as fluorescence labels. *Analyst* **2006**, *131*, 394–401.
3. Feng, P.; Weagant, S.D.; Grant, M.A. Enumeration of Escherichia coli and the coliform bacteria. *Bacteriol. Anal. Man.* **2002**, *8*, 102–135.

4. Barreiros dos Santos, M.; Agusil, J.; Prieto-Simon, B.; Sporer, C.; Teixeira, V.; Samitier, J. Highly sensitive detection of pathogen Escherichia coli O157:H7 by electrochemical impedance spectroscopy. *Biosens. Bioelectron.* **2013**, *45*, 174–180.
5. Brichta-Harhay, D.; Arthur, T.; Bosilevac, J.; Guerini, M.; Kalchayanand, N.; Koohmaraie, M. Enumeration of Salmonella and Escherichia coli O157:H7 in ground beef, cattle carcass, hide and faecal samples using direct plating methods. *J. Appl. Microbiol.* **2007**, *103*, 1657–1668.
6. Jiang, X.; Chen, K.; Wang, J.; Shao, K.; Fu, T.; Shao, F.; Lu, D.; Liang, J.; FrahatáFoda, M.; Han, H. Solid-state voltammetry-based electrochemical immunosensor for Escherichia coli using graphene oxide–Ag nanoparticle composites as labels. *Analyst* **2013**, *138*, 3388–3393.
7. Mannoor, M.S.; Zhang, S.; Link, A.J.; McAlpine, M.C. Electrical detection of pathogenic bacteria via immobilized antimicrobial peptides. *Proc. Natl. Acad. Sci. USA* **2010**, *107*, 19207–19212.
8. Salam, F.; Uludag, Y.; Tothill, I.E. Real-time and sensitive detection of Salmonella Typhimurium using an automated quartz crystal microbalance (QCM) instrument with nanoparticles amplification. *Talanta* **2013**, *115*, 761–767.
9. Subramanian, A.; Irudayaraj, J.; Ryan, T. A mixed self-assembled monolayer-based surface plasmon immunosensor for detection of *E. coli* O157:H7. *Biosens. Bioelectron.* **2006**, *21*, 998–1006.
10. Linman, M.J.; Sugerman, K.; Cheng, Q. Detection of low levels of Escherichia coli in fresh spinach by surface plasmon resonance spectroscopy with a TMB-based enzymatic signal enhancement method. *Sens. Actuators B Chem.* **2010**, *145*, 613–619.
11. He, R.-X.; Zhang, M.; Tan, F.; Leung, P.H.M.; Zhao, X.-Z.; Chan, H.L.W.; Yang, M.; Yan, F. Detection of bacteria with organic electrochemical transistors. *J. Mater. Chem.* **2012**, *22*, 22072–22076.
12. Viswanathan, S.; Rani, C.; Ho, J.A.A. Electrochemical immunosensor for multiplexed detection of food-borne pathogens using nanocrystal bioconjugates and MWCNT screen-printed electrode. *Talanta* **2012**, *94*, 315–319.
13. Abu-Rabeah, K.; Ashkenazi, A.; Atias, D.; Amir, L.; Marks, R. Highly sensitive amperometric immunosensor for the detection of Escherichia coli. *Biosens. Bioelectron.* **2009**, *24*, 3461–3466.
14. Wang, J.; Chen, G.; Jiang, H.; Li, Z.; Wang, X. Advances in nano-scaled biosensors for biomedical applications. *Analyst* **2013**, *138*, 4427–4435.
15. Mairhofer, J.; Roppert, K.; Ertl, P. Microfluidic systems for pathogen sensing: A review. *Sensors* **2009**, *9*, 4804–4823.
16. Environmental Protection Agency, Region 1—EPA New England. *Beaches and Coasts, Questions and Answers*; EPA: Boston, MA, USA, 2014.
17. Standard Methods for the Examination of Water and Wastewater. *CWA Table IA.—List of Approved Biological Test Procedures*; American Water Works Association: Washington D.C., WA, USA, 2014.
18. IDEXX Corporation. *A Comparison of IDEXX Coliform and E. coli Tests*; IDEXX: Westbrook, ME, USA, 2014.

19. Zhu, P.; Shelton, D.R.; Li, S.; Adams, D.L.; Karns, J.S.; Amstutz, P.; Tang, C.M. Detection of *E. coli* O157:H7 by immunomagnetic separation coupled with fluorescence immunoassay. *Biosens. Bioelectron.* **2011**, *30*, 337–341.
20. Wright, D.; Chapman, P.; Siddons, C. Immunomagnetic separation as a sensitive method for isolating Escherichia coli O157 from food samples. *Epidemiol. Infect.* **1994**, *113*, 31–39.
21. Varshney, M.; Li, Y.; Srinivasan, B.; Tung, S. A label-free, microfluidics and interdigitated array microelectrode-based impedance biosensor in combination with nanoparticles immunoseparation for detection of Escherichia coli O157:H7 in food samples. *Sens. Actuators B Chem.* **2007**, *128*, 99–107.
22. Qiu, J.; Zhou, Y.; Chen, H.; Lin, J.M. Immunomagnetic separation and rapid detection of bacteria using bioluminescence and microfluidics. *Talanta* **2009**, *79*, 787–795.
23. Wang, J. Survey and summary from DNA biosensors to gene chips. *Nucleic Acids Res.* **2000**, *28*, 3011–3016.
24. Luo, X.; Hsing, I.M. Electrochemical techniques on sequence-specific PCR amplicon detection for point-of-care applications. *Analyst* **2009**, *134*, 1957–1964.
25. Jayamohan, H.; Sant, H.J.; Gale, B.K. Applications of microfluidics for molecular diagnostics. In *Microfluidic Diagnostics*; Springer: New York City, NY, USA, 2013; pp. 305–334.
26. Setterington, E.B.; Alocilja, E.C. Electrochemical biosensor for rapid and sensitive detection of magnetically extracted bacterial pathogens. *Biosensors* **2012**, *2*, 15–31.
27. Nam, J.M.; Thaxton, C.S.; Mirkin, C.A. Nanoparticle-based bio-bar codes for the ultrasensitive detection of proteins. *Science* **2003**, *301*, 1884–1886.
28. Nam, J.M.; Stoeva, S.I.; Mirkin, C.A. Bio-bar-code-based DNA detection with PCR-like sensitivity. *J. Am. Chem. Soc.* **2004**, *126*, 5932–5933.
29. Wang, J.; Rincón, O.; Polsky, R.; Dominguez, E. Electrochemical detection of DNA hybridization based on DNA-templated assembly of silver cluster. *Electrochem. Commun.* **2003**, *5*, 83–86.
30. Wang, J.; Liu, G.; Munge, B.; Lin, L.; Zhu, Q. DNA-Based Amplified Bioelectronic Detection and Coding of Proteins. *Angew. Chem. Int. Ed.* **2004**, *43*, 2158–2161.
31. Wang, J.; Liu, G.; Engelhard, M.H.; Lin, Y. Sensitive immunoassay of a biomarker tumor necrosis factor-α based on poly (guanine)-functionalized silica nanoparticle label. *Anal. Chem.* **2006**, *78*, 6974–6979.
32. Ding, C.; Zhang, Q.; Zhang, S. An electrochemical immunoassay for protein based on bio bar code method. *Biosens. Bioelectron.* **2009**, *24*, 2434–2440.
33. Zhang, D.; Huarng, M.C.; Alocilja, E.C. A multiplex nanoparticle-based bio-barcoded DNA sensor for the simultaneous detection of multiple pathogens. *Biosens. Bioelectron.* **2010**, *26*, 1736–1742.
34. Pratiwi, F.W.; Rijiravanich, P.; Somasundrum, M.; Surareungchai, W. Electrochemical immunoassay for Salmonella Typhimurium based on magnetically collected Ag-enhanced DNA biobarcode labels. *Analyst* **2013**, *138*, 5011–5018.
35. Wang, Q.; Su, J.; Xu, J.; Xiang, Y.; Yuan, R.; Chai, Y. Dual amplified, sensitive electrochemical detection of pathogenic sequences based on biobarcode labels and functional graphene modified electrode. *Sens. Actuators B Chem.* **2012**, *163*, 267–271.

36. Stoeva, S.I.; Lee, J.S.; Thaxton, C.S.; Mirkin, C.A. Multiplexed DNA detection with biobarcoded nanoparticle probes. *Angew. Chem.* **2006**, *118*, 3381–3384.
37. Gordon, N. Ultra-Sensitive Detection of Extremely Low Level Biological Analytes Using Electrochemical Signal Amplification and Biosensor. USPTO 14/173,064, 5 February 2014.
38. ATCC. *ATCC Bacterial Culture Guide*; ATCC: Manassas, VA, USA, 2014.
39. Life Technologies. *Dynabeads MAX E. Coli O157 Kit*; Life Technologies: Carlsbad, CA, USA, 2014.
40. KPL Inc. *Biotin-Labeled BacTrace Anti-E. coli O157:H7 Antibody Datasheet*; KPL: Gaithersburg, MD, USA, 2014.
41. Chen, L.; Tang, Y.; Wang, K.; Liu, C.; Luo, S. Direct electrodeposition of reduced graphene oxide on glassy carbon electrode and its electrochemical application. *Electrochem. Commun.* **2011**, *13*, 133–137.
42. Kim, J.; Elsnab, J.; Gehrke, C.; Li, J.; Gale, B.K. Microfluidic integrated multi-walled carbon nanotube (MWCNT) sensor for electrochemical nucleic acid concentration measurement. *Sens. Actuators B Chem.* **2013**, *185*, 370–376.
43. Roy, S.; Soin, N.; Bajpai, R.; Misra, D.; McLaughlin, J.A.; Roy, S.S. Graphene oxide for electrochemical sensing applications. *J. Mater. Chem.* **2011**, *21*, 14725–14731.
44. Du, D.; Zou, Z.; Shin, Y.; Wang, J.; Wu, H.; Engelhard, M.H.; Liu, J.; Aksay, I.A.; Lin, Y. Sensitive immunosensor for cancer biomarker based on dual signal amplification strategy of graphene sheets and multienzyme functionalized carbon nanospheres. *Anal. Chem.* **2010**, *82*, 2989–2995.
45. Wang, J. *Analytical Electrochemistry*; John Wiley & Sons: Hoboken, NJ, USA, 2006.
46. Foudeh, A.M.; Didar, T.F.; Veres, T.; Tabrizian, M. Microfluidic designs and techniques using lab-on-a-chip devices for pathogen detection for point-of-care diagnostics. *Lab Chip* **2012**, *12*, 3249–3266.
47. Brownson, D.A.; Banks, C.E. Graphene electrochemistry: An overview of potential applications. *Analyst* **2010**, *135*, 2768–2778.
48. Muti, M.; Sharma, S.; Erdem, A.; Papakonstantinou, P. Electrochemical Monitoring of Nucleic Acid Hybridization by Single-Use Graphene Oxide-Based Sensor. *Electroanalysis* **2011**, *23*, 272–279.
49. Huang, K.J.; Niu, D.J.; Sun, J.Y.; Han, C.H.; Wu, Z.W.; Li, Y.L.; Xiong, X.Q. Novel electrochemical sensor based on functionalized graphene for simultaneous determination of adenine and guanine in DNA. *Colloids Surf. B Biointerfaces* **2011**, *82*, 543–549.
50. Bonanni, A.; Ambrosi, A.; Pumera, M. Nucleic acid functionalized graphene for biosensing. *Chem. A Eur. J.* **2012**, *18*, 1668–1673.
51. Ambrosi, A.; Bonanni, A.; Sofer, Z.; Cross, J.S.; Pumera, M. Electrochemistry at chemically modified graphenes. *Chem. A Eur. J.* **2011**, *17*, 10763–10770.
52. Hummers Jr, W.S.; Offeman, R.E. Preparation of graphitic oxide. *J. Am. Chem. Soc.* **1958**, *80*, 1339–1339.
53. Johnston, D.H.; Glasgow, K.C.; Thorp, H.H. Electrochemical measurement of the solvent accessibility of nucleobases using electron transfer between DNA and metal complexes. *J. Am. Chem. Soc.* **1995**, *117*, 8933–8938.

CHAPTER 5

ANODIZED TITANIA NANOTUBE ARRAY MICROFLUIDIC DEVICE FOR PHOTOCATALYTIC APPLICATION: EXPERIMENT AND SIMULATION

©2015 Elsevier B.V. Reprinted, with permission, from Elsevier. This was published in Applied Catalysis B: Environmental, Volumes 174-175, 2015, Pages 167-175, DOI:10.1016/j.apcatb.2015.02.041. Authors are Harikrishnan Jayamohan, York R. Smith, Lauryn C. Hansen, Swomitra K. Mohanty, Bruce K. Gale, and Mano Misra.

Applied Catalysis B: Environmental 174–175 (2015) 167–175

Contents lists available at ScienceDirect

Applied Catalysis B: Environmental

journal homepage: www.elsevier.com/locate/apcatb

Anodized titania nanotube array microfluidic device for photocatalytic application: Experiment and simulation

Harikrishnan Jayamohan[a], York R. Smith[b,*], Lauryn C. Hansen[b], Swomitra K. Mohanty[c], Bruce K. Gale[a], Mano Misra[b,c,**]

[a] Department of Mechanical Engineering, University of Utah, Salt Lake City, UT 84112, USA
[b] Department of Metallurgical Engineering, University of Utah, Salt Lake City, UT 84112, USA
[c] Department of Chemical Engineering, University of Utah, Salt Lake City, UT 84112, USA

ARTICLE INFO

Article history:
Received 22 October 2014
Received in revised form 25 February 2015
Accepted 27 February 2015
Available online 2 March 2015

Keywords:
Anodization
Titania nanotubes
Photocatalysis
Microfluidic reactors
Simulation

ABSTRACT

Microfluidic photocatalytic reactors have advantages over conventional bulk reactors such as large surface-area-to-volume ratio and high control of fluid flow. Although titania nanotubular arrays (TNA) have shown enhanced photocatalytic degradation compared to nanoparticle films in a batch reactor configuration, their application in a microfluidic format has yet to be explored. The photocatalytic performance of a microfluidic reactor with TNA catalyst was compared with the performance of microfluidic format with TiO_2 nanoparticulate (commercial P25) catalyst. The microfluidic device was fabricated using non-cleanroom based soft lithography, making it suitable for economical large scale manufacturing. The photocatalytic performance was evaluated at different flow rates ranging from 25 to 200 μL/min. The TNA microfluidic system demonstrated enhanced photocatalytic performance over microfluidic TiO_2 nanoparticulate layers, especially at higher flow rates (50–200 μL/min). For instance, 12 μm long TNA was able to achieve 82% fractional conversion of 18 mM methylene blue in comparison to 55% conversion in case of the TiO_2 nanoparticulate layer at a flow rate of 200 μL/min. A computational model of the microfluidic format was developed to evaluate the effect of diffusion coefficient and rate constant on the photocatalytic performance. The improved performance of the TNA photocatalyst over the nanoparticle film can be attributed to higher generation of oxidizing species.

© 2015 Elsevier B.V. All rights reserved.

1. Introduction

Water based pollutants are a big concern and serious challenge in both developed and developing nations. Photocatalytic environmental remediation has been widely investigated for the degradation of water based pollutants [1]. Recently, nanomaterials such as nanoparticles, nanowires and nanoporous films have been applied to photocatalytic reactions due to their interesting properties over bulk materials. Many studies have used photocatalysts in the form of a powder. However, the use of powdered photocatalysts necessitates their downstream recovery, which can be costly. The immobilization or growth of photocatalysts as a film eliminates this drawback. Many studies involve conventional macroscale reactors with limited mass transport and poor photon transport. This can potentially limit the degradation performance of the system [2–4]. The use of microfluidic system has the potential to reduce such aforementioned reactor limitations.

Microfluidic systems have inherent advantages such as large surface to volume ratio, smaller diffusion distance, uniform irradiation over the whole catalytic surface, self-refreshing property [5] and large mass transfer efficiency [6,4]. Microfluidic photocatalytic reactors have demonstrated higher photocatalytic efficiency compared to conventional reactors. For example, Lei et al. reported reaction rate constants in microreactors to be 100 times more than in bulk reactors [3]. In bulk reactors, there is a loss of photons reaching the photocatalyst surface due to scattering effects in the liquid [7]. In contrast, in microfluidic reactors, the thin layer of liquid over the catalyst ensures that less photons are lost due to scattering. Microfluidic reactors can also be used for rapid screening of photocatalysts [4,8].

Of the semiconductor materials studied for photocatalytic environmental remediation, titanium dioxide (e.g., nanoparticles, nanowires, nanotubes) is widely used due to its desirable

* Corresponding author. Tel.: +1 801 581 6386; fax: +1 801 581 4937.
** Corresponding author at: Department of Metallurgical Engineering, University of Utah, Salt Lake City, UT 84112, USA. Tel.: +1 801 581 6386; fax: +1 801 581 4937.
E-mail addresses: york.smith@utah.edu (Y.R. Smith), mano.misra@utah.edu (M. Misra).

http://dx.doi.org/10.1016/j.apcatb.2015.02.041
0926-3373/© 2015 Elsevier B.V. All rights reserved.

properties. Titanium dioxide has successfully demonstrated photocatalytic degradation of a wide spectrum of metallic and organic pollutants [9]. Titania nanotube arrays (TNA) synthesized by anodization have received interest in last few decades in areas such as sensing, drug-delivery, energy conversion/storage, and catalysis, for example [10–12]. Macak et al. reported the use of high-aspect ratio TNA for enhanced photocatalytic properties compared to TiO_2 nanoparticulate layers [13]. Although the TNA layer was five times shorter than the P25 nanoparticulate layer, it still exhibited enhanced photocatalytic performance compared to the latter. In their study, the photocatalytic experiments were performed in a batch reactor configuration. Most of the current literature on photocatalytic microfluidic systems involve TiO_2 nanoparticle film as a photocatalyst [14,15,3,16,17]. Subsequently, a more efficient degradation system could be realized by integrating TNA in a microfluidic system. Moreover, microfluidic devices integrated with TNA can potentially be used for other applications such as photocatalytic syntheses of chemicals such as L-pipecolinic acid, for example [18].

A potential disadvantage with current microfluidic photocatalytic degradation systems is that the microfluidic devices needed are often complex and difficult to fabricate especially when clean-room techniques are involved. This is especially critical when a large-scale array of microfluidic channels is required [4]. For example, previous reports on microfluidic photocatalytic devices used clean-room techniques to fabricate the mold for the microfluidic device [14,3,6] or to pattern the photocatalyst substrate [2] or CNC milling to pattern the substrate [19]. In contrast, in this study the microreactor mold was fabricated using laser patterned polymethyl methacrylate (PMMA) sheets [20,21] and polydimethylsiloxane (PDMS) was used to fabricate the device. A widely used material for microfluidic devices, PDMS, has desirable properties such as optical transparency, chemical inertness, and easy and rapid fabrication [22,17].

In this work, we demonstrate the use of self-ordered TNA for photocatalytic degradation in a microfluidic reactor. The degradation performance of TNA was also compared to P25 TiO_2 nanoparticle films in a similar microfluidic format. The degradation kinetics of a model pollutant (methylene blue) in a microfluidic channel with TNA vs. P25 TiO_2 particles as catalyst under solar irradiation (AM 1.5, ~100 mW/cm^2) was used in this study. Most of the existing work on microfluidic photocatalytic system, however, have been done under UV light [2,6,17], limiting the practical application.

We have also developed a model using COMSOL Multiphysics to examine how convection and diffusion of the reactant/pollutant molecules affect the performance of the microfluidic surface reactor system. Although models have been developed to understand the nature and reaction kinetics between a photocatalyst and reactant in batch reactors [23–26], a model that would explain the behavior of such a system in a microfluidic flow based scenario has yet to be explored.

2. Experimental

2.1. Preparation and characterization of TNA and P25 film

Titania nanotube arrays were synthesized by electrochemical anodization similar to an earlier reported protocol [27,28]. In short, Ti foils (0.02032 cm thick) were cut into 3 cm × 2 cm and anodized under sonication (Branson 5510 ultrasonic bath) in an electrolytic solution consisting of ethylene glycol (Fisher Scientific, Waltham, MA), deionized (DI) water (2 wt.%) and ammonium fluoride (0.5 wt.%, Fischer Scientific) at 30 °C bath temperature. One side of the Ti foil was masked using Kapton tape to restrict oxide growth to only one side of the Ti strip. A two electrode configuration with platinum (Pt) mesh as the cathode was used for anodization. The anodization was carried out at an applied potential of 60 V (D.C.) (Agilent, E3647A) for different time intervals (60 min for long tubes, 30 min for medium tubes and 15 min for short tubes). The thus formed TNA were rinsed with DI water, air-dried and cut to the dimension of the microfluidic channel. The TNA samples were subsequently annealed in an atmosphere of N_2/H_2 (2% H_2) at 500 °C (1.6 °C/min ramp rate) for 2 h.

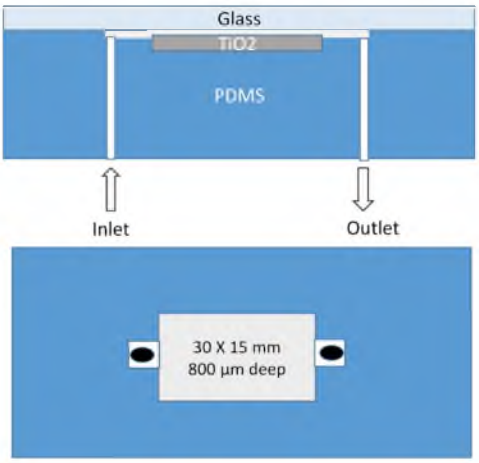

Fig. 1. Top and side view of the microfluidic device.

The P25 films were prepared by doctor blade method [29]. A fine paste of Degussa P25 was made with dilute nitric acid (pH 3–4) using a mortar and pestle. Scotch tape (3M) was used as a mold to form a film the same dimensions of the channel (30 mm × 15 mm) on a Ti foil. Subsequently the P25 film was calcined in air for 2 h at 450 °C. The morphology of the thus formed P25 TiO_2 and TNA films were characterized using a field emission scanning electron microscope (SEM) (Hitachi, S-4800). The crystalline properties of the films were examined using X-ray diffraction (Rigaku MiniFlex 600) with CuKα radiation (λ = 0.1542 nm) from 2θ = 20–80° with a step size = 0.01° and dwell time = 0.5°/min.

2.2. Fabrication of microfluidic channel and integration of TNA substrate

The microfluidic device was fabricated by soft lithography similar to a previous procedure [30]. A laser was used to create the mold for the microfluidic channel on a PMMA sheet (800 µm thick) and transferred onto a plastic petri dish. The dimensions of the channel are as shown in Fig. 1. A 20 mL mixture of PDMS (base to curing agent ratio – 1:10) was poured onto the mold and cured at 60 °C for 4 h to create the PDMS layer. Subsequently, inlet and outlet channels were bored onto the PDMS channel. Then the thin film catalyst (TNA or P25 film) was embedded (using a double-sided tape) into the PDMS channel. The TNA or P25 layer was placed facing the glass slide. The glass slide was bonded to the PDMS layer via corona surface treatment for 4 min and subsequently baked at 60 °C for 2 h [31].

2.3. Evaluation of the photocatalytic degradation

The photocatalytic degradation of the device was evaluated using methylene blue (MB) as a model pollutant. This dye is non-biodegradable and commonly used in the textile industry. As

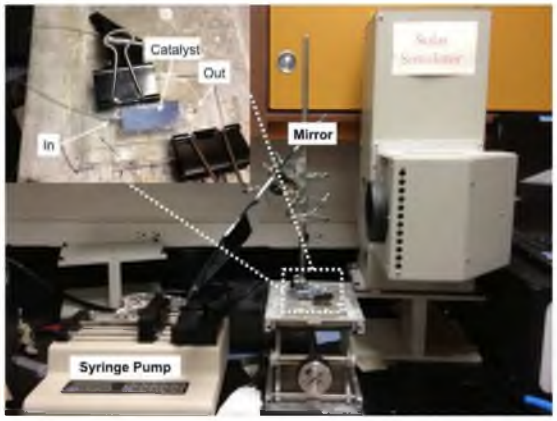

Fig. 2. Experimental setup used for microfluidic photodegradation of MB. The inset shows the actual microfluidic reactor with the TNA catalyst embedded.

a result, this molecule is widely used for testing photocatalytic activity [32,33,13]. A depiction of the experimental setup used to evaluate the photocatalytic performance is shown in Fig. 2. In a typical experiment run, 5 mL of 18 mM aqueous solution of MB was injected through the inlet into the microfluidic device using a syringe pump (KD Scientific, Manassas, VA) via Tygon tubing (0.02 in. inner diameter) at different flow rates ranging from 25 to 200 μL/min. The microfluidic device was irradiated with AM 1.5 simulated solar light. The intensity of the light was measured at the surface of the microfluidic device using a handheld power meter (Nova, Ophir-Spiricon, UT) to be ~100 mW/cm^2. The syringe pump was used to flow 1 mL of the MB solution through the device with the simulated solar light irradiation before any sample was collected. This was to ensure steady state is reached before the MB degradation is measured. The degraded MB solution was collected and the concentration was analyzed by monitoring the decrease in characteristic absorption peak at $\lambda = 664$ nm using a UV–vis spectrophotometer (Shimadzu Corp., Japan). The fractional conversion (X) was calculated by:

$$X = \frac{A_0 - A}{A_0} \quad (1)$$

where A_0 is the initial concentration absorbance value, and A is the absorbance value of the degraded solution. The experiment was repeated in the absence of AM 1.5 light to evaluate the amount of MB adsorbed on the catalyst. All photocatalytic degradation experiments were repeated 3–5 times and the fractional conversion values averaged. Error bars on all plots are $\pm\sigma$ of the experimental data.

3. Numerical modeling

A finite element model to simulate the degradation of MB in the microfluidic channel was created in COMSOL Multiphysics 4.3b. For simplicity, the model assumes the catalytic surface to be a flat surface rather than nano-structured. The model also assumes that the bulk MB solution is transported to the catalyst surface at the bottom of the channel and degraded.

3.1. Microchannel geometry

Fluid flows using 3-D model geometries were developed. Fig. 3 shows the geometry of the 3-D model used in the simulations. The x and y dimensions of the channel match the geometry of the microchannel fabricated for the experiments. The z dimension is assumed to be 600 μm. This is because the overall height of the channel is 800 μm and the thickness of the Ti foil/catalyst layer is approximated as 200 μm.

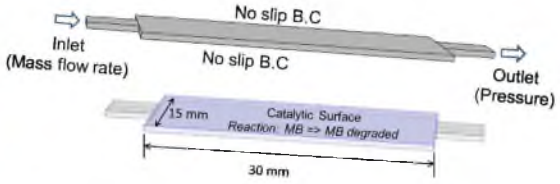

Fig. 3. Boundary conditions used in simulation of the 3D model.

3.2. Fluid flow

The Navier–Stokes equations for conservation of momentum (2) and the continuity equation for conservation of mass (3) are used to model the laminar flow of a single phase Newtonian fluid in the micro-channel.

$$\rho\left(\frac{\partial \vec{u}}{\partial t}\right) + \vec{u}\cdot\nabla\vec{u} = -\nabla\vec{p} + \mu\nabla^2\vec{u} \quad (2)$$

$$\rho\nabla\vec{u} = 0 \quad (3)$$

In Eqs. (2) and (3), u is the flow velocity field, μ is the dynamic viscosity of the fluid, ρ is the fluid density and p is the fluid pressure. At the walls of the microfluidic channel, no-slip boundary conditions are applied. Eqs. (2) and (3) assume the system is under steady-state conditions with negligible body forces and uniform fluid density. The inlet fluid mass flow rate was specified and a no-slip boundary is assumed at the channel surfaces. Based on the given boundary conditions the velocity and pressure fields are computed inside the microfluidic channel.

3.3. Species concentration

The equation for convection-diffusion of the species in the fluid is given by (assuming constant diffusion coefficient)

$$\frac{\partial \vec{c}}{\partial t} = -D\nabla^2\vec{c} + R - \vec{u}\cdot\nabla\vec{c} \quad (4)$$

where c and D are the concentration and the diffusion coefficient of the species, respectively, in a fluid flowing with velocity u and R is the reaction rate in the bulk solution. The diffusion coefficient of MB is assumed to be 1.6×10^{-10} m^2/s [34].

3.4. Degradation reaction

The overall degradation of MB happens at the catalytic surface only and not the bulk solution. The boundary fluxes at the catalytic surfaces thus are denoted by

$$R_i = n\cdot(-D_i\delta c_i + c_i u) \quad (5)$$

where the reaction rate $R_i = kc$ and k is the forward reaction rate constant. The model solves for concentration profile of the product (degraded MB) along the channel based on the given flow conditions and reaction parameters.

4. Results and discussion

4.1. Characterization

Figs. 4 and 5 show the SEM image of the annealed TNA of different lengths. The nanotube lengths are approximately 12 μm

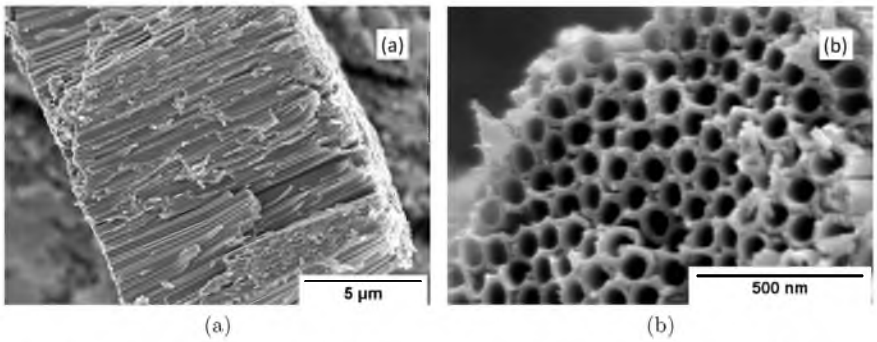

Fig. 4. SEM images of TNA anodized at 60 V for 1 h duration, showing the sidewall morphology (a) and top morphology (b).

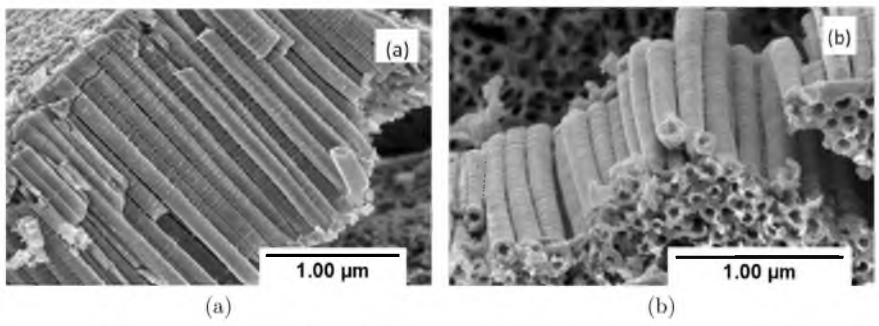

Fig. 5. SEM images of TNA anodized at 60 V for 15 min anodization, showing the sidewall (a) and top morphology (b).

(1 h anodization, Fig. 4), 7 μm (30 min anodization – not shown) and 3 μm (15 min anodization, Fig. 5). The TNA tubes have an approximate inner diameter of 80 nm with an average wall thickness of 15 nm. In comparison, the TiO_2 P25 layer (Fig. 6) has particles and agglomerates of 20–50 nm size with a layer thickness of approximately 40 μm.

The crystalline structure is one of the critical factors in the catalytic performance of TiO_2 at a liquid–solid interface [35,13,36,37]. The XRD patterns of the annealed P25 and TNA catalysts are shown in Fig. 7. The diffraction patterns have been indexed to standard JCPDS cards. From the peak positions and the relative intensities, it is evident that both P25 (Fig. 7a) and TNA (Fig. 7b) contain two titania crystalline phases, anatase (labeled A) and rutile (labeled R). The underlying titanium support (labeled T) is also evident in both samples. It is evident that the predominant phase is anatase.

4.2. Degradation performance of the microfluidic reactor: effect of flow rate and nanotube length

The results of the degradation at different flow rates over TNA (12 μm) and TiO_2 P25 in the presence and absence of AM 1.5 irradiation are presented in Fig. 8a. At the lowest flow rate, both the TiO_2 P25 and 12 μm thick TNA catalysts show similar degradation performance. As the flow rate increases from 50 to 200 μL/min, the fractional conversion of the P25 catalyst decreases from 0.93 to 0.55. In contrast, the TNA fractional conversion remains relatively

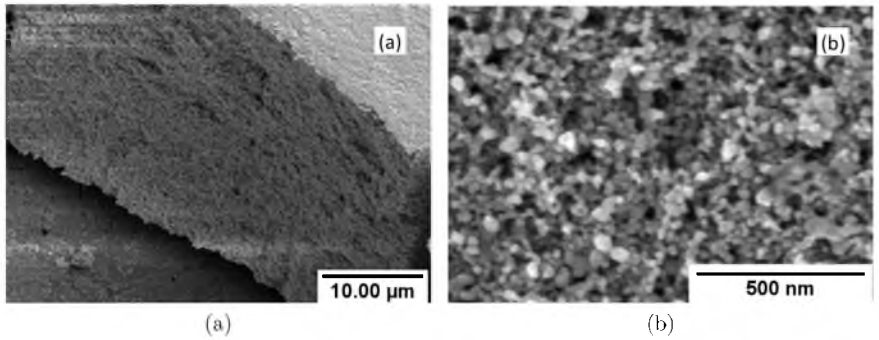

Fig. 6. SEM images of P25 TiO_2 layer prepared by doctor blade method, showing the film sidewall morphology (a) and top morphology (b).

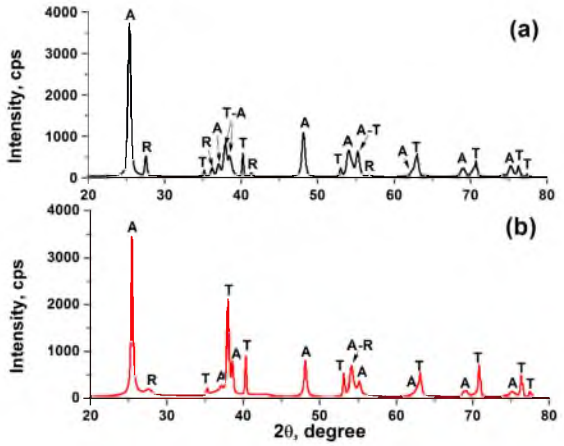

Fig. 7. X ray diffraction patterns of annealed (a) P25 photocatalyst and (b) 12 μm TNA photocatalyst. For both photocatalysts, both anatase (indexed labeled A) and rutile (index labeled R) crystal phases are identified. The underlying titanium substrate (indexed labeled T) is also identified.

constant over the flow rate range of 50–200 μL/min. The thickness of the TNA and P25 oxide layer has shown to be correlated to the level of degradation performance in batch reactor systems [13]. It is interesting to note that, even though the P25 layer is more than three times as thick (40 μm) as the longer TNA (12 μm), the degradation performance is much higher in the case of 12 μm TNA. The results of the fractional conversion in the absence of AM 1.5 light gives an indication of how much dye is adsorbed on the catalyst. It is observed that the P25 film adsorbs more dye at a flow rate of 25 μL/min compared to TNA. For higher flow rates, the dye adsorption remains relatively constant and is approximately the same for both P25 and TNA. At the lowest flow rate, the molecules have more time to adsorb and equilibrate with the catalyst surface. The higher dye adsorption on the P25 film compared to the TNA film is possibly due to a larger surface area of the P25 film over the 12 μm TNA film. However, it should be noted that the ability of a dye molecule to adsorb onto a titania surface is predisposed to the surface charge of that catalyst (i.e., isoelectric point) and of the dye molecule [38]. In nanomaterials, this can vary depending upon the synthesis method adopted, polymorph, crystallographic planes, as well as crystallite size [12]. The degradation performance for different lengths of TNA catalyst was also examined (Fig. 8b). The shorter TNA lengths (7 and 3 μm) have a degradation performance lower than that of the P25 film within the flow rate domain. It should be noted, that the decrease in fractional conversion with an increase in flow rate from

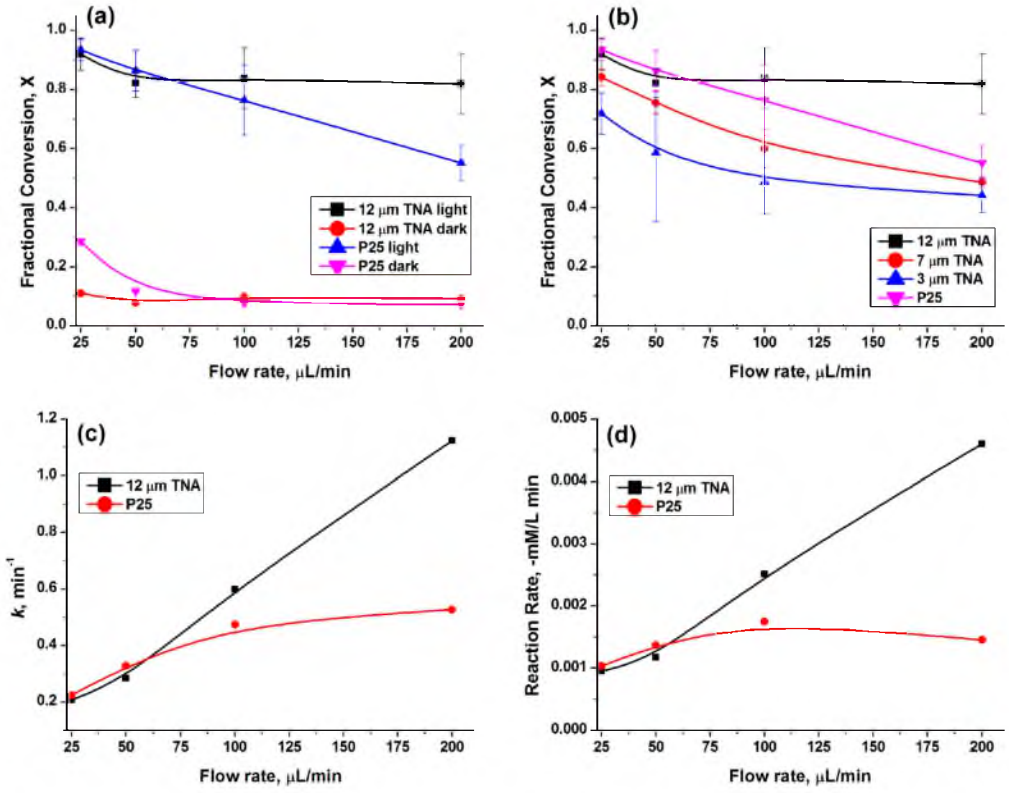

Fig. 8. (a) Effect of flow rate on MB degradation for 12 μm TNA and P25 TiO_2 film catalyst in the presence and absence of AM 1.5 irradiation (~100 mW/cm^2). (b) Effect of TNA length (12, 7 and 3 μm) on MB degradation at different flow rates under AM 1.5 irradiation (~100 mW/cm^2). (c) Pseudo-first order rate constant of MB degradation at different flow rates for TNA vs. P25 layer. (d) Reaction rate for photocatalytic MB degradation at different flow rates for TNA vs. P25 layer.

50 to 200 μL/min for 7 and 3 μm TNA is less than that of the P25 catalyst over the same range.

4.3. Evaluation of photocatalytic degradation

The mechanism for the photocatalytic degradation of MB has been discussed in previous published work [13,39]. In short, the adsorbed MB molecules on the catalyst surface are oxidized by the photoinduced holes of the TiO_2 catalyst to form $^{\bullet}MB^{+}$ radicals. These radicals further react with O_2 to form $[MBOO^{\bullet}]^{+}$, subsequently the heteropolyaromatic ring is broken and is eventually degraded to mineral acids and CO_2 [39]. However, it should be noted, the degradation mechanism when using P25 under these experimental conditions is likely different than when TNA are used as the photocatalyst. The UV portion of AM 1.5 irradiation is a small contribution; moreover P25 is only UV photoactive. Whereas the synthesis method used to prepare TNA in this study results in doped carbon and sub-stoichiometric titania, which contributes to visible light photoactivity [28,12,40,41]. Visible light photocatalysis is achievable using P25, however the mechanism is different and based on dye/ligand-sensitization phenomena [42,43]. Although the degradation pathway and product distribution may be different for each system, the objective of this study is to examine the overall photoconversion of each system based on flow parameters.

Heterogeneous photocatalytic degradation is not an elementary process, i.e., there are several reaction intermediates; moreover, the reaction intermediate species and/or dissolved oxidizing species can act as catalysts for the degradation of other intermediate species. As a result, the reaction order can change along the reaction coordinate. To overcome such complexities, we can assume that the non-degraded MB is in large excess compared to other degradation products. This is generally an adopted approach when examining the kinetics of photocatalytic reactions and is commonly referred as pseudo-order rate kinetics. Kinetic studies on the photocatalytic degradation of azo dyes using TNA [38] and titania nanoparticle films [44] show that they follow a pseudo first order kinetics, and under certain operating conditions, follow the Langmuir–Hinshelwood mechanism. If we assume that the rate-limiting step is the surface reaction, the concentration of oxidizing species ($OH^{\bullet}$ radicals and holes) is assumed to be in large excess. The reaction rate is then assumed to be proportional to the flow rate or residence time (or dye molecules adsorbed). By assuming plug flow within the microfluidic channel and an isothermal pseudo-first order irreversible reaction, the dye concentration (C_A) can be expressed as:

$$C_A = C_{A0} \cdot e^{-k\tau} \tag{6}$$

where C_{A0} is the initial dye concentration, k is the pseudo-first order rate constant, and τ is the residence time. The pseudo-first order rate constant and reaction rate as a function of flow rate for 12 μm TNA and P25 photocatalysts were calculated and plotted in Fig. 8c and d. From these plots it is evident that for the TNA photocatalyst, as the flow rate increases the reaction rate and rate constant increase over the entire domain of flow rates. This indicates that the surface reaction occurs fast and the kinetics is diffusion limited over the flow rate domain. For the P25 film, the reaction rate and pseudo-first order rate constant, plateaus at 100 μL/min and remains constant thereafter, thus for flow rates >100 μL/min, the kinetics for the P25 films is reaction limited. It is worth noting, the range of Reynolds numbers for these flow rates is 0.05–0.4 (for 25–200 μL/min) and is still well within the laminar flow regime (i.e., no turbulent mixing effects). Thus the degradation kinetics can be explained in terms of the diffusion of reacting species, and the photocatalysts ability to suppress charge carrier recombination.

Another possible explanation for the higher fractional conversion at higher flow rates (50–200 μL/min) is that the roughness might be inducing localized mixing at higher flow rates in the case of TNA. At low Reynolds numbers (<2300) and given a relative roughness of 0.02 (for the TNA layer in this study), the surface roughness does not normally affect the flow in macro systems [45]. But in the case of microfluidic systems, it has been reported that nanoscale surface roughness does cause flow perturbations in low Reynolds number flows (Re = 0.06–6.5) [46]. The induced flow perturbations could possibly contribute to the mixing of MB and generated oxidizing species, resulting in an enhanced degradation.

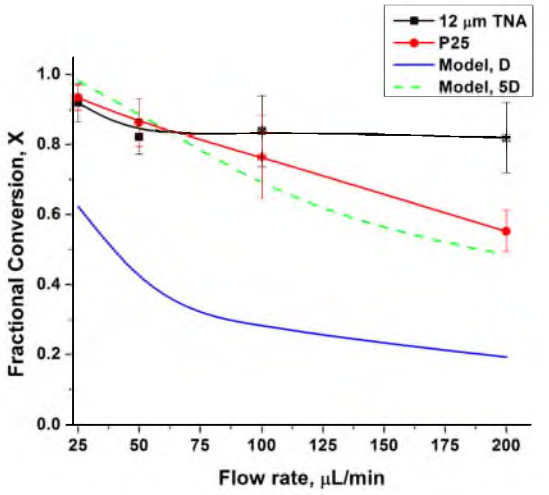

Fig. 9. Results of actual degradation (TNA and P25) in comparison to simulation data for the photocatalytic degradation of methylene blue (18 mM initial concentration). By increasing the diffusion coefficient (D), the simulation data begins to match the experimental data.

Titania nanotube arrays have been reported to have higher photocatalytic efficiency compared to P25 layers in spite of their lower surface area compared to the latter [47]. The TNA nanotubes provide an optimized geometry that has a shorter carrier-diffusion path in the tube walls and lower recombination rates of photo-generated electron–hole pairs in comparison with P25 layer. In the case of P25, the charge carriers have to travel between single nanoparticles, where higher interfacial grain boundaries may lead to increased charge recombination rates. Also, the diffusion path of the dye molecules from bulk solution to the active surface area on a tubular geometry is much shorter compared to the tortuous path in porous structured P25 [48]. Therefore, the enhanced degradation performance of the TNA photocatalyst vs. the P25 photocatalyst may be attributed to better charge separation and diffusion of reacting species.

4.4. Simulation results

The results of the simulation showing fractional conversion of MB in comparison to experimental results (12 μm TNA and P25 catalyst) at different flow rates are shown in Fig. 9. The fractional conversion as per the simulation is lower than what is observed during the experiment for TNA and P25 TiO_2 catalyst (Fig. 8). This may be because the simulation assumes a smooth planar surface, unlike in the case of TNA and P25, which have porous, nanostructured surfaces. Due to the length scales involved, it is computationally expensive to incorporate the exact geometry of a nanostructured surface in the current model. One method to overcome this limitation is to increase the diffusivity of MB to account for the enhanced mass transfer due to a larger surface area and

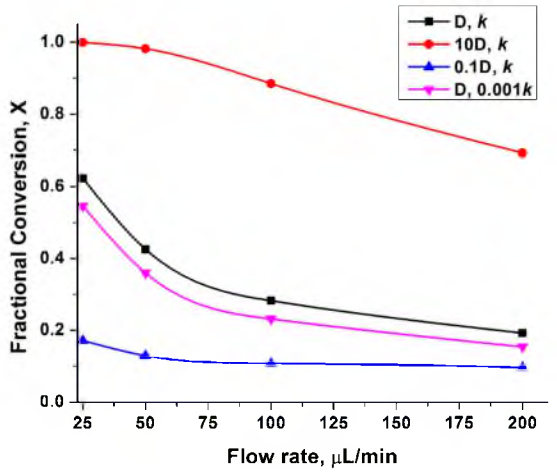

Fig. 10. Simulation on the effect of diffusion coefficient and pseudo-first order rate constant on the degradation of methylene blue. The simulation results are more sensitive to changes in the diffusion coefficient than to the reaction rate constant.

higher number of reactive sites. For example, by increasing the actual diffusion coefficient of MB by five times (5*D*), the simulation results begin to match the experimental results obtained with P25 photocatalyst (Fig. 9).

The better performance of TNA can be attributed to lower recombination rates of photogenerated electron–hole pairs [13]. This can be assumed equivalent to increasing the rate constant. To examine this modeling analog, we have conducted simulations of fractional conversion at different flow rates while varying the diffusion coefficient ($D = 1.6 \times 10^{-10}$ m^2/s for methylene blue [34,49]) and pseudo-first order rate constant ($k = 0.2238$ min^{-1}), respectively (Fig. 10). The pseudo-first order rate constant was calculated from experimental results of P25 TiO_2 catalyst at 25 μL/min. At this flow rate, the reaction rate and pseudo-first order rate constant are nearly the same for both photocatalysts; moreover, the degradation is least affected by mass transport. It is evident from the simulation that increasing the diffusion coefficient or the rate constant results in increased fractional conversion. It is interesting to note, the effect of rate constant on the fractional conversion is less than that of the diffusion coefficient. For example, reducing the rate constant by three orders of magnitude (0.001*k*) only results in an 18% reduction in fractional conversion at flow rate of 100 μL/min. In comparison, a drop in diffusion coefficient by an order of magnitude (*D* to 0.1*D*) resulted in a 62% reduction in fractional conversion at flow rate of 100 μL/min. From the results of these simulations the diffusion of reacting species plays a larger role than rate constant.

But an enhancement in diffusion coefficient by five times the actual value seems an unlikely real world scenario even when a nanostructured surface is present. For instance, at a diffusion coefficient of 5*D*, it takes 225 s for a MB molecule to diffuse the height of the microfluidic channel. While at a flow rate of 200 L/min the MB molecule advects across the length (30 mm) of the channel in 81 s. Hence it is unlikely that during this time period, the MB molecule would diffuse from the bulk to the surface of the TNA catalyst. In the model developed in this study, the assumption is that the MB molecules have to diffuse to the surface of the catalyst to be degraded. An alternate theory can be examined based on diffusion of oxidizing species from surface of the catalyst to the bulk solution. Based on existing work, we know that oxidizing species ($OH^{\bullet}$, $^{\bullet}O_2^-$, H_2O_2) are generated at the surface of the TNA catalyst by reaction of the photogenerated electron–holes in an aqueous solution [50–52,13,53]). While the lifetime of $OH^{\bullet}$, $^{\bullet}O_2$ radicals are very short, hydrogen peroxide (H_2O_2) molecules can remain stable and potentially diffuse from catalyst surface to MB present in solution. For instance, Fujishima reported long-range photocatalytic bactericidal effect (up to 50 μm) from the surface of TiO_2 films and proposed H_2O_2 and other oxygen species as likely agents [54]. Remote bleaching of methylene blue in gas phase at a distance of 500 μm away from the surface of UV irradiated TiO_2 films has been reported [55,52]. With a diffusion coefficient of 1.71×10^{-9} m^2/s [56], it would take 26 s for the H_2O_2 molecule to diffuse half the height of the microfluidic channel. We assume the generation of the H_2O_2 and other oxidizing species are limited by their concentration near surface of TNA catalyst. Hence at larger flow rates larger amounts of H_2O_2 molecules are carried away from the catalyst surface by the flow, resulting in a faster generation of H_2O_2 molecules. These molecules could potentially mix with the MB not just in microfluidic channel but also once the sample is collected. This would account for the higher conversion achieved at larger flow rates. Since the height of the TNA array would determine the amount of the oxidizing species generated, the longer the TNA array tubes, the better the degradation performance [13]. This fits well with the results observed in this study for different nanotube lengths (Fig. 8b).

4.5. Degradation performance of the microfluidic reactor – system performance comparison with current literature

The degradation performance of other titania-based photocatalytic microfluidic systems has been complied and compared (Table 1). Although all of the studies mentioned in Table 1 use methylene blue, it is difficult to compare the performance of TNA photocatalyst with these systems due to the different channel geometries, flow-rates, pollutant concentration and photocatalyst surface area involved. The degradation performance in these systems is reported as a function of irradiation time [2] or the effective residence time [6]. In the case of microfluidic surface reactors, the Pêclet number determines whether diffusion or advection is the dominating means of pollutant mass transport to the photocatalyst surface. Hence we have converted the results of these studies as a function of dimensionless Pêclet number

$$Pe = \frac{(L \times U)}{D} \tag{7}$$

where *L* is the characteristic length, *U* the flow velocity, and *D* is the mass diffusion coefficient. The Pêclet number is a measure of relative importance of advection to diffusion [57,58]. The dimensionless Pêclet numbers corresponding to the flow rates 200, 100, 50 and 25 μL/min are 8*P*, 4*P*, 2*P* and *P* (*P* = 9639). These equivalent Pêclet numbers enable comparison with other microfluidic surface reaction systems of varied geometries with the exception for the system reported by Qin et al.[6] (electrospun nanofibrous TiO_2), the maximum Pêclet number of the microfluidic systems are less than Pêclet numbers for this study (38,556). Hence the advection to diffusive mass transport is higher in the microfluidic system in this study compared to the other two studies mentioned. Since the irradiance intensity and wavelength of light source are different for the other studies in Table 1, an absolute degradation performance comparison is not possible. But in terms of comparison based on the nature of convective flow in the microfluidic system, the results of this study demonstrates a much larger advective flow conditions than the other two studies mentioned earlier [3,17]. For instance, the Pêclet number defines how rapidly the inlet pollutant is carried by the moving fluid towards the catalyst relative to how fast the degraded products are transferred from the catalyst surface to the center of the fluid flow for removal [59]. Hence the larger the Pêclet

Table 1
Summary of reported titania-based photocatalytic microfluidic systems for MB degradation.

Photocatalyst	Irradiance intensity (mW/cm^2)	Wavelength &lamp source	Flow rates ($\mu L/min$)	Peclet number range	Initial concentration of MB (M)	Percent conversion reported
TiO_2 coated fiber glass	2	310–400 nm, 150 W mercury lamp	33.3–200	541–3248	20×10^{-6}	45–90% [17]
Electrospun nanofibrous TiO_2	50	365 nm, UV-LED lamp	25–100	20,300–81,198	31×10^{-6}	55–95% [6]
P25 TiO_2 film	100	AM 1.5 simulated solar light	150–900	2256–13,533	30×10^{-6}	48–94% [3]
P25 TiO_2 film	100	AM 1.5 simulated solar light	25–100	9639–38,556	18×10^{-3}	55–93% (this study)
TNA	100	AM 1.5 simulated solar light	25–100	9639–38,556	18×10^{-3}	82–92% (this study)

number, a higher throughput of fluid in the microfluidic system can be realized.

5. Conclusion

The photocatalytic degradation of a model compound, methylene blue, was examined in a microfluidic system using TNA photocatalyst under simulated AM 1.5 irradiation. The microfluidic device was constructed using a non-clean room, inexpensive, rapid prototyping technique. When compared to a film of commercial P25 photocatalyst, TNA demonstrated enhanced degradation over the range of flow rates examined. Analysis of the degradation kinetics reveals that a 12 μm TNA photocatalyst operates under diffusion limited conditions for all flow rates studied, while the P25 photocatalyst film operates under reaction limited conditions at higher flow rates. The improved performance of the TNA photocatalyst over P25 can be attributed to better diffusion of reacting species and improved charge separation. A comparison with other titania-based photocatalytic microfluidic systems reported in the literature based on the dimensionless Péclet number is discussed.

A finite element model was developed to simulate the degradation of MB in the microfluidic channel utilizing COMSOL Multiphysics. From the model developed, the effect of diffusion coefficient and rate constant is discussed. The effect of the diffusion coefficient on the fractional conversion is more sensitive than that of the rate constant. The model can be easily modified to suit other channel geometries, pollutants with different diffusion coefficients, or different values of rate constants.

Acknowledgement

The work presented here was supported by the Utah Science Technology and Research (USTAR) initiative.

References

[1] H. Lachheb, E. Puzenat, A. Houas, M. Ksibi, E. Elaloui, C. Guillard, J.-M. Herrmann, Photocatalytic degradation of various types of dyes (Alizarin s, Crocein Orange G, Methyl Red, Congo Red, Methylene Blue) in water by UV-irradiated titania, Appl. Catal. B: Environ. 39 (1) (2002) 75–90.
[2] Z. Han, J. Li, W. He, S. Li, Z. Li, J. Chu, Y. Chen, A microfluidic device with integrated ZnO nanowires for photodegradation studies of methylene blue under different conditions, Microelectron. Eng. 111 (2013) 199–203.
[3] L. Lei, N. Wang, X. Zhang, Q. Tai, D.P. Tsai, H.L. Chan, Optofluidic planar reactors for photocatalytic water treatment using solar energy, Biomicrofluidics 4 (4) (2010) 043004.
[4] L. Helen, et al., Microfluidic reactors for photocatalytic water purification, Lab Chip 14 (6) (2014) 1074–1082.
[5] N. Wang, X. Zhang, B. Chen, W. Song, N.Y. Chan, H.L. Chan, Microfluidic photoelectrocatalytic reactors for water purification with an integrated visible-light source, Lab Chip 12 (20) (2012) 3983–3990.
[6] Z. Meng, X. Zhang, J. Qin, A high efficiency microfluidic-based photocatalytic microreactor using electrospun nanofibrous TiO_2 as a photocatalyst, Nanoscale 5 (11) (2013) 4687–4690.
[7] A. Kar, Y.R. Smith, V. Subramanian, Improved photocatalytic degradation of textile dye using titanium dioxide nanotubes formed over titanium wires, Environ. Sci. Technol. 43 (9) (2009) 3260–3265.
[8] H. Zhang, J.-J. Wang, J. Fan, Q. Fang, Microfluidic chip-based analytical system for rapid screening of photocatalysts, Talanta 116 (2013) 946–950.
[9] M.R. Prairie, L.R. Evans, B.M. Stange, S.L. Martinez, An investigation of titanium dioxide photocatalysis for the treatment of water contaminated with metals and organic chemicals, Environ. Sci. Technol. 27 (9) (1993) 1776–1782.
[10] H. Jayamohan, Y.R. Smith, B.K. Gale, M. Misra, S.K. Mohanty, Platinum functionalized titania nanotube array sensor for detection of trichloroethylene in water, in: Sensors, 2013 IEEE, IEEE, 2013, pp. 1–4.
[11] Y.-Y. Song, F. Schmidt-Stein, S. Bauer, P. Schmuki, Amphiphilic TiO_2 nanotube arrays: an actively controllable drug delivery system, J. Am. Chem. Soc. 131 (12) (2009) 4230–4232.
[12] Y.R. Smith, R.S. Ray, K. Carlson, B. Sarma, M. Misra, Self-ordered titanium dioxide nanotube arrays: anodic synthesis and their photo/electro-catalytic applications, Materials 6 (7) (2013) 2892–2957.
[13] J.M. Macak, M. Zlamal, J. Krysa, P. Schmuki, Self-organized TiO_2 nanotube layers as highly efficient photocatalysts, Small 3 (2) (2007) 300–304.
[14] H. Lindstrom, R. Wootton, A. Iles, High surface area titania photocatalytic microfluidic reactors, AIChE J. 53 (3) (2007) 695–702.
[15] D. Daniel, I.G. Gutz, Microfluidic cell with a TiO_2-modified gold electrode irradiated by an UV-LED for in situ photocatalytic decomposition of organic matter and its potentiality for voltammetric analysis of metal ions, Electrochem. Commun. 9 (3) (2007) 522–528.
[16] N. Tsuchiya, K. Kuwabara, A. Hidaka, K. Oda, K. Katayama, Reaction kinetics of dye decomposition processes monitored inside a photocatalytic microreactor, Phys. Chem. Chem. Phys. 14 (14) (2012) 4734–4741.
[17] L. Li, R. Chen, X. Zhu, H. Wang, Y. Wang, Q. Liao, D. Wang, Optofluidic microreactors with TiO_2-coated fiberglass, ACS Appl. Mater. Interfaces 5 (23) (2013) 12548–12553.
[18] G. Takei, T. Kitamori, H.-B. Kim, Photocatalytic redox-combined synthesis of L-pipecolinic acid with a titania-modified microchannel chip, Catal. Commun. 6 (5) (2005) 357–360.
[19] H. Aran, D. Salamon, T. Rijnaarts, G. Mul, M. Wessling, R. Lammertink, Porous photocatalytic membrane microreactor (P2M2): a new reactor concept for photochemistry, J. Photochem. Photobiol. A: Chem. 225 (1) (2011) 36–41.
[20] D.C. Duffy, J.C. McDonald, O.J. Schueller, G.M. Whitesides, Rapid prototyping of microfluidic systems in poly(dimethylsiloxane), Anal. Chem. 70 (23) (1998) 4974–4984.
[21] J. Kim, R. Surapaneni, B.K. Gale, Rapid prototyping of microfluidic systems using a PDMS/polymer tape composite, Lab Chip 9 (9) (2009) 1290–1293.
[22] E. Sollier, C. Murray, P. Maoddi, D. Di Carlo, Rapid prototyping polymers for microfluidic devices and high pressure injections, Lab Chip 11 (22) (2011) 3752–3765.
[23] H.T. Chang, N.-M. Wu, F. Zhu, A kinetic model for photocatalytic degradation of organic contaminants in a thin-film TiO_2 catalyst, Water Res. 34 (2) (2000) 407–416.
[24] M. Dijkstra, H. Panneman, J. Winkelman, J. Kelly, A. Beenackers, Modeling the photocatalytic degradation of formic acid in a reactor with immobilized catalyst, Chem. Eng. Sci. 57 (22) (2002) 4895–4907.
[25] N. Daneshvar, M. Rabbani, N. Modirshahla, M. Behnajady, Kinetic modeling of photocatalytic degradation of Acid Red 27 in UV/TiO_2 process, J. Photochem. Photobiol. A: Chem. 168 (1) (2004) 39–45.
[26] H. Yatmaz, A. Akyol, M. Bayramoglu, Kinetics of the photocatalytic decolorization of an azo reactive dye in aqueous ZnO suspensions, Ind. Eng. Chem. Res. 43 (19) (2004) 6035–6039.
[27] Y.R. Smith, R. Gakhar, A. Merwin, S.K. Mohanty, D. Chidambaram, M. Misra, Anodic titania nanotube arrays sensitized with Mn- or Co-doped CdS nanocrystals, Electrochim. Acta 135 (2014) 503–512.
[28] S.K. Mohapatra, M. Misra, V.K. Mahajan, K.S. Raja, Design of a highly efficient photoelectrolytic cell for hydrogen generation by water splitting: application of $TiO_{2-x}C_x$ nanotubes as a photoanode and Pt/TiO_2 nanotubes as a cathode, J. Phys. Chem. C 111 (24) (2007) 8677–8685.
[29] G.P. Smestad, M. Gratzel, Demonstrating electron transfer and nanotechnology: a natural dye-sensitized nanocrystalline energy converter, J. Chem. Educ. 75 (6) (1998) 752.

[30] Y. Xia, G.M. Whitesides, Soft lithography, Annu. Rev. Mater. Sci. 28 (1) (1998) 153–184.
[31] M.A. Eddings, M.A. Johnson, B.K. Gale, Determining the optimal PDMS–PDMS bonding technique for microfluidic devices, J. Micromech. Microeng. 18 (6) (2008) 067001.
[32] A. Houas, H. Lachheb, M. Ksibi, E. Elaloui, C. Guillard, J.-M. Herrmann, Photocatalytic degradation pathway of methylene blue in water, Appl. Catal. B: Environ. 31 (2) (2001) 145–157.
[33] K. Rajeshwar, M. Osugi, W. Chanmanee, C. Chenthamarakshan, M. Zanoni, P. Kajitvichyanukul, R. Krishnan-Ayer, Heterogeneous photocatalytic treatment of organic dyes in air and aqueous media, J. Photochem. Photobiol. C: Photochem. Rev. 9 (4) (2008) 171–192.
[34] M. Resende, P. Vieira, R. Sousa Jr., R. Giordano, R. Giordano, Estimation of mass transfer parameters in a Taylor-Couette-Poiseuille heterogeneous reactor, Braz. J. Chem. Eng. 21 (2) (2004) 175–184.
[35] H.-F. Zhuang, C.-J. Lin, Y.-K. Lai, L. Sun, J. Li, Some critical structure factors of titanium oxide nanotube array in its photocatalytic activity, Environ. Sci. Technol. 41 (13) (2007) 4735–4740.
[36] J. Augustynski, The role of the surface intermediates in the photoelectrochemical behaviour of anatase and rutile TiO_2, Electrochim. Acta 38 (1) (1993) 43–46.
[37] R. Beranek, H. Tsuchiya, T. Sugishima, J. Macak, L. Taveira, S. Fujimoto, H. Kisch, P. Schmuki, Enhancement and limits of the photoelectrochemical response from anodic TiO_2 nanotubes, Appl. Phys. Lett. 87 (24) (2005) 243114.
[38] Y.R. Smith, A. Kar, V. Subramanian, Investigation of physicochemical parameters that influence photocatalytic degradation of methyl orange over TiO_2 nanotubes, Ind. Eng. Chem. Res. 48 (23) (2009) 10268–10276.
[39] T. Zhang, T. Oyama, A. Aoshima, H. Hidaka, J. Zhao, N. Serpone, Photooxidative n-demethylation of methylene blue in aqueous TiO_2 dispersions under UV irradiation, J. Photochem. Photobiol. A: Chem. 140 (2) (2001) 163–172.
[40] Y.R. Smith, B. Sarma, S.K. Mohanty, M. Misra, Light-assisted anodized TiO_2 nanotube arrays, ACS Appl. Mater. Interfaces 4 (11) (2012) 5883–5890.
[41] Y.-C. Nah, I. Paramasivam, P. Schmuki, Doped TiO_2 and TiO_2 nanotubes: synthesis and applications, ChemPhysChem 11 (13) (2010) 2698–2713.
[42] S. Kim, W. Choi, Visible-light-induced photocatalytic degradation of 4-chlorophenol and phenolic compounds in aqueous suspension of pure titania: demonstrating the existence of a surface-complex-mediated path, J. Phys. Chem. B 109 (11) (2005) 5143–5149.
[43] T. Wu, G. Liu, J. Zhao, H. Hidaka, N. Serpone, Evidence for H_2O_2 generation during the TiO_2-assisted photodegradation of dyes in aqueous dispersions under visible light illumination, J. Phys. Chem. B 103 (23) (1999) 4862–4867.
[44] V. Subramanian, P.V. Kamat, E.E. Wolf, Mass-transfer and kinetic studies during the photocatalytic degradation of an azo dye on optically transparent electrode thin film, Ind. Eng. Chem. Res. 42 (10) (2003) 2131–2138.
[45] L.F. Moody, Friction factors for pipe flow, Trans. ASME 66 (8) (1944) 671–684.
[46] R. Jaeger, J. Ren, Y. Xie, S. Sundararajan, M.G. Olsen, B. Ganapathysubramanian, Nanoscale surface roughness affects low Reynolds number flow: experiments and modeling, Appl. Phys. Lett. 101 (18) (2012) 184102.
[47] J. Krýsa, G. Waldner, H. Měšťánková, J. Jirkovský, G. Grabner, Photocatalytic degradation of model organic pollutants on an immobilized particulate TiO_2 layer: roles of adsorption processes and mechanistic complexity, Appl. Catal. B: Environ. 64 (3) (2006) 290–301.
[48] S.-Z. Chu, S. Inoue, K. Wada, S. Hishita, K. Kurashima, Self-organized nanoporous anodic titania films and ordered titania nanodots/nanorods on glass, Adv. Funct. Mater. 15 (8) (2005) 1343–1349.
[49] V. Swaminathan, R. Tchao, S. Jonnalagadda, Physical characterization of thin semi-porous poly(L-lactic acid)/poly(ethylene glycol) membranes for tissue engineering, J. Biomater. Sci. Polym. Ed. 18 (10) (2007) 1321–1333.
[50] C.S. Turchi, D.F. Ollis, Mixed reactant photocatalysis: intermediates and mutual rate inhibition, J. Catal. 119 (2) (1989) 483–496.
[51] D.F. Ollis, H. Al-Ekabi, Photocatalytic purification and treatment of water and air, in: Proceedings of the 1st International Conference on TiO_2 Photocatalytic Purification and Treatment of Water and Air, 8–13 November 1992, London, Ontario, Canada, Elsevier Science Ltd, 1993.
[52] A. Fujishima, T.N. Rao, D.A. Tryk, Titanium dioxide photocatalysis, J. Photochem. Photobiol. C: Photochem. Rev. 1 (1) (2000) 1–21.
[53] Y.S. Sohn, Y.R. Smith, M. Misra, V. Subramanian, Electrochemically assisted photocatalytic degradation of methyl orange using anodized titanium dioxide nanotubes, Appl. Catal. B: Environ. 84 (3) (2008) 372–378.
[54] Y. Kikuchi, K. Sunada, T. Iyoda, K. Hashimoto, A. Fujishima, Photocatalytic bactericidal effect of TiO_2 thin films: dynamic view of the active oxygen species responsible for the effect, J. Photochem. Photobiol. A: Chem. 106 (1) (1997) 51–56.
[55] T. Tatsuma, S.-i. Tachibana, T. Miwa, D.A. Tryk, A. Fujishima, Remote bleaching of methylene blue by UV-irradiated TiO_2 in the gas phase, J. Phys. Chem. B 103 (38) (1999) 8033–8035.
[56] R.C. Pena, J. Gamboa, M. Bertotti, T.R. Paixao, Studies on the electrocatalytic reduction of hydrogen peroxide on a glassy carbon electrode modified with a ruthenium oxide hexacyanoferrate film, Int. J. Electrochem. Sci. 6 (2) (2011) 394.
[57] T.M. Squires, S.R. Quake, Microfluidics: fluid physics at the nanoliter scale, Rev. Mod. Phys. 77 (3) (2005) 977.
[58] R.B. Bird, W.E. Stewart, E.N. Lightfoot, Transport Phenomena, John Wiley & Sons, 2007.
[59] K.S. Elvira, X.C. i Solvas, R.C. Wootton, The past, present and potential for microfluidic reactor technology in chemical synthesis, Nat. Chem. 5 (11) (2013) 905–915.

CHAPTER 6

DEGRADATION OF ORGANIC AND BIOLOGICAL CONTAMINANTS: PHOTOCATALYTIC MICROFLUIDIC REACTORS UTILIZING TITANIA NANOTUBES ON TITANIUM MESH

6.1 Abstract

Microfluidic reactors are being increasingly applied to photocatalytic degradation of contaminants in water. They have advantages like large surface-area-to-volume ratio and high control of fluid flow. They still suffer from drawbacks due to limited mass transport associated with laminar flow in microfluidic channels. The use of titania nanotubes synthesized on a mesh show improved photocatalytic performance in comparison to nanotubes synthesized on foil in a microreactor. At the lowest flow rate (25 μL\min), the fractional conversion increased from 20% for foil to 46% in the case of nanotubes on mesh. The enhanced photocatalytic performance is due to shorter diffusion distance and induction of flow perturbation in the case of mesh format. Also, the radially outward oriented nanotubes formed over the circumference of the titanium wire leads to the efficient capture of both reflected and refracted light. The device was also applied to inactivation of *E. coli* O157:H7. At a flow rate of 50 μL\min, the titania nanotubes on a mesh microreactor was able to achieve >99% inactivation of *E. coli*.

6.2 Introduction

According to estimates, 1.2 billion people lack access to safe drinking water, which contributes to the death of 3900 children daily [1]. Hence, access to clean water is a worldwide need. In both industrialized and developing nations, chemical and biological contaminants are finding their way into water bodies due to increasing human activity

[1]. Cleanup and reuse of polluted wastewater is an attractive solution to some of these issues. Low-cost and high-efficiency water remediation technologies are needed to achieve the same [2]. Conventional wastewater treatment technologies such as adsorption or coagulation merely concentrate the pollutants present by transferring them to other phases [2]. Other conventional methods such as sedimentation, filtration, chemical, and membrane technologies are expensive and potentially generate toxic secondary pollutants [1].

Advanced Oxidation Processes (AOP) could solve some of the issues associated with conventional water treatment methods. These processes work by the generation of highly reactive transitory species (*e.g.* H_2O_2, $OH^{\bullet}$, $O_2^{\bullet -}$, O_3) for mineralization of chemical and biological pollutants present in water [2]. Among these AOPs, photocatalytic environmental remediation employing semiconductor photocatalysts has been widely applied for remediation of water-based pollutants [3, 2]. Nanomaterial semiconductor photocatalysts have been used due to their interesting properties over bulk materials. Many studies have used powdered photocatalysts suspended in solution [4, 5]. However, the use of powdered photocatalysts necessitates their downstream recovery. This can lead to increased operational and capital costs [5, 6]. Also, the use of powdered catalyst particles limits the depth of penetration of light due to strong adsorption and scattering [7, 8]. The immobilization or growth of photocatalysts as a film on a substrate eliminates many of these drawbacks [6].

Microfluidic reactors (microreactors) have been increasingly applied to water remediation over conventional macroscale reactors [9, 10]. This is because conventional macroscale reactors have limitations due to mass transport and poor photon transport [5]. In the case of microreactors, the thin layer of liquid over the catalyst ensures lesser photons are lost due to scattering [11]. Microreactors can be advantages over conventional macroscale reactors due to large surface to volume ratio, smaller diffusion distance, and large mass transfer efficiency [12]. Microfluidic photocatalytic reactors have been reported to have higher photocatalytic efficiency compared to conventional reactors [10].

Titanium dioxide (TiO_2) has been widely applied to photocatalytic degradation of chemical and biological pollutants [13, 6, 14, 15]. Titania nanotube arrays (TNA) are of particular interest due to their simple synthesis and improved ability to transport photogenerated charges as compared to their titanium dioxide nanoparticle (TNP) counterpart [16]. Titania nanotube arrays have shown to have enhanced photocatalytic properties compared to TNP layers in a macroscale batch reactor configuration [17]. Further, by electrochemical anodization, TNA can be synthesized on different titanium (Ti) metal substrates, having

varied geometries (thin wires [8], meshes [16], and curved surfaces [18]).

TiO_2 based catalysts in the form of TNA [11] and TNP [19, 10, 5] have been applied in microreactors for photocatalytic degradation. We recently reported the application of TNA synthesized on a foil (TNA_{foil}) for degradation of methylene blue (MB) in a microreactor [11]. The TNA_{foil} had enhanced photocatalytic performance over P25 TNP layer when used in a microfluidic format.

Current microfluidic formats face a major drawback due to limited mass-transport. This is because in a microfluidic format, the flow is typically laminar and mass transport is primarily through diffusion [5]. To overcome this limitation, Li et al. reported the use of a fiberglass coated with P25 TNP layer for the degradation of MB [5]. The new design yielded higher degradation over a conventional microreactor platform involving P25 TNP layer embedded on a flat surface.

Although TNA_{foil} has shown promising results for photocatalytic applications, the use of metal foils has limitations (such as the opacity, inefficient use of Ti, and reduced flexibility). As an alternative, metal meshes provide an approach that allows for high flexibility, efficient Ti utilization, and transparency. Such a format has shown has shown to be effective in applications such as dye-sensitized solar cells [20].

We report the use of TNA grown on a titanium mesh (TNA_{mesh}) for photocatalytic degradation of MB and inactivation of *E. coli* O157:H7 in a microfluidic format. The microfluidic device was fabricated using non-cleanroom-based technique which makes it suitable for large-scale applications [21]. The degradation performance is compared to that of previously reported data using TNA_{foil} at different flow rates in a geometrically similar microreactor [11]. We also report the use of TNA_{mesh} for the photocatalytic inactivation of *E. coli*. The use of TNA for inactivation of pathogens in a flow through system has yet to be fully explored.

6.3 Experimental

6.3.1 Preparation and Characterization of TNA on Foil and Mesh

Titania nanotube arrays grown on a titanium mesh were synthesized by electrochemical anodization similar to an earlier reported protocol [16]. In short, Titanium gauze (50 mesh woven from 0.102 mm dia wire, 64% open area) was obtained from Alfa Aesar and cut into 3x2 cm^2 dimensions. The Ti gauze was first washed with isopropanol and DI water under sonication for 10 mins each, and then electropolished in 1 °C glacial acetic acid/perchloric acid (9:1 volume ratio) at 60 V under sonication for 1 min [22]. The electrochemical anodization was carried out at an applied potential of 60 V (D.C.)(Agilent, E3647A) for

60 min. The thus formed TNA_{mesh} was rinsed with DI water, air dried, and subsequently annealed in an atmosphere of N_2 (2% H_2) at 500 °C (1.6 °C/min ramp rate) for 2 h.

The morphology of the thus formed TNA_{mesh} film was characterized using a field emission scanning electron microscope (SEM) (Hitachi, S-4800).

6.3.2 Fabrication of Microfluidic Channel and Integration of TNA_{mesh} Substrate

The microfluidic device was fabricated by soft lithography [21] similar to that reported in our earlier study [11]. In short, the mold was cut on a tape using a laser, polydimethylsiloxane (PDMS) mix poured onto the mold, and cured in an oven to create the PDMS layer. Subsequently, inlet and outlet channels were bored onto the PDMS channel and the TNA_{mesh} catalyst was embedded into the PDMS channel. Finally, a corona activated glass slide was bonded to the PDMS layer.

6.3.3 Evaluation of the Photocatalytic Degradation of Methylene Blue

The photocatalytic degradation of the device was evaluated using methylene blue (MB) as a model pollutant. Methylene blue is a nonbiodegradable dye and is used for characterizing photocatalytic performance [23, 24, 17]. The experimental setup used to evaluate the photocatalytic performance of the device is depicted in Fig. 6.1. In a typical experimental run, 4 ml of 18 mM aqueous solution of MB was injected through the inlet into the microfluidic device using a syringe pump (KD Scientific, Manassas, VA) via Tygon tubing (0.02 inch/0.0508 mm inner diameter) at different flow rates ranging from 25-200 μL/min. The microfluidic device was irradiated with AM 1.5 simulated solar light (100 mW/cm^2). The intensity of the light was measured at the surface of the microfluidic device using a handheld power meter (Nova, Ophir-Spiricon, UT). The degraded MB solution was collected and the concentration was determined by monitoring the change in characteristic absorption peak at $\lambda = 664$ nm using a UV-vis spectrophotometer (Shimadzu Corp., Japan). The fractional conversion was given by:

$$X(\%) = \frac{A_0 - A}{A_0} 100 \tag{6.1}$$

where A_0 is the initial concentration absorbance value, and A is the absorbance value of the degraded solution. The experiment was repeated in the absence of AM 1.5 light to evaluate the amount of MB adsorbed on the catalyst. The fractional conversion was normalized with respect to the substrate area exposed to normal incident light [8]. The results were compared to normalized fractional conversion of MB using a TNA_{foil} (12 μm and 7 μm nanotube lengths) reported in our earlier work [11].

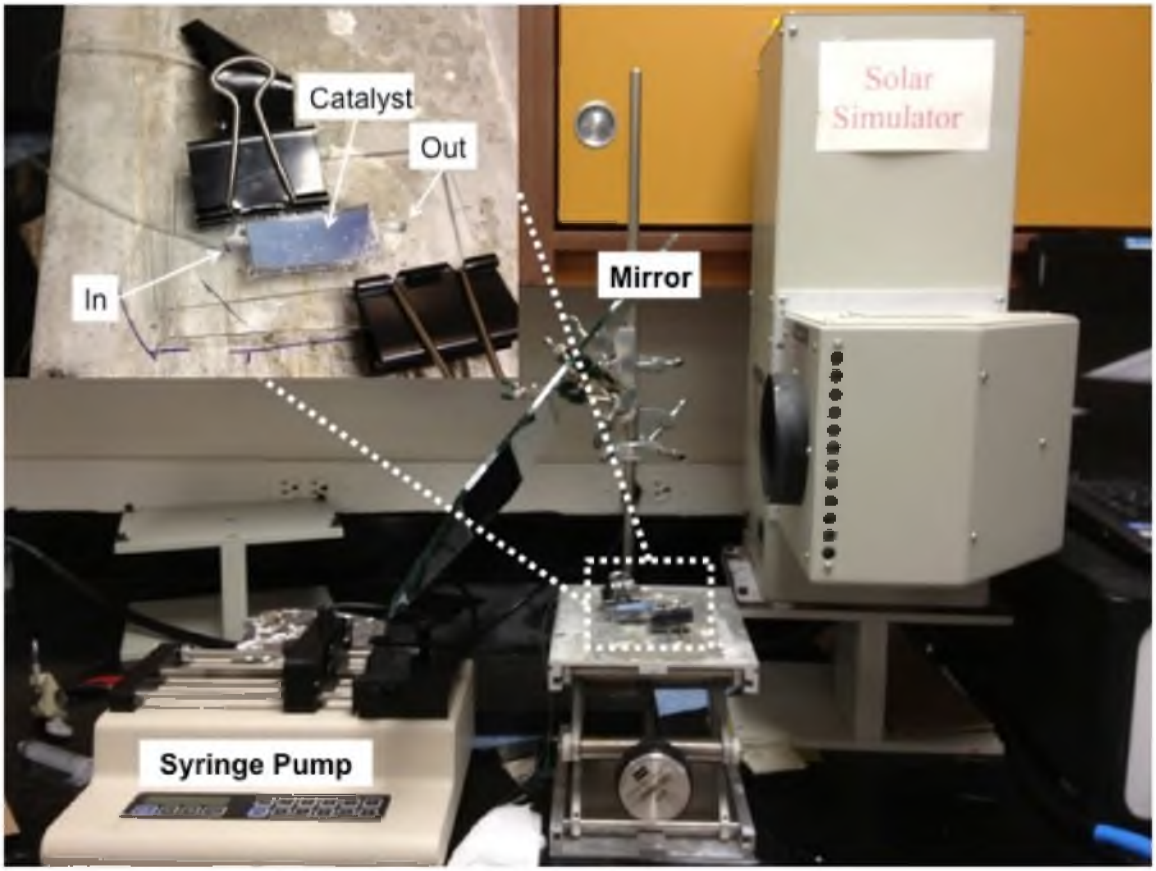

Figure 6.1. Experimental setup. Reproduced with permission from Elsevier [11].

6.3.4 Evaluation of the Photocatalytic Inactivation of *E. coli*

The photocatalytic inactivation of *E. coli* was evaluated using TNA_{mesh} in a microreactor as described above. *E. coli* O157:H7 (nonpathogenic strain, Catalog no. 700728, ATCC) was used to prepare different concentrations (1000 and 10000 CFUs/mL) of *E. coli* in 1X PBS solution [25]. The experimental setup is the same as that for MB degradation mentioned in the section above. A four mL sample of the *E. coli* solution was taken in a syringe, 3 mL of which was injected using a syringe pump through the inlet into the microfluidic device. The flow rates were varied from 25-200 μL/min in the absence and presence of AM 1.5 simulated solar light (100 mW/cm^2). The intensity of the light was varied from 10-100 mW/cm^2 to evaluate the effect on inactivation. The inactivated *E. coli* solution was collected and plated on agar (Difco Nutrient Agar, Catalog no. 213000, Becton Dickinson, Sparks, MD), incubated at 37°C for 12 h, and subsequently counted to calculate the final concentration (C_f). The 1 mL stock solution left in the syringe was also plated after the experimental run (to avoid any nonphotocatalytic, room temperature-based inactivation of *E. coli* during the experimental run) to determine the initial concentration (C_0). The survival ratio was calculated by:

$$X(\%) = \frac{C_0}{C_f} 100 \tag{6.2}$$

where C_f is the final concentration (CFU/mL) of *E. coli* post inactivation in the microfluidic device, and C_0 is the initial concentration (CFU/mL) of *E. coli* (solution solution left in the syringe). The experiment was repeated in the absence of AM 1.5 light to evaluate the amount of *E. coli* adsorbed/trapped in the catalyst. The experiment was also performed in the presence of AM 1.5 light in the microreactor without the catalyst embedded in it to evaluate the effect of light inactivation only on *E. coli*.

6.4 Results and Discussion

6.4.1 Properties of Titania Nanotubes

The morphology of the TNA_{mesh} was characterized by SEM (Figs. 6.2, 6.3, and 6.4). From Fig. 6.2, fissures and bundling of nanotubes are observed in TNA_{mesh} (unlike TNA formed on a planer substrate\TNA_{foil}). These are due to the curvature-induced stress during formation of nanotubes and the outward radial growth of the nanotubes on a curved Ti substrate [8, 20]. Such a morphology is observed in TNA formed on wire-type substrates [26]. The nanotube lengths are approximately 8 μm (1 h anodization). The TNA_{mesh} tubes have an approximate inner diameter of 80 nm and wall thickness in the range 15-20 nm.

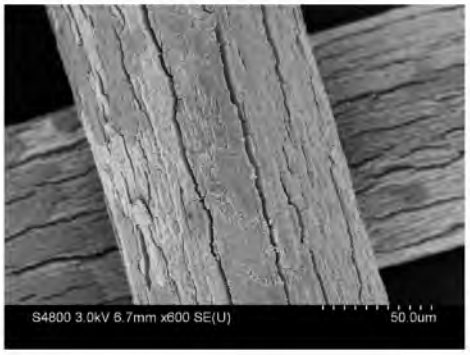

Figure 6.2. SEM images of TNA_{mesh} anodized at 60 V for 1 h, showing the low-magnified overall image of nanotubes on the anodized mesh.

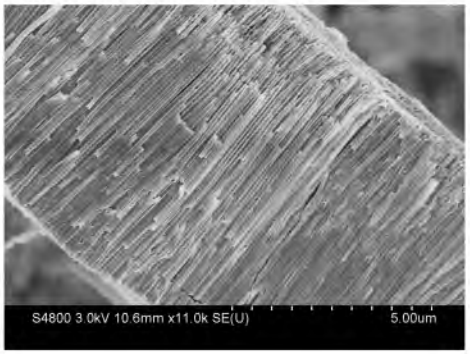

Figure 6.3. SEM images of TNA_{mesh} anodized at 60 V for 1 h, showing the sidewall morphology of nanotubes on the anodized mesh.

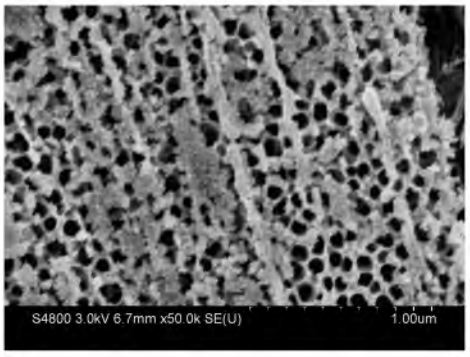

Figure 6.4. SEM images of TNA_{mesh} anodized at 60 V for 1 h, showing the top morphology of nanotubes on the anodized mesh.

Though the orientation of nanotubes differ, the morphology (nanotube height and diameter) of the TNA_{mesh} is very similar to the TNA_{foil} [11].

6.4.2 Degradation Efficiency (MB) of the Microfluidic Reactor- Effect of Flow Rates

The results of the degradation at different flow rates over TNA_{mesh} (8 μm) vs. TNA_{foil} (12 μm) with AM 1.5 irradiation are presented in Fig. 6.5. Both the TNA_{mesh} and TNA_{foil} catalysts show a similar trend of drop in degradation in the 25-50 μL/min domain. This is intuitive since an increase in flow rate would mean less time for the MB to diffuse and come in contact with the catalyst. However, it is interesting to note that the degradation performance of both the TNA_{mesh} and TNA_{foil} catalysts remain steady over the 50-200 μL/min domain. Such a trend has been previously observed [11], and is primarily due to the faster generation of oxidizing species with increased flow rate [11].

The TNA_{mesh} shows a higher fractional conversion compared to TNA_{foil} in the flow domain under consideration. At the lowest flow rate (25 μL/min), TNA_{mesh} exhibits a fractional conversion more than twice that of TNA_{foil}. At the highest flow rate (200 μL/min), TNA_{mesh} has a fractional conversion 1.5 times higher than TNA_{foil}. This is in spite of the fact that nanotube length on TNA_{mesh} is 66% lower than that on TNA_{foil} and the nanotube length [11].

6.4.3 Inactivation (*E. coli*)- Effect of Flow Rates

The results of the inactivation of *E. coli* at different flow rates over TNA_{mesh} are presented in Fig. 6.6. From the results, it is evident that in the given flow range (50-200 μL\min), there is very little inactivation (1-16%) of *E. coli* due to adsorption by the catalyst (absence of AM 1.5). Also, at the lowest flow rate (50 μL\min), there is very little inactivation (<8 %) of *E. coli* due to AM 1.5 light in the absence of TNA_{mesh} catalyst (not shown). This also indicates that the inactivation is primarily due to photocatalytic generation of species by TiO_2 and not due to the inactivation by the UV component of light.

For the 1000 CFUs\mL starting concentration, at the lowest flow rate (50 μL\min), almost 100% of the *E. coli* is inactivated using the TNA_{mesh} catalyst. Even at the highest flow rate, more than 92% of *E. coli* is inactivated. As the starting concentration increases by a order of magnitude, survival ratio increases from <1% to 6% (Fig. 6.7).

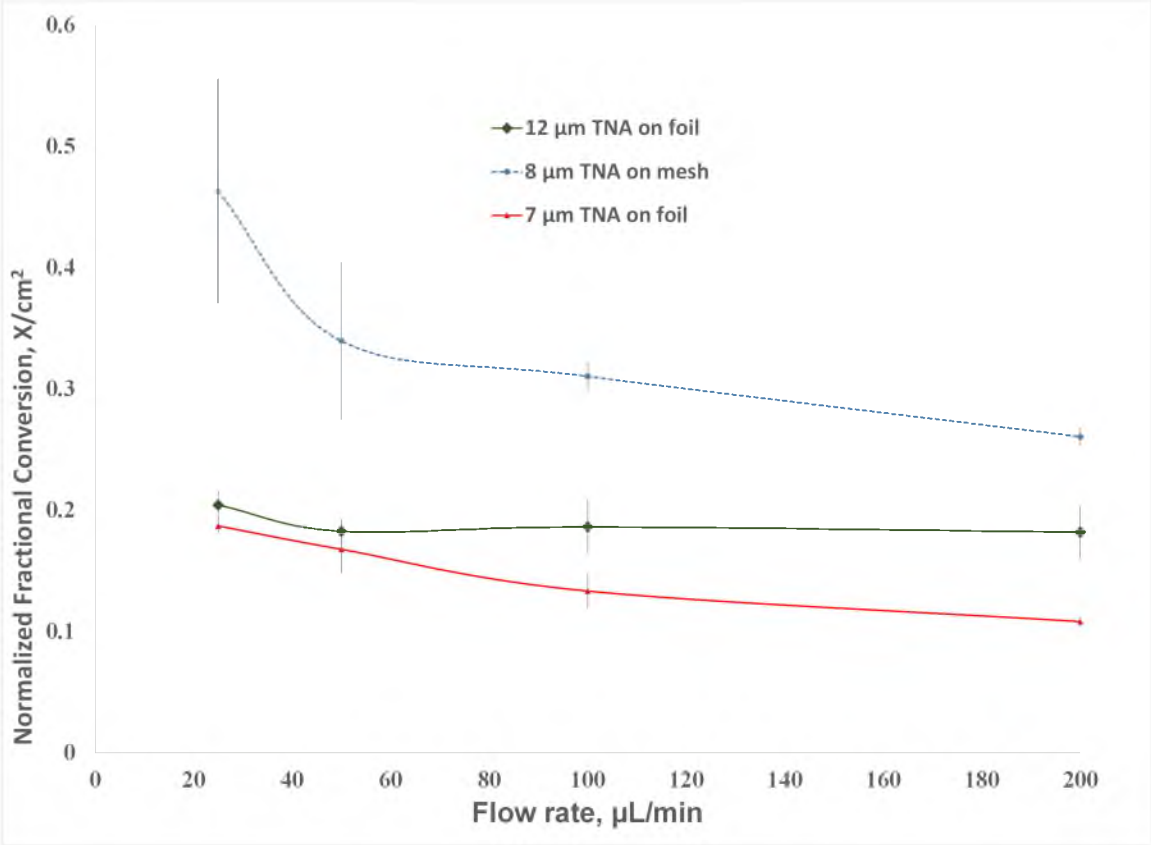

Figure 6.5. Effect of flow rate on MB degradation for TNA_{mesh} and TNA film catalyst in the presence and absence of AM 1.5 light (1000 CFU/mL starting concentration). The fractional conversion is normalized with respect to substrate area exposed to normal incident light.

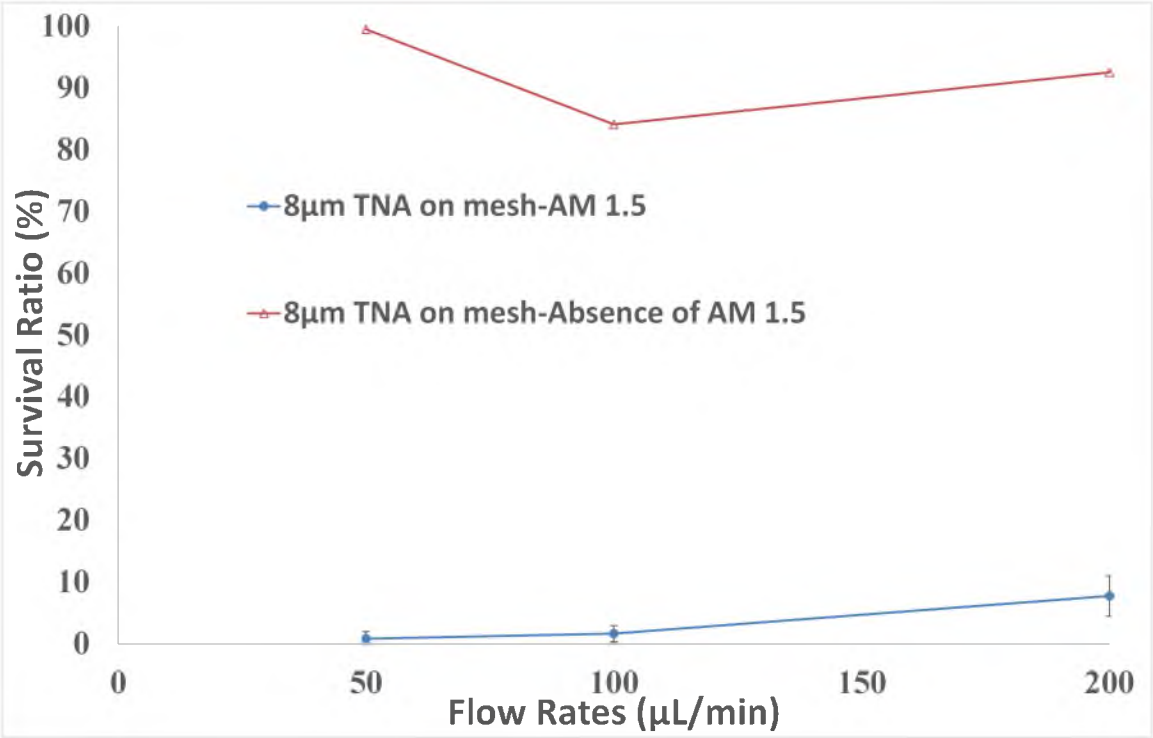

Figure 6.6. Effect of flow rate on *E. coli* inactivation for TNA_{mesh} in the presence and absence of AM 1.5 light (1000 CFU\mL starting concentration).

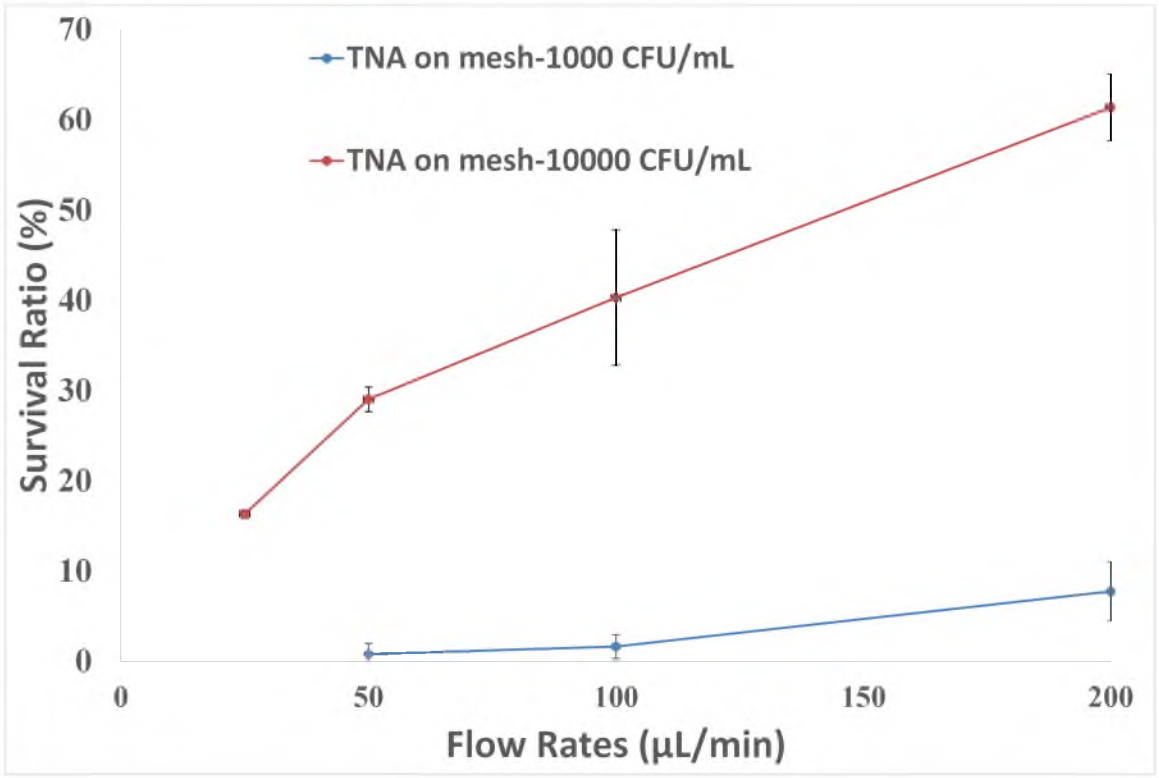

Figure 6.7. Effect of flow rate on *E. coli* inactivation at different starting concentration for TNA_{mesh} in the presence of AM 1.5 light.

6.4.4 Inactivation Efficiency of *E. coli*- Effect of Light Intensity

With a drop in light intensity, there is commensurate drop in *E. coli* inactivation. A 50% drop in light intensity results in a 50% drop in inactivation. From Fig. 6.8, the relationship between inactivation rate and light intensity is linear. This indicates the process is reaction dominated [27], *i.e.* the process has not reached a limiting light intensity where the electron-hole pair recombination limits further increase in inactivation. This means by further increasing the light intensity, the inactivation rate can be increased or a higher flow rate/process throughput can be achieved (at a given inactivation rate). This could be due to the low light scattering observed in the case of TNA_{mesh} format.

6.5 Discussion

The mechanism of photocatalytic MB degradation is well reported in literature [17]. The MB dye molecules adsorbed on the surface of the catalyst are oxidized by the photoinduced holes generated by the TiO_2 catalyst to form a radical $^{\bullet}MB^{+}$. These radicals further react with O_2 to form $[MBOO^{\bullet}]^{+}$, the heteropolyaromatic ring is broken, and subsequent degradation occurs [28].

Titanium nanotubes formed on titanium wires have been reported to demonstrate higher dye degradation performance in comparison to TNA_{foil} using a conventional macroscale non-flow-through format [8]. The higher degradation of the former was attributed to the geometry wherein the wires are juxtaposed next to one another [8]. Also, on wire and mesh substrates, titania nanotubes grow radially outwards in a uniform and compact manner. Such a configuration enables them to not only to utilize the absorbed light, but also the reflected and refracted light as well [26]. In the case of microfluidic format, the enhanced photocatalytic degradation of MB using the TNA_{mesh} catalyst can be attributed to the short transport length [5]. Unlike in the case of TNA_{foil}, the TNA_{mesh} catalyst remains suspended across height of the channel (Fig. 6.9). Hence, the MB molecules do not have to diffuse all the way to bottom of the microfluidic channel to reach a catalyst surface. Thus the mass transport is enhanced in the case of TNA_{mesh} in comparison to TNA_{foil}. Another reason for the enhanced performance can be attributed to the flow perturbation induced by the mesh [5].

The application of TiO_2 photocatalysts for *E. coli* inactivation was first reported by Yoshihiko et al. [29]. The mechanism of degradation of bacteria is similar to that for MB viz. due to the generation of reactive oxygen species/ROS ($OH^{\bullet}$, O_2^{-}, $HOO^{\bullet}$, H_2O_2) by TNA [30, 31]. The photo generated hole sites in the valance band of titania reacts with the water to form hydroxyl radicals ($OH^{\bullet}$), while the electrons promoted to the conduction

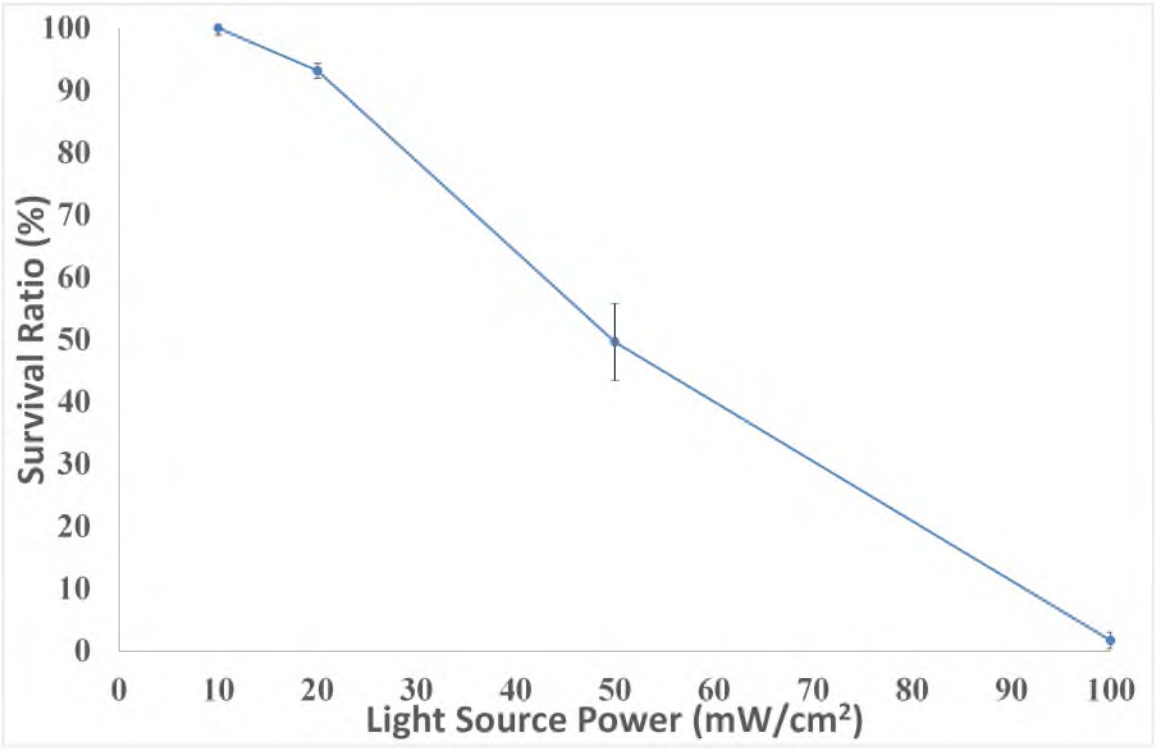

Figure 6.8. Effect of light intensity on *E. coli* degradation for TNA_{mesh} (1000 CFU\mL starting concentration, 100 μL/min).

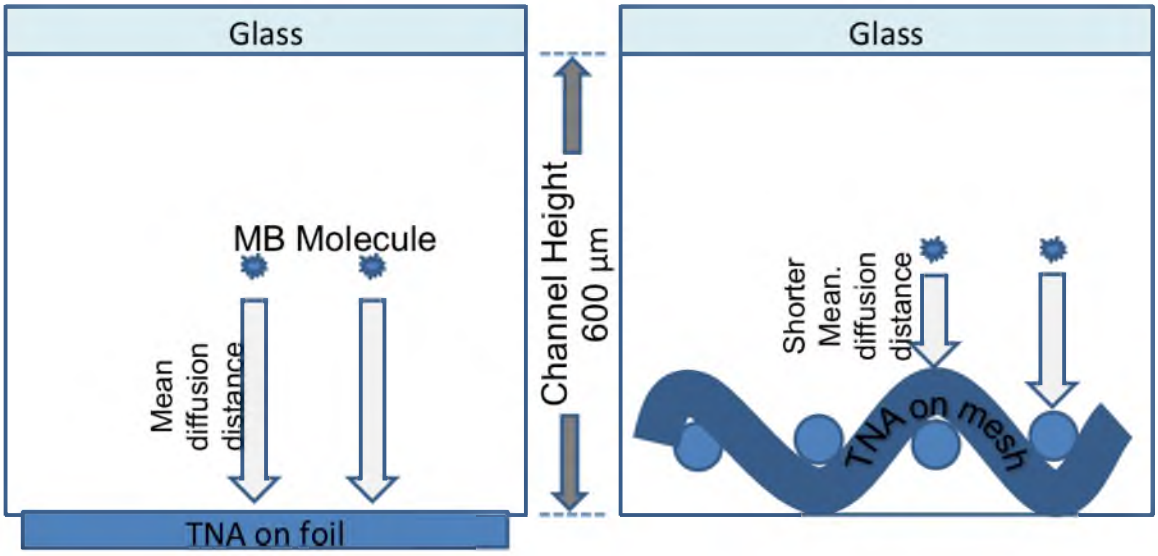

Figure 6.9. TNA_{foil} and TNA_{mesh} catalyst layouts in the microfluidic channel

band react with molecular oxygen to form superoxide ions and H_2O_2. These further react with water to form additional hydroxl radicals. An alternative mechanism involving the direct oxidation of bacteria through the photogenerated holes has been ruled out [32]. The photogenerated radicals are responsible for the inactivation of bacteria, by oxidizing organic material up to complete mineralization [32, 14]. The generated radicals attack the bacterial cell wall, leading to punctures [33, 32]. They cause the degradation of lipopolysaccharide, a cell wall constituent, and promote peroxidation of the lipid membrane [34, 35]. This results in the increase in the permeability of cells, the leakage of intracellular molecules, penetration of ROS into the cytoplasmic inner membrane, and finally induces bacterial cell death [36].

The use of microfluidic photocatalytic systems involving TNA_{mesh} could be used to harvest clean and inexpensive energy from the sun for photocatalytic water remediation. They can be used for industrial applications by scaling up the microreactors. These could also be used as portable water treatment devices especially in developing countries. The technique could be also be used in conjunction with current ultraviolet purifiers, wherein the power consumption can be significantly reduced, or the time for effective water treatment can be significantly reduced.

6.6 Conclusion

The photocatalytic degradation performance using TNA_{mesh} and TNA_{foil} catalyst in a microreactor was compared at different flow rates under simulated AM 1.5 light. The experimental results show that TNA_{mesh} exhibited enhanced degradation of MB pollutant in comparison TNA_{foil}. The improved photocatalytic performance of the TNA_{mesh} is attributed to shorter diffusion distance and induction of flow perturbation in the case of TNA_{mesh}. Also in the case of TNA_{mesh}, the nanotubes grow radially outwards in a uniform and compact manner, enabling them to utilize absorbed, reflected, and refracted light [26]. The microreactor was applied to the inactivation of *E. coli* O157:H7.

6.7 References

[1] M. A. Shannon, P. W. Bohn, M. Elimelech, J. G. Georgiadis, B. J. Mariñas, and A. M. Mayes, "Science and technology for water purification in the coming decades," *Nature*, vol. 452, no. 7185, pp. 301–310, 2008.

[2] M. N. Chong, B. Jin, C. W. Chow, and C. Saint, "Recent developments in photocatalytic water treatment technology: a review," *Water research*, vol. 44, no. 10, pp. 2997–3027, 2010.

[3] H. Lachheb, E. Puzenat, A. Houas, M. Ksibi, E. Elaloui, C. Guillard, and J.-M. Herrmann, "Photocatalytic degradation of various types of dyes (alizarin s, crocein orange g, methyl red, congo red, methylene blue) in water by uv-irradiated titania," *Applied Catalysis B: Environmental*, vol. 39, no. 1, pp. 75–90, 2002.

[4] R. W. Matthews, "Photo-oxidation of organic material in aqueous suspensions of titanium dioxide," *Water Research*, vol. 20, no. 5, pp. 569–578, 1986.

[5] L. Li, R. Chen, X. Zhu, H. Wang, Y. Wang, Q. Liao, and D. Wang, "Optofluidic microreactors with tio2-coated fiberglass," *ACS applied materials & interfaces*, vol. 5, no. 23, pp. 12 548–12 553, 2013.

[6] N. Baram, D. Starosvetsky, J. Starosvetsky, M. Epshtein, R. Armon, and Y. Ein-Eli, "Enhanced inactivation of e. coli bacteria using immobilized porous tio 2 photoelectrocatalysis," *Electrochimica Acta*, vol. 54, no. 12, pp. 3381–3386, 2009.

[7] N. M. Mahmoodi, M. Arami, and N. Y. Limaee, "Photocatalytic degradation of triazinic ring-containing azo dye (reactive red 198) by using immobilized tio 2 photoreactor: Bench scale study," *Journal of hazardous materials*, vol. 133, no. 1, pp. 113–118, 2006.

[8] A. Kar, Y. R. Smith, and V. Subramanian, "Improved photocatalytic degradation of textile dye using titanium dioxide nanotubes formed over titanium wires," *Environmental science & technology*, vol. 43, no. 9, pp. 3260–3265, 2009.

[9] Z. Han, J. Li, W. He, S. Li, Z. Li, J. Chu, and Y. Chen, "A microfluidic device with integrated zno nanowires for photodegradation studies of methylene blue under different conditions," *Microelectronic Engineering*, vol. 111, pp. 199–203, 2013.

[10] L. Lei, N. Wang, X. Zhang, Q. Tai, D. P. Tsai, and H. L. Chan, "Optofluidic planar reactors for photocatalytic water treatment using solar energy," *Biomicrofluidics*, vol. 4, no. 4, p. 043004, 2010.

[11] H. Jayamohan, Y. R. Smith, L. C. Hansen, S. K. Mohanty, B. K. Gale, and M. Misra, "Anodized titania nanotube array microfluidic device for photocatalytic application: Experiment and simulation," *Applied Catalysis B: Environmental*, vol. 174, pp. 167–175, 2015.

[12] Z. Meng, X. Zhang, and J. Qin, "A high efficiency microfluidic-based photocatalytic microreactor using electrospun nanofibrous tio2 as a photocatalyst," *Nanoscale*, vol. 5, no. 11, pp. 4687–4690, 2013.

[13] M. R. Prairie, L. R. Evans, B. M. Stange, and S. L. Martinez, "An investigation of titanium dioxide photocatalysis for the treatment of water contaminated with metals and organic chemicals," *Environmental science & technology*, vol. 27, no. 9, pp. 1776–1782, 1993.

[14] G. Prasad, G. Agarwal, B. Singh, G. Rai, and R. Vijayaraghavan, "Photocatalytic inactivation of bacillus anthracis by titania nanomaterials," *Journal of hazardous materials*, vol. 165, no. 1, pp. 506–510, 2009.

[15] Y. R. Smith, R. S. Ray, K. Carlson, B. Sarma, and M. Misra, "Self-ordered titanium dioxide nanotube arrays: Anodic synthesis and their photo/electro-catalytic applications," *Materials*, vol. 6, no. 7, pp. 2892–2957, 2013.

[16] Y. R. Smith and V. Subramanian, "Heterostructural composites of tio2 mesh- tio2 nanoparticles photosensitized with cds: A new flexible photoanode for solar cells," *The Journal of Physical Chemistry C*, vol. 115, no. 16, pp. 8376–8385, 2011.

[17] J. M. Macak, M. Zlamal, J. Krysa, and P. Schmuki, "Self-organized tio2 nanotube layers as highly efficient photocatalysts," *Small*, vol. 3, no. 2, pp. 300–304, 2007.

[18] B. Chen and K. Lu, "Influence of patterned concave depth and surface curvature on anodization of titania nanotubes and alumina nanopores," *Langmuir*, vol. 27, no. 19, pp. 12 179–12 185, 2011.

[19] H. Lindstrom, R. Wootton, and A. Iles, "High surface area titania photocatalytic microfluidic reactors," *AIChE journal*, vol. 53, no. 3, pp. 695–702, 2007.

[20] Z. Liu, V. Subramania, and M. Misra, "Vertically oriented tio2 nanotube arrays grown on ti meshes for flexible dye-sensitized solar cells," *The Journal of Physical Chemistry C*, vol. 113, no. 31, pp. 14 028–14 033, 2009.

[21] M. A. Eddings, M. A. Johnson, and B. K. Gale, "Determining the optimal pdms–pdms bonding technique for microfluidic devices," *Journal of Micromechanics and Microengineering*, vol. 18, no. 6, p. 067001, 2008.

[22] B. Chen, K. Lu, and J. A. Geldmeier, "Highly ordered titania nanotube arrays with square, triangular, and sunflower structures," *Chemical Communications*, vol. 47, no. 36, pp. 10 085–10 087, 2011.

[23] A. Houas, H. Lachheb, M. Ksibi, E. Elaloui, C. Guillard, and J.-M. Herrmann, "Photocatalytic degradation pathway of methylene blue in water," *Applied Catalysis B: Environmental*, vol. 31, no. 2, pp. 145–157, 2001.

[24] K. Rajeshwar, M. Osugi, W. Chanmanee, C. Chenthamarakshan, M. Zanoni, P. Kajitvichyanukul, and R. Krishnan-Ayer, "Heterogeneous photocatalytic treatment of organic dyes in air and aqueous media," *Journal of Photochemistry and Photobiology C: Photochemistry Reviews*, vol. 9, no. 4, pp. 171–192, 2008.

[25] H. Jayamohan, B. K. Gale, B. Minson, C. J. Lambert, N. Gordon, and H. J. Sant, "Highly sensitive bacteria quantification using immunomagnetic separation and electrochemical detection of guanine-labeled secondary beads," *Sensors*, vol. 15, no. 5, pp. 12 034–12 052, 2015.

[26] Y. R. Smith, B. Sarma, S. K. Mohanty, and M. Misra, "Single-step anodization for synthesis of hierarchical tio 2 nanotube arrays on foil and wire substrate for enhanced photoelectrochemical water splitting," *international journal of hydrogen energy*, vol. 38, no. 5, pp. 2062–2069, 2013.

[27] Y. R. Smith, A. Kar, and V. Subramanian, "Investigation of physicochemical parameters that influence photocatalytic degradation of methyl orange over tio2 nanotubes," *Industrial & Engineering Chemistry Research*, vol. 48, no. 23, pp. 10 268–10 276, 2009.

[28] T. Zhang, T. Oyama, A. Aoshima, H. Hidaka, J. Zhao, and N. Serpone, "Photooxidative n-demethylation of methylene blue in aqueous tio2 dispersions under uv irradiation," *Journal of Photochemistry and Photobiology A: Chemistry*, vol. 140, no. 2, pp. 163–172, 2001.

[29] Y. Kikuchi, K. Sunada, T. Iyoda, K. Hashimoto, and A. Fujishima, "Photocatalytic bactericidal effect of tio 2 thin films: dynamic view of the active oxygen species responsible for the effect," *Journal of photochemistry and photobiology A: Chemistry*, vol. 106, no. 1, pp. 51–56, 1997.

[30] A. Fujishima, T. N. Rao, and D. A. Tryk, "Titanium dioxide photocatalysis," *Journal of Photochemistry and Photobiology C: Photochemistry Reviews*, vol. 1, no. 1, pp. 1–21, 2000.

[31] M. Cho, H. Chung, W. Choi, and J. Yoon, "Different inactivation behaviors of ms-2 phage and escherichia coli in tio2 photocatalytic disinfection," *Applied and environmental microbiology*, vol. 71, no. 1, pp. 270–275, 2005.

[32] K. P. Kühn, I. F. Chaberny, K. Massholder, M. Stickler, V. W. Benz, H.-G. Sonntag, and L. Erdinger, "Disinfection of surfaces by photocatalytic oxidation with titanium dioxide and uva light," *Chemosphere*, vol. 53, no. 1, pp. 71–77, 2003.

[33] T. Saito, T. Iwase, J. Horie, and T. Morioka, "Mode of photocatalytic bactericidal action of powdered semiconductor tio 2 on mutans streptococci," *Journal of Photochemistry and Photobiology B: Biology*, vol. 14, no. 4, pp. 369–379, 1992.

[34] K. Sunada, Y. Kikuchi, K. Hashimoto, and A. Fujishima, "Bactericidal and detoxification effects of tio2 thin film photocatalysts," *Environmental Science & Technology*, vol. 32, no. 5, pp. 726–728, 1998.

[35] P.-C. Maness, S. Smolinski, D. M. Blake, Z. Huang, E. J. Wolfrum, and W. A. Jacoby, "Bactericidal activity of photocatalytic tio2 reaction: toward an understanding of its killing mechanism," *Applied and environmental microbiology*, vol. 65, no. 9, pp. 4094–4098, 1999.

[36] Z.-X. Lu, L. Zhou, Z.-L. Zhang, W.-L. Shi, Z.-X. Xie, H.-Y. Xie, D.-W. Pang, and P. Shen, "Cell damage induced by photocatalysis of tio2 thin films," *Langmuir*, vol. 19, no. 21, pp. 8765–8768, 2003.

CHAPTER 7

CONCLUSION

Several key scientific contributions have been made by the author in the area of applying nanomaterials in microfluidic format for sensing and remediation. A brief summary of the scientific contributions and conclusions drawn are presented hereafter along with suggestions for future work.

7.1 Platinum Functionalized Titania Nanotube Array Sensor for Detection of Trichloroethylene in Water

7.1.1 Conclusions

- A platinum functionalized TNA sensor for amperometric detection of TCE in water sample was reported.
- The TNA was synthesized using an electrochemical anodization technique and platinum was photocatalytically deposited on the nanotubes.
- The sensor showed current response to TCE in water at concentrations ranging from 10 ppm to 1000 ppm.
- The sensor exhibited a response to TCE at room temperature, making it less power intensive.
- The sensor can easily be incorporated into a point-of-use field-based system.

7.1.2 Contributions

- The Pt functionalized TNA sensor can be used for detection of other gases like O_2, H_2, formaldehyde etc.
- A mechanism for the sensor current response based on the reaction of TCE with chemisorbed reactive oxygen species (primarily O^-) was proposed. The knowledge can be applied to other metal oxide semiconductor sensors.

7.1.3 Future Work

The mechanism of amperometric response of the sensor involves reaction of chemisorbed reactive oxygen species on the surface of the sensor with volatile organic compounds (VOCs) [1]. Hence, the sensor can be applied to detection of other VOCs. Functionalization of the sensor with other metals (Pd, Co) could be explored for detection of other VOCs [2]. The deposition of metals via. different modes (electrochemical, photodeposition, vapor phase deposition) need to explored and characterized using XPS, SEM to optimize the sensor. Detection of VOCs from exhaled breath is a possible method for early diagnosis of several pulmonary diseases [2]. Hence, the platform can be modified into a breathalyzer with potential applications in health care diagnostics. The amount of platinum on the surface of the TNA can be modified to optimize the response to the sensor. The bias voltage can also be optimized to improve current response. To enhance the sensitivity of the sensor, TNA could be integrated into an interdigitated electrode format [3].

7.2 Highly Sensitive Bacteria Quantification Using Immunomagnetic Separation and Electrochemical Detection of Guanine-labeled Secondary Beads

7.2.1 Conclusions

- The protocol reported can detect *E. coli* from 100 mL samples with demonstrated limit of detection of 3 CFU/mL (S/N=3).
- IMS indicated a 95% extraction efficiency of *E. coli* with much less nonspecific capture (0.4%).
- The use of polyG functionalized secondary beads in addition to the magnetic beads incorporates signal amplification and potential multiplexing capability.
- Fluorescence imaging was performed to confirm selective binding of polyG functionalized secondary beads on the electrode surface and to demonstrate minimal nonspecific binding.
- The demonstrated limit of detection was 67 times lower than the most sensitive technique reported in literature.

7.2.2 Contributions

- A protocol for ultra-sensitive indirect electrochemical detection and quantification of *E. coli* O157:H7 was reported.

- The use of the protocol for detection of *E. coli* O157:H7 seeded in waste water effluent samples was demonstrated. Hence, the protocol can be used for real-world applications.

- The protocol can be applied to quantification of other pathogens using magnetic beads functionalized with antibodies specific to the pathogen strain.

7.2.3 Future Work

The protocol needs to be integrated into an automated system for use in field-based detection of *E. coli*. Miniaturized electrodes fabricated on chip needs to be used instead of glassy carbon electrodes for such a system. Since in a commercial system, long-term stability of the probes on the electrode is critical, the same needs to be evaluated. The system can be multiplexed by using secondary beads functionalized with a different polyG sequence (and using corresponding complementary probe sequence on the electrode). The hybridization parameters needs to be optimized to ensure minimum nonspecific binding between noncomplimentary DNA sequences. These include factors like temperature, salt concentration in buffer, hybridization time, etc. [4]. Future work would include optimization of the number of magnetic beads, number and size of nonmagnetic beads, polyguanine oligonucelotide concentration, and antibody concentrations. In the reported protocol, it is possible that the magnetic bead and secondary bead might compete to bind to the same site on *E. coli*. Hence, the ratio of these beads needs to be optimized. Another area of improvement is the reduction in variability of the electrochemical signal during DPV in acetate buffer solution (supporting electrolyte) containing 5 μM $Ru(bpy)_3^{2+}$. The use of other supporting electrolytes like PBS and KCl can also be explored. The effect of DPV scan parameters on the variability needs to be studied using statistical techniques (factor analysis).

7.3 Anodized Titania Nanotube Array Microfluidic Device for Photocatalytic Application: Experiment and Simulation

7.3.1 Conclusions

- A microfluidic reactor with TNA catalyst embedded in it was applied to photocatalytic degradation of methylene blue.

- The performance was evaluated at different flow rates ranging from 25 to 200 μL/min.

- The degradation performance was demonstrated to be better in comparison to microfluidic format with TiO_2 nanoparticulate (commercial P25) catalyst especially at higher flow rates (50-200 μL/min).

- The microfluidic reactor was fabricated using non-cleanroom-based soft lithography, making it suitable for economical large-scale manufacturing.

- A computational model of the microfluidic format was developed in a COMSOL Multiphysics® (finite element analysis) software to evaluate the effect of diffusion coefficient and rate constant on the photocatalytic performance.

7.3.2 Contributions

- The microfluidic reactor can be used for other photocatalytic applications and not just for degradation. For instance, the device can be used for photocatalytic syntheses of chemicals without much modification.

- The COMSOL model developed simulates the conversion of MB in the microreactor, including the effect of diffusion coefficient and rate constant. This model can applied to any microfluidic surface-based catalytic conversion system. By modifying the diffusion coefficient and rate constant, the model can be used for other chemicals/pollutants and catalysts. The model can easily be modified to fit other channel geometries.

7.3.3 Future Work

Improvements in the format have been incorporated into work done in Chapter 6, especially in the area of using the reactor for inactivation of pathogens.

7.4 Degradation of Organic and Biological Contaminants: Photocatalytic Microfluidic Reactors Utilizing Titania Nanotubes on Titanium Mesh

7.4.1 Conclusions

- A microreactor with TNA grown on a mesh showed enhanced photocatalytic performance over the device with TNA grown on a mesh (described in Chapter 5) for degradation of methylene blue.

- The device was also able to achieve >99% inactivation of E. coli O157:H7 at a flow rate of 50 μL/min.

7.4.2 Contributions

- A photocatalytic microfluidic reactor with TNA grown on a mesh was developed.
- The system can be applied to degradation of any chemical and biological agents in water, which can be mineralized with oxidizing agents (H_2O_2, $OH^{\bullet}$, $O_2^{\bullet -}$, O_3).

7.4.3 Future Work

The device can be applied to inactivation of other pathogens like viruses, which are harder to remove using conventional techniques like filtration. The TNA catalyst can also be functionalized with metals (Pt, Pd, Mn, Co), semiconductor material (CdS, PbS, Bi_2S_3, CdSe, CdTe, InP) to further improve their performance in the microfluidic format under visible light [5, 6]. The deposition using different modes (electrochemical, photodeposition, vapor phase deposition) needs to explored and characterized using XPS, SEM to understand surface coverage etc. To improve the photocatalytic efficiency of the system under visible light, doping of TNA with nitrogen can be done. Nitrogen doping could narrow the band gap of titania to extend the adsorption of catalyst to the visible light region [7].

7.5 Publications

Three manuscripts have been published from this work, with one manuscript in process of being submitted. A book chapter on microfluidic diagnostics was also published. These publications are as follows:

1. H. Jayamohan, H. J. Sant, and B. K. Gale, " Applications of microfluidics for molecular diagnostics," in *Microfluidic Diagnostics.* Springer, 2013, pp. 305-334.
2. H. Jayamohan, Y. R. Smith, B. K. Gale, M. Misra, and S. K. Mohanty,"Platinum functionalized titania nanotube array sensor for detection of trichloroethylene in water," *Proc. Sensors 2013 (Baltimore, MD, 3-6 November 2013)* IEEE, pp. 1-4, 2013.
3. H. Jayamohan, Y. R. Smith, L. C. Hansen, S. K. Mohanty, B. K. Gale, and M. Misra,"Anodized titania nanotube array microfluidic device for photocatalytic application:Experiment and simulation," *Applied Catalysis B: Environmental*, vol. 174, pp. 167-175, 2015.
4. H. Jayamohan, B. K. Gale, B. J. Minson, C. J. Lambert, N. Gordon, and H. J. Sant,"Highly Sensitive Bacteria Quantification Using Immunomagnetic Separation and Electrochemical Detection of Guanine-Labeled Secondary Beads," *Sensors*, vol. 15, pp. 12034-12052, 2015.

7.6 References

[1] H. Jayamohan, Y. R. Smith, B. K. Gale, M. Misra, and S. K. Mohanty, "Platinum functionalized titania nanotube array sensor for detection of trichloroethylene in water," *Proc. Sensors 2013 (Baltimore, MD, 3–6 November 2013) IEEE*, pp. 1–4, 2013.

[2] D. Bhattacharyya, Y. R. Smith, M. Misra, and S. K. Mohanty, "Electrochemical detection of methyl nicotinate biomarker using functionalized anodized titania nanotube arrays," *Materials Research Express*, vol. 2, no. 2, p. 025002, 2015.

[3] S. C. Colindres, K. Aguir, F. Cervantes Sodi, L. V. Vargas, J. A. M. Salazar, and V. G. Febles, "Ozone sensing based on palladium decorated carbon nanotubes," *Sensors*, vol. 14, no. 4, pp. 6806–6818, 2014.

[4] M. Tsuruoka, K. Yano, K. Ikebukuro, H. Nakayama, Y. Masuda, and I. Karube, "Optimization of the rate of dna hybridization and rapid detection of methicillin resistant staphylococcus aureus dna using fluorescence polarization," *Journal of biotechnology*, vol. 48, no. 3, pp. 201–208, 1996.

[5] Y. R. Smith, B. Sarma, S. K. Mohanty, and M. Misra, "Formation of tio 2–wo 3 nanotubular composite via single-step anodization and its application in photoelectrochemical hydrogen generation," *Electrochemistry Communications*, vol. 19, pp. 131–134, 2012.

[6] Y. R. Smith, "Self-ordering titania nanotube arrays: Electrochemical anodization, functionalization, and application," Ph.D. dissertation, University of Utah, 2014.

[7] Y. Cong, J. Zhang, F. Chen, and M. Anpo, "Synthesis and characterization of nitrogen-doped tio2 nanophotocatalyst with high visible light activity," *The Journal of Physical Chemistry C*, vol. 111, no. 19, pp. 6976–6982, 2007.